The Thesis Committee for Yao Fu
Certifies that this is the approved version of the following thesis

Leak-Off Test (LOT) Models

APPROVED BY
SUPERVISING COMMITTEE:

Supervisor:

Kenneth E. Gray

Hugh C. Daigle

Leak-Off Test (LOT) Models

By

Yao Fu, B.S. P.E.

Thesis

Presented to the Faculty of the Graduate School of

The University of Texas at Austin

in Partial Fulfillment

of the Requirements

for the Degree of

Master of Science in Engineering

The University of Texas at Austin

May 2014

Dedication

To my parents.

Acknowledgements

I am grateful for the opportunity to study and conduct research as a graduate student in the petroleum engineering department at the University of Texas at Austin, my educational and research experiences were outstanding and I owe thanks to many who made it enjoyable.

I would like to express my sincere gratitude to my supervisor, Dr. Kenneth E. Gray, for his guidance, support, patience, and motivation throughout my graduate study. It wouldn't be possible to achieve this milestone without him. I would also like to thank Dr. Hugh C. Daigle for reading this thesis and providing valuable comments and suggestions.

I would like to thank the research stuff of Wider Windows Industrial Affiliate Program: Dr. Eric B. Becker III, Dr. Evgeny Podnos, and Dr. Zhi Ye for their guidance and assistance.

I would like to thank all my colleagues in the research group for their assistance, including Lucas Barros, Yongcun Feng, Arjang Gandomkar, Anthony Ho, Xiaorong Li, Cesar Soares, and Scott Wallace.

I would like to thank the sponsoring companies of my research: BP, Chevron, Marathon Oil Company, National Oilwell Varco, Occidental Petroleum, and Conoco Phillips. I would like to mention Fernando E. Ziegler and John Jones of Marathon Oil Company, they spent hours of their valuable time to help me improving my understanding of formation pressure testing.

I would like to thank Emily and my friends for their company and support.

Abstract

Leak-Off Test (LOT) Models

Yao Fu, M.S.E.

The University of Texas at Austin, 2014

Supervisor: Kenneth E. Gray

A leak-off test is one of the most common procedures to test the fracture pressure of the exposed formations. After cementing and drilling out of the casing shoe, the LOT is run to verify that the casing, cement, and formation can withstand the pressure needed to safely drill the next section of the well. The equivalent mud weight obtained from the test is recorded and reported to government agencies as the strength of the casing shoe. Drilling engineers also rely on the reading from the LOT and use it as the maximum pressure that may be imposed on the formation to avoid fracturing. Exceeding the maximum pressure may result in serious consequences such as lost circulation, one of the most costly events in drilling operations. Therefore, accurate determination of formation fracture gradient is critical and can avoid a variety of well control problems.

Considerable efforts to model LOT and leak-off behaviors have been done in the past. Altun (2001) and Paknejad (2007) each presented a unique method to estimate leak-off volume by dividing the pressurized system into four sub-systems: mud compression, casing expansion, fluid leakage, and borehole expansion. The volume response from each sub-system is then combined to represent the total volume pumped during a LOT.

However, neither model included the expansion volumes of cement sheath and formation rock outside of the casing; these volumes are not trivial and should not be neglected. In addition, both models use only pump pressure to calculate volumes generated during a LOT. The actual downhole pressure and the pressure acting from the outside are ignored.

In this study, the volume contributions from cement sheath expansion and formation rock expansion are calculated using single cylinder Lame's equation. The results are added with Altun's borehole expansion volume, mud compression volume, and fluid leakage volume to represent the total volume for the enhanced Altun model. Secondly, a Wider Windows mechanical expansion model is developed based on the concentric cylinder theory. This model simulates the compounded effect of casing, cement, and formation expansion along the cased hole based on pressures inside the wellbore and out in the far-field stress region. The volume generated from concentric cylinder expansion is then combined with Altun's mud compression volume and fluid leakage volume to simulate the total volume pumped during a LOT.

The developed models were verified using three sets of field LOT data obtained from literature and compared with the original Altun model. The results confirmed that leak-off volume along the cased hole should be analyzed as a compounded effect of casing, cement, and formation expansion. Overall, the WW models accurately simulate both leak-off volume and leak-off behaviors.

Table of Contents

List of Tables

List of Figures

Chapter 1: Introduction

1.1 MOTIVATION

In conventional drilling operations, wellbore pressure must be kept within the mud weight window at any depth. The lower limit of the window is described by the naturally occurring formation pore pressure. If the wellbore pressure falls below the formation pore pressure, a "kick" can take place as formation fluids enter the wellbore causing well control problems. On the other hand, the upper limit of the window is characterized by the maximum pressure that the formation can withstand without losing integrity, such pressure is often referred to as the formation fracture pressure. If the wellbore pressure is high enough to exceed the formation fracture pressure, cracks can be generated at the open hole to provide flow paths for drilling fluid to enter the formation. The serious consequences of fractured formation include lost circulation, which is one of the most costly events in drilling operations. The margin for safe drilling operation, especially offshore, is often very narrow. Therefore understanding and recognizing both the formation pore pressure and the formation fracture pressure is critical to ensure safe drilling practices.

The drilling industry relies on two main methods to estimate the formation fracture pressure: the direct method and the indirect method. The direct method involves pressure testing of the open hole formation after drilling out of the previous casing shoe, such tests include the leak-off test (LOT), formation integrity test (FIT), extended leak-off test (XLOT), and pump-in and flow-back test. On the other hand, the indirect method often utilizes empirical correlations such as the Eaton correlation, Hubbert and Willis equations, and etc. Drilling planning engineers also rely on the basin-wide fracture pressure correlations in mature fields where the fracture pressure gradients are well characterized by studying existing LOTs and XLOTs. Numerous studies have been published such as "A comparison of leak-off test and extended leak-off test data for stress estimation" by Addis

et al. in 1998 and "An investigation of leak-off test data for estimating in-situ stress magnitudes: application to a Basinwide study in the North Sea" by Edwards et al. in 1998.

Altun et al. (1999) published the first ever LOT model aimed to better analyze LOT results in formations that give non-linear relationships between the pumped volume and the observed pump pressure. The model is divided into four sub-systems: mud compression, casing expansion, borehole expansion, and fluid leakage. It was concluded that the non-linear behavior solely results from fluid leaking into the formation. Paknejad (2007) followed Altun's model by changing only the fluid leakage term to better describe LOT behaviors in shallow marine sediments. However, neither of the models include the volumes and compressibilities of the cement sheaths and rock formations outside the casing. These additional volume changes to the total leak-off volume response during a LOT are not trivial and should not be neglected.

Therefore, the main objective of this thesis is to incorporate the volumes generated from expanding the cement sheath and formation rock outside of the casing. It is also important to understand the physical meaning behind each of the terms shown on the conventional LOT and XLOT plots. Therefore, they are carefully examined and the different opinions are summarized in this thesis work.

1.2 THESIS ORGANIZATION

The thesis consists of four chapters. After the introduction chapter, chapter 2 will provide the literature review of LOTs and XLOTs including the nomenclatures and physical meanings, factors affecting leak-off behavior, non-linear LOT interpretation, and surface and downhole LOT data comparison. Chapter 3 will provide the overview of the past LOT models developed by Altun (1999) and Paknejad (2007). Chapter 4 covers the new developments in LOT modeling including the "enhanced" Altun model and the Wider

Windows mechanical expansion models. Finally, chapter 5 will state the conclusions for this thesis work.

Chapter 2 Literature Review

Chapter 2 begins with an overview of generalized LOT and XLOT plots. After the overview, terms on the generalized plots, their physical meanings, and different opinions associated with them will be explored. In addition, factors affecting leak-off behaviors, non-linear LOT interpretations, and surface/downhole LOT data comparison will be discussed in this chapter.

2.1 Generalized LOT and XLOT plots

A typical LOT plot is shown in Figure 2.1, illustrated by Postler (1997). Most LOT plots exhibit a linear trend of the pressure buildup curve initially. At point A, the data trend line starts to deviate from linearity, and the pressure at this point is often referred to as leak-off pressure (LOP) or fracture initiation pressure (FIP). After point A, pressure continues to increase to point B as pumping continues. At point B, the pump is stopped, and the observed pressure is called the maximum test pressure or maximum observed pressure. When the pump stops, the pressure decreases rapidly and then levels off. The inflection point, point C, is commonly considered to be the minimum formation stress. Point D, where the pressure levels off, is called the fracture closure pressure. The physical meaning of these points will be further discussed in section 2.2.

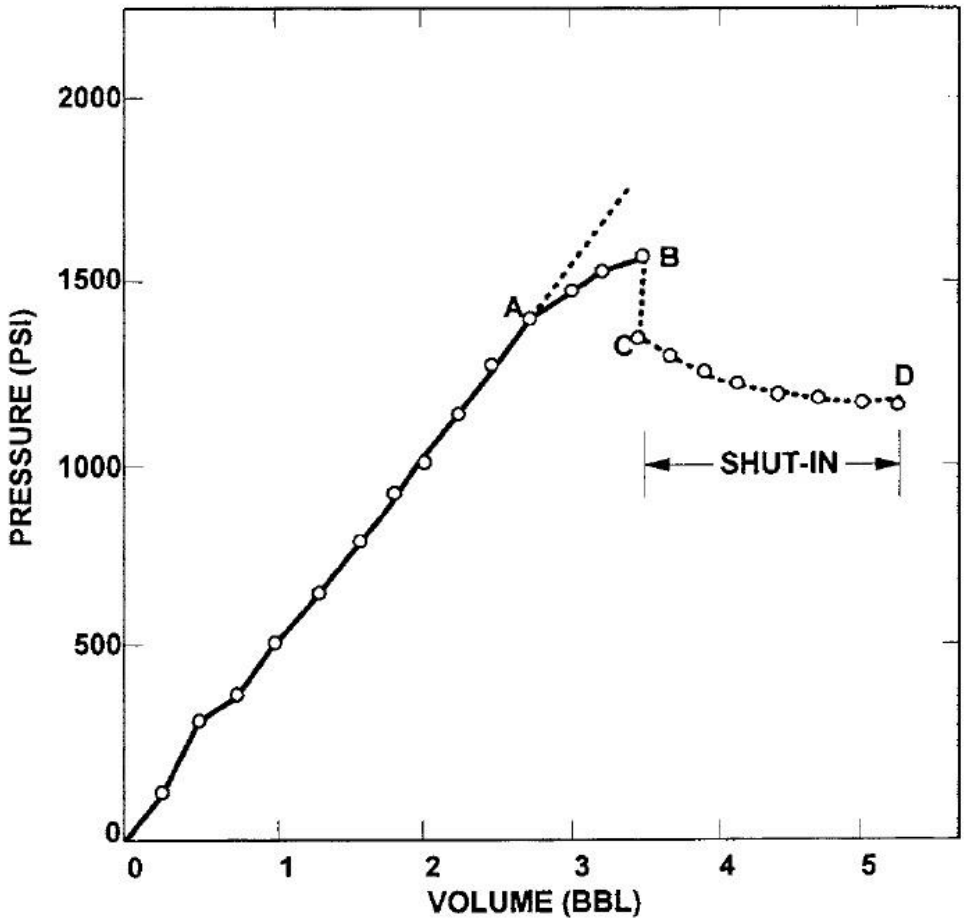

Figure 2.1 Typical LOT plot (Modified after Postler, 1997)

An idealized XLOT is shown in Figure 2.2. The XLOT generally has two pumping cycles: the first pumping cycle is identical to a LOT; the second pumping cycle starts after bleeding off pressure and allowing the well to flowback, the pressures and volume observed during flowback are recorded before pumping starts again. The descriptions of events and definitions of key points on the plot will be discussed in section 2.2.

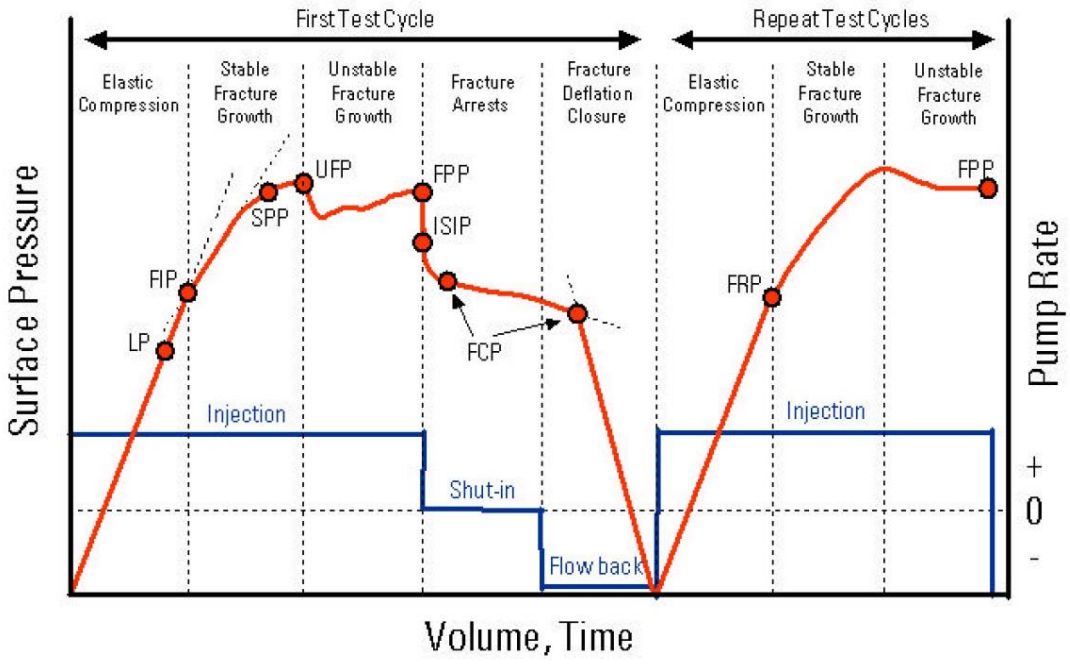

Figure 2.2 Idealized XLOT plot (Lee, 2004; originally developed by API RP 66 work group)

2.2 NOMENCLATURES AND PHYSICAL MEANINGS

This section will discuss the nomenclature and the physical meanings behind each term shown in Figure 2.2.

2.2.1 Limit Pressure

The limit pressure (LP) is the pressure limit set for a FIT or sometimes referred to as a limit test. Since the FIT is normally performed during drilling of production wells in mature fields where local fracture gradient is well characterized at a certain depth, the LP is set below the FIP to avoid fracturing the formation. During the test, surface pressure is applied to pressurize the well to a desired equivalent mud weight (EMW) at the open hole.

2.2.2 Fracture Initiation Pressure

FIP or commonly called the LOP is defined as the point where the pressure buildup trend line deviates from linearity by bending to the right. Many theories have been published in effort to explain the complex physical nature in the wellbore at this point.

Early publications (prior to 2000) commonly suggested that FIP represents fracture opening at the open hole. Postler (1997) suggested that a small, stable fracture is opened in the wellbore at this pressure. As the fracture opens, mud flows into the opened fracture and fluid is lost through the permeable faces of the fracture. When fluid is lost to the formation via the opened fracture, more mud is pumped into the well, hence change the slope of the pressure buildup curve (Postler, 1997).

Addis et al. (1998) explained the LOP by examining the compressibility of the system during a LOT. Before reaching the LOP, the compressibility of the pressurized system stays constant. However, at LOP, the compressibility of the system increases, causing the rate of pressure buildup to decline. Therefore, a deflection point can be observed on the LOT plot.

Edwards et al. (1998) agreed with Postler's theory by suggesting that fractures are opened at the wellbore at LOP. Furthermore, LOP is classified into two sub-classes. In class 1, a fracture is opened at the wellbore of a previously intact formation, therefore the LOP is close to the formation breakdown pressure. However, in class 2, a fracture is reopened at the wellbore due to drilling induced fractures or naturally cracked pre-existing fractures. In this case, the LOP is a good estimation of the minimum horizontal stress (Edwards, 1998). The two classes of LOP and their corresponding LOPs are shown in figure 2.3.

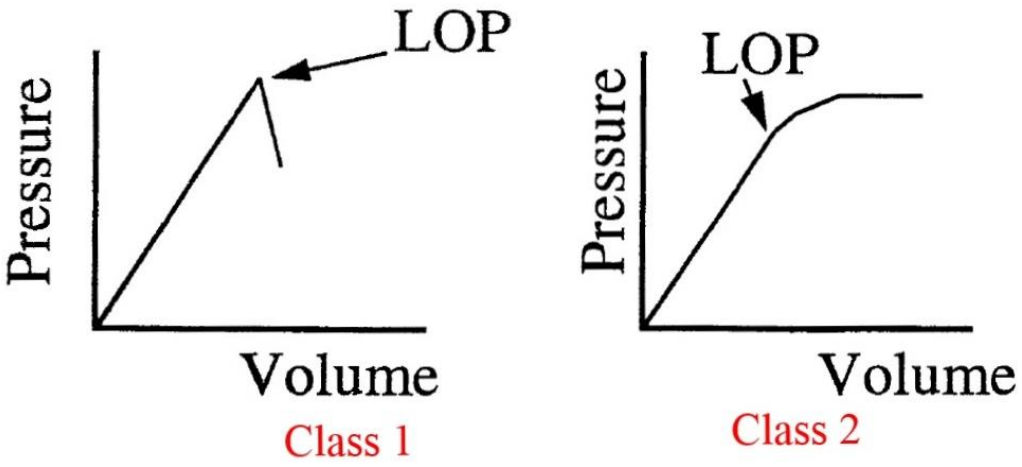

Figure 2.3 Two classes of leak-off pressure (Edwards, 1998)

Some of the recent publications agreed with Postler (1997)'s theory that a fracture is opened in the wellbore of the open hole when the pressure buildup line first starts to deviate from linearity (Økland et al. 2002; Lee et al. 2004; van Oort et al. 2007; Li et al. 2009; Aadnoy et al. 2009; Heger et al. 2011).

Li et al. (2009) further suggested that the LOP is observed when the opening of the rock starts to dominate since fluid can enter the formation through permeable paths in the rock.

Zoback (2007) indicated that the pressure buildup trend line starts to deviate from linearity when the volume of the pressurized system increases due to fracturing and the LOP should equal to the fracture propagation pressure (FPP), as shown in Figure 2.4.

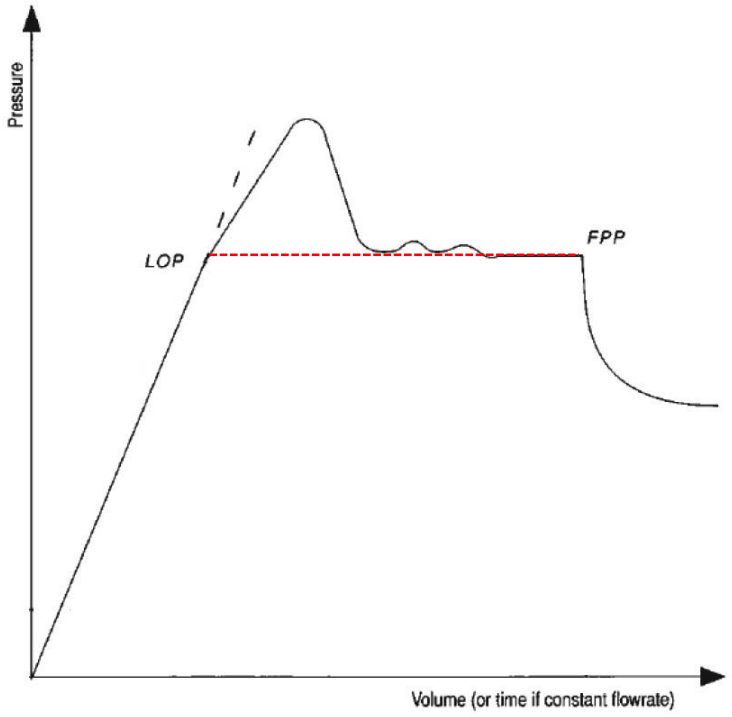

Figure 2.4 Zoback's LOP (Zoback, 2007, modified after Gaarenstroom et al. 1993)

In contrast, Wojtanowicz et al. (2001) suggested that instead of opening a fracture at the wellbore, the formation remains intact at the LOP and only fails beyond the LOP. The compressibility of the pressurized system changes at LOP, causing the pressure buildup trend line to bend to the right.

The leak-off test procedure by Nabors Drilling International Limited also suggested that the fractures are not created at the LOP. Instead, LOP represents formation intake pressure, further pumping beyond LOP will eventually create fractures at the wellbore (Aadnoy, 2009).

Økland et al. (2002) suggested that LOP can also represent formation breakdown. In this case, no clear deflection point can be observed during pressure building up, therefore formation breakdown is achieved and the pressure at this point is called the FIP. A rapid

drop in pressure is observed while pumping continues, indicating the volume of the induced crack increases faster than the pump rate, shown in Figure 2.5.

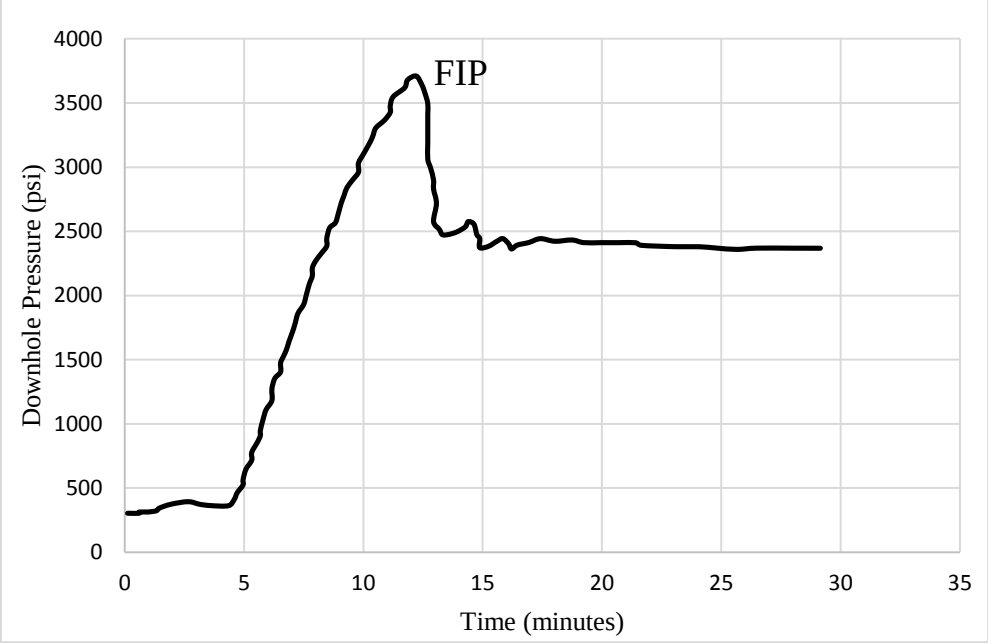

Figure 2.5 Fracture initiation as leak-off pressure (Modified after Økland, 2002)

2.2.3 Stop Pump Pressure

The stop pump pressure (SPP) is usually the highest pressure achieved during a LOT. Pressure continues to increase from FIP to SPP as injection of fluid continues. Stable fracture growth is observed during this period, meaning most pressure and fluid are lost along the length of the fracture (Postler, 1997). However, the pressure at the tip of the fracture remains near FIP and it requires additional pressure buildup to propagate the fracture. For a LOT, the pump is stopped at this point, a rapid drop in pressure is observed because of fluid loss in the open fracture and the loss of pump friction pressure (Postler, 1997). The EMW observed at SPP is recorded and reported to regulatory authorities as the strength of the casing shoe (van Oort, 2007). During the shut-in period, a slight decrease in pressure can be observed. This is caused by fluid loss to the permeable formation

(Postler, 1997). Drilling operation resumes when pressure stabilizes and no additional problems are reported.

2.2.4 Unstable Fracture Pressure

Unstable fracture pressure (UFP), or breakdown pressure, occurs when the stored energy overcomes the pressure loss along the faces of the fracture to transmit additional pressure to the tip of the fracture. Van Oort (2007) suggests that at UFP, fracture growth is primarily in length ranging from tens to thousands of feet. Similarly, Alberty (1999) concluded that massive loss occurs at breakdown pressure due to the fracture being extended away from the wellbore into the far-field region. It is recommended to stop the test before UFP to avoid lost circulation. A cement squeeze job is required to repair the damages created by uncontrollable fracture growth to ensure casing shoe integrity.

Figure 2.6 shows an example of two-stage fracture growth from LOP to UFP. The LOP is recorded at approximately 830 psi for the initial test. Then pressure continues to increase until it reaches UFP of 1300 psi. Consequently, a rapid drop in pressure can be observed to indicate uncontrollable fracture growth. The repeated test shows an identical LOP at near 830 psi. However, a short stable crack growth period and a smaller breakdown pressure are both observed for the repeated test because breakdown has already occurred during the first pumping cycle. A slight decrease in pressure after the UFP can also be seen from the repeated cycle.

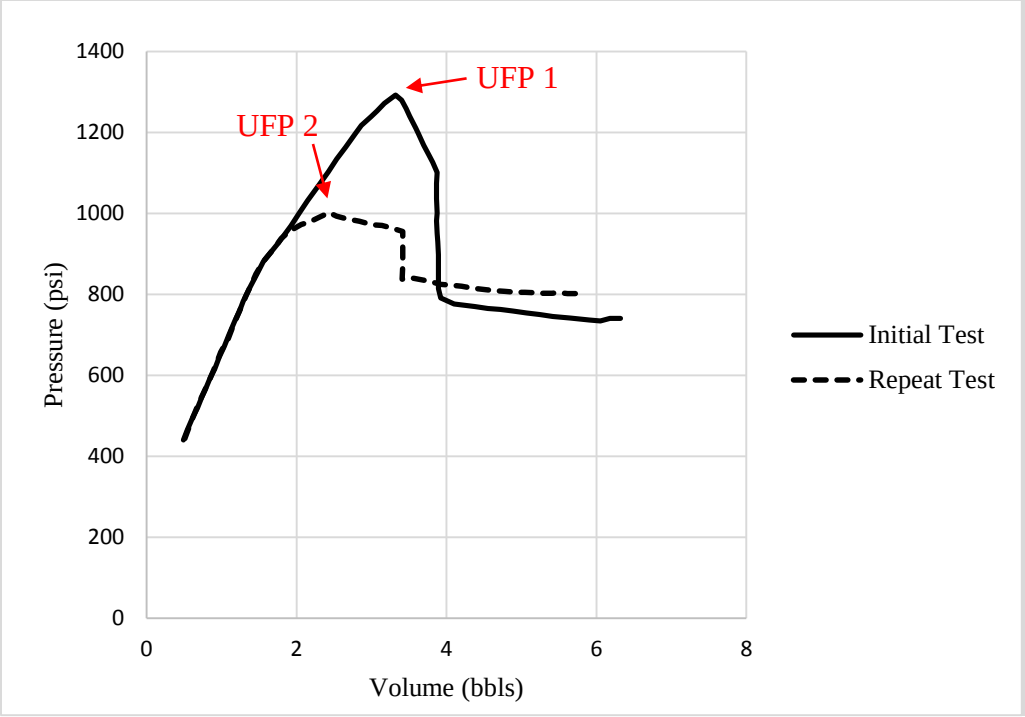

Figure 2.6 Two-stage fracture growth (Modified after Postler, 1997)

2.2.5 Fracture Propagation Pressure

Fracture propagation pressure (FPP) is below UFP. Whereas UFP represents formation breakdown, FPP represents uncontrolled fracture propagation. Many believe that the FPP for the first pumping cycle of an XLOT should equal to the FPP recorded for the second pumping cycle. Van Oort (2007) illustrated this relationship by modifying the generalized XLOT plot originally developed by API RP 66 work group, shown in Figure 2.7.

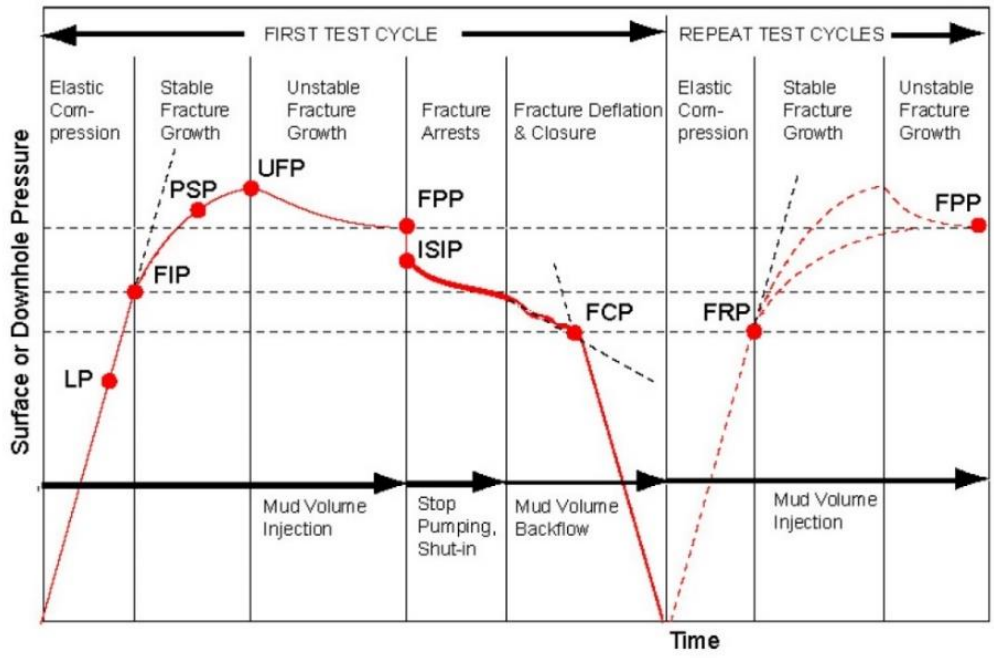

Figure 2.7 Fracture propagation pressures for an XLOT (van Oort, 2007; modified after API RP 66 work group).

Økland et al. (2002) studied FPP using field data from Statoil and presented an interesting observation on fracture propagation, shown in Figure 2.8. It can be seen that fracture propagation features a saw-tooth shape. This is because as fracture propagates, the FPP decreases. Therefore, as long as the pressure inside the fracture is above minimum horizontal stress, propagation would occur in a mini-breakdown fashion, causing the fracture to grow in steps.

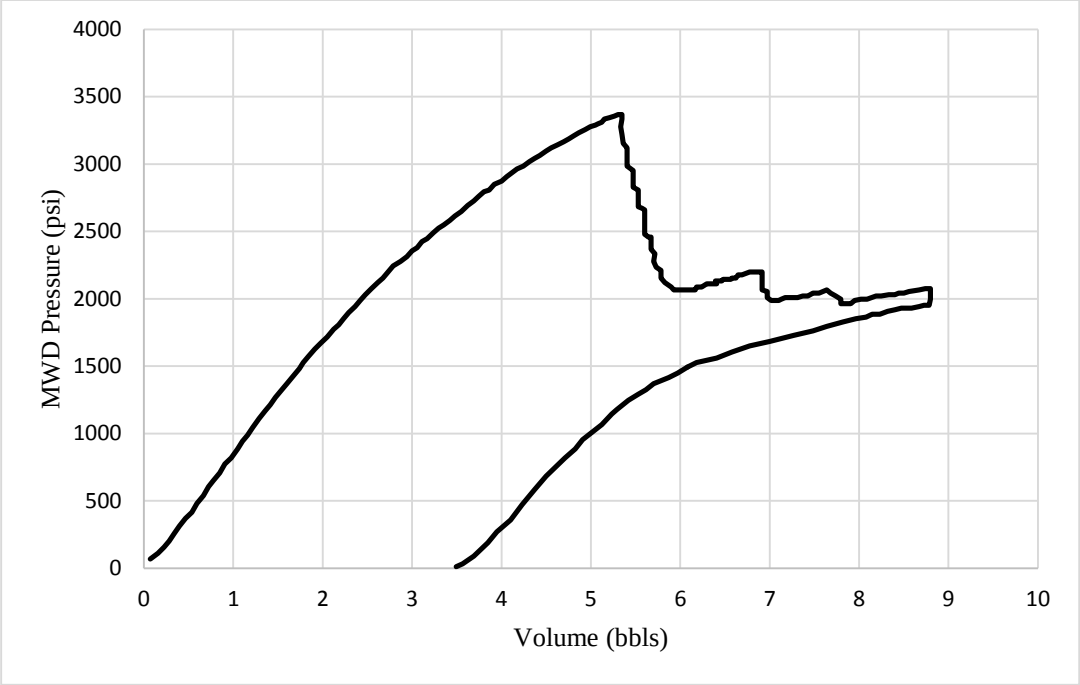

Figure 2.8 Fracture tip "mini-breakdowns" (Modified after Økland, 2002)

2.2.6 Instantaneous Shut In Pressure

Instantaneous shut in pressure (ISIP) is observed immediately after shut-in. When the pump stops, a rapid drop in pressure occurs, caused by the loss of pump friction pressure and the loss of fluids to the fractures (Postler, 1997). Alberty (1999) suggested that fractures created during a LOT would collapse at ISIP, therefore ISIP indicates fracture closure. Similarly, Postler (1997) concluded that because most fractures generated during a LOT extend to the far field stress region, the ISIP is a good estimation of the undistorted minimum horizontal stress as it represents the stresses at the fracture tip. In addition, based on field observations, if the ISIP is lower than half of the LOP, it is likely that a leak channel exists in the surface equipment, casing, or cement (Postler, 1997).

2.2.7 Fracture Closure Pressure

It is not easy to determine the fracture closure pressure (FCP) from a conventional LOT plot or XLOT plot. However, the FCP is commonly recognized as the best estimation of far-field minimum horizontal stress (Økland et al. 2002 and van Oort 2007).

For a LOT, FCP occurs when pressure levels off after shut-in. At this pressure, fluid loss is limited to loss through permeable faces of the wellbore, assuming all the fractures generated are closed.

For an XLOT, FCP can be obtained by either plotting pressure vs. time during the shut-in phase or pressure vs. volume during the flowback phase (Økland et al. 2002 and van Oort 2007). In either method, a change in slope of the data points indicates fracture closure and the corresponding pressure is reported as the FCP, as shown in Figure 2.9 and Figure 2.10.

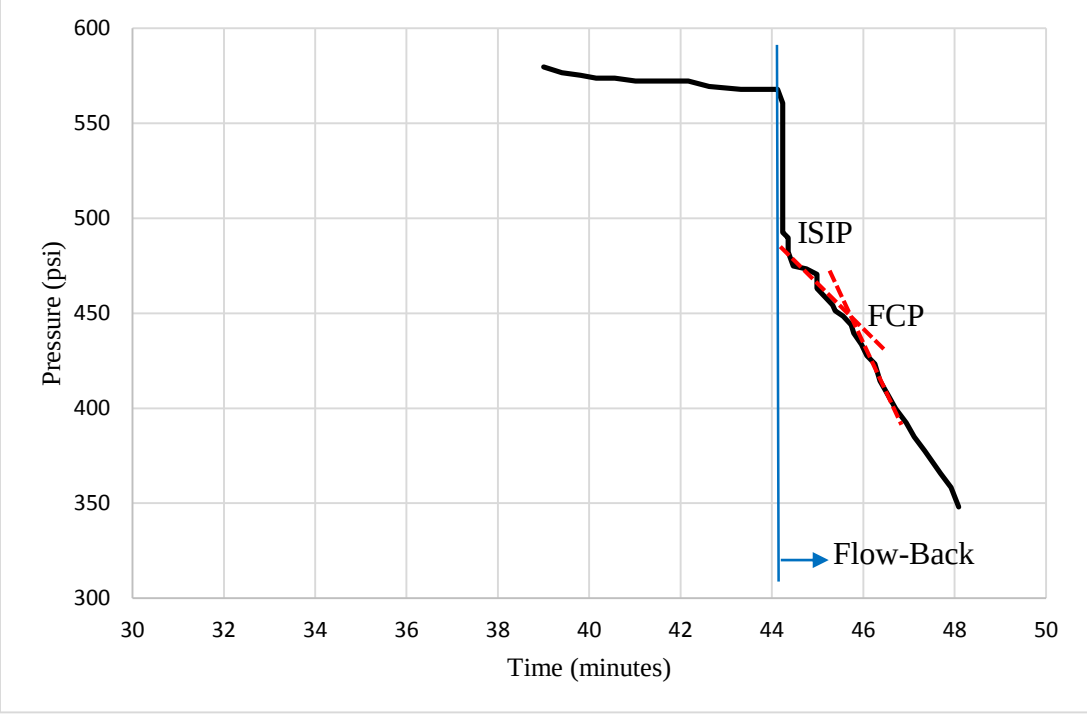

Figure 2.9 FCP during flow back phase (Modified after van Oort, 2007)

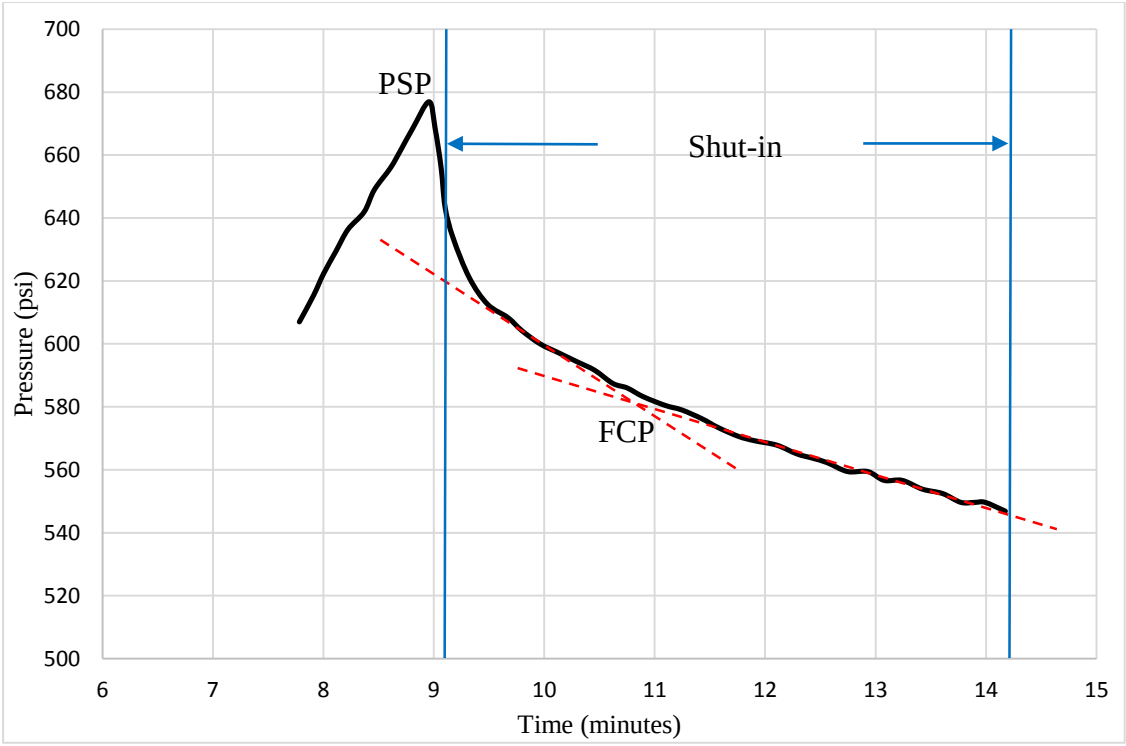

Figure 2.10 FCP during shut-in phase (Modified after van Oort, 2007)

2.2.8 Fracture Reopening Pressure

Fracture reopening pressure (FRP) occurs during the second pumping cycle of an XLOT when the fracture opens again. Many believe that the magnitude of FRP should be less than the magnitude of LOT because the rock releases the tensile strength when the fractures are created during the first pumping cycle (Edwards, 1998; Økland et al. 2002; van Oort 2007). However, Økland (2002) has shown that the FRP may increase over time due to changing conditions at the wellbore wall, including fracture healing caused by the interaction between WBM and shales. Figure 2.11 shows the relationship between the LOPs for an XLOT, the difference in magnitude represents the rock tensile strength.

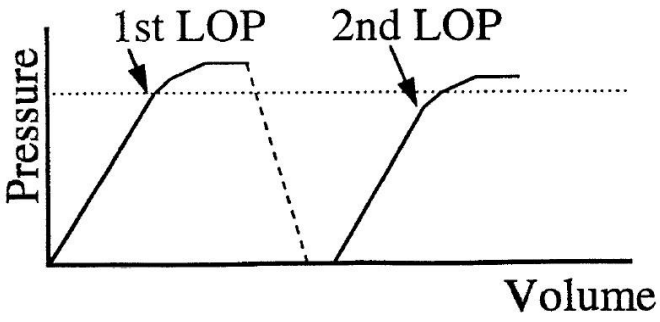

Figure 2.11 Leak-off pressures for two pumping cycles (Edwards, 1998)

Van Oort (2007) concluded that because the fractures are reopened for the second pumping cycle, the FRP should be equal or close to the FCP for the first pumping cycle. However, Økland et al. (2002) suggests that based on field data, the FRP can also be higher than FCP, as shown in Figure 2.12.

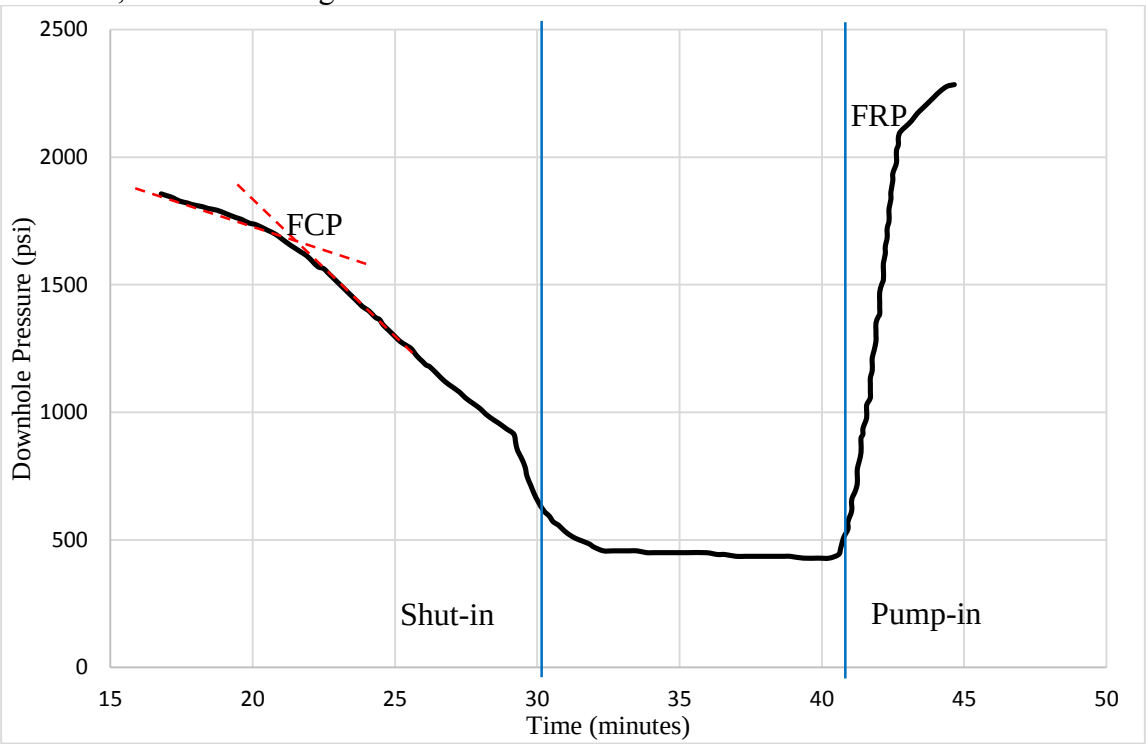

Figure 2.12 Fracture reopening pressure higher than fracture closure pressure (Modified after Økland, 2002)

2.3 FACTORS AFFECTING LEAK-OFF BEHAVIOR

2.3.1 Wellbore Distortion Effect and Plastic Rocks

The natural subsurface stress field is distorted while drilling a well. A highly stressed, compressive layer of rock is present near the wellbore since it must bear the load that was previously supported by the rock removed during drilling. This effect causes the stress concentration to be higher near the wellbore and decreases with distance away from the well. As illustrated by Hubbert and Willis (1957), the stress concentration approaches the undistorted far-field stress within a couple borehole diameters. This observation implies that the magnitude of pressure required to initiate fracture must be higher than the undistorted minimum stress. It also suggests that fracture propagation requires less pressure than fracture opening since the stress concentration is higher near the wellbore. This agrees with most field observations (Postler, 1997).

Most rocks exhibit elastic behavior up to the point of failure. It was found that drilling through an unconsolidated sand or consolidated sand with low horizontal stress ratio can create a plastic strained zone around the wellbore. Horsrud (1982) suggested that the cause of reduced rock strength is because of the breakdown of intergranular cementation bonds. As a result, there can exist two distinct stress regions: a near wellbore plastic region and a far field elastic region. In this case, the pressure needed to initiate a fracture at the wellbore will be lower than the pressure required to propagate the fracture.

Horsrud (1982) closely investigated the wellbore distortion phenomena by performing multiple numerical studies. An example is shown in Figure 2.13. It can be seen that a fracture is opened in the wellbore when the fluid pressure is equal to the tangential stress. However, the fracture will only extend a short distance and will not extend into the elastic region because the pressure cannot overcome the far-field stresses.

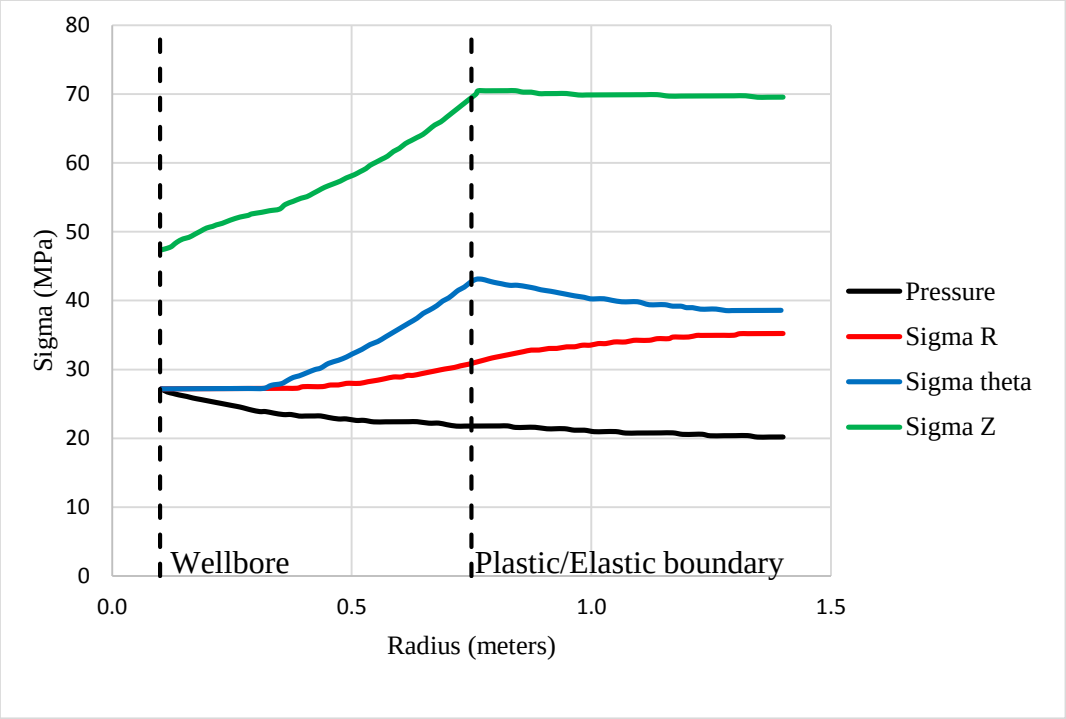

Figure 2.13 Numerical fracture study in near wellbore plastic region (Modified after Horsrud, 1982)

Similar to Horsrud's numerical study, Postler (1997) presented a field LOT to show the different behaviors in plastic and elastic regions. It can be seen from Figure 2.14 that a fracture is initiated at around 850 psi and propagates from 850 psi to 900 psi within the plastic region. However, propagation stops at 900 psi when the fracture tip reaches the plastic/elastic boundary. A second linear portion is observed representing pressure buildup. At 1100 psi the stored energy finally overcomes the far-field stress and the fracture is opened again into the elastic region.

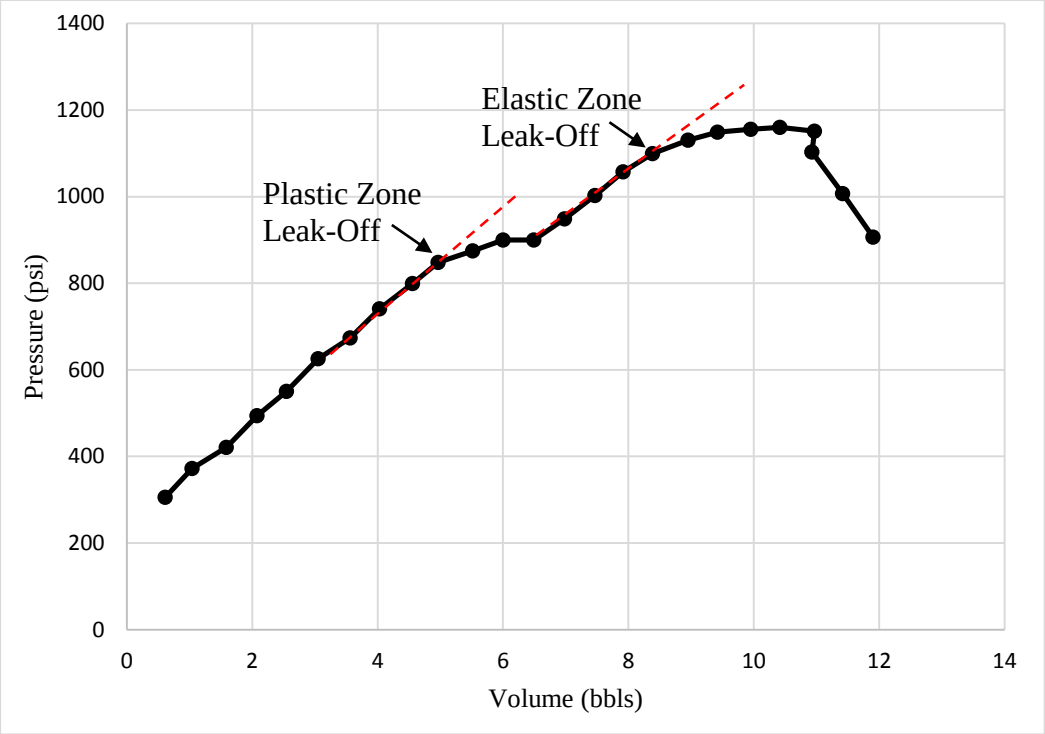

Figure 2.14 Two Stage Fracture Growth (Modified after Postler, 1997)

2.3.2 Mud Compressibility and Thermal Expansion

Although recent advancements in downhole technologies enables real-time downhole measurement for LOT, it is still a common practice to calculate EMW and fracture gradient based on surface measurements. As a result, this can lead to problems managing narrow drilling margins if the EMW is not corrected for the effect of mud compressibility and thermal expansion (van Oort, 2007).

Mud compressibility correction is important for drilling deepwater wells. In deepwater environment, drilling mud passes through the drilling risers before reaching the BOP. Because the temperature outside the risers is almost always cooler than the temperature at the drill floor, the mud gets cooled down, and the effective density of the mud as it enters the BOP can be much higher than the mud density recorded at surface. This can lead to underestimation of the EMW at a particular casing shoe when analyzing a

LOT if the changes in mud density are not recognized. Luckily, most drilling fluid suppliers have taken account of the mud compressibility effect in their hydraulics simulation packages (van Oort, 2007).

When drilling in high pressure and high temperature (HPHT) environments, thermal expansion effects can cause the mud to expand towards the bottom of the well, resulting in a downhole mud density that is less than the surface mud density. Therefore, it is also important to recognize the effect on mud density caused by thermal expansion when calculating the shoe strength using surface measurements (van Oort, 2007).

2.3.3 Mud Type

The types of mud used during a LOT has profound influence on stable fracture growth caused by the fracture tip screen-out phenomena (van Oort, 2007). Stable fracture growth, as discussed in section 2.2.3, is characterized by pressure and fluid loss along the length of the fracture. For a LOT performed using WBM, the buildup of external filter cakes can effectively isolate the fracture tip. On the contrary, for a LOT performed using OBM or SBM, wettability contrast between the rock and the mud causes very little filtration loss (Aadnoy, 2009). Therefore, neither mud can effectively build-up filter cakes to screen-out the fracture tip, the fracture tip is therefore in communication with the hydraulic force of the mud at all times, which leads to a lower and constant fracture propagation pressure than for LOT performed using WBM (van Oort, 2007; Aadnoy, 2009).

2.3.4 Temperature

Change in temperature can alter the near wellbore thermal stress and affect leak-off behaviors. For example, heating a formation can increase the thermal stress around the wellbore, resulting in higher FIP and FPP; on the other hand, cooling the formation can

decrease the near wellbore thermal stress, causing the rock to exhibit lower FIP and FPP. Previous studies have shown that thermal effects in sandstone ranges from 2.5 psi/°C to 52.2 psi/°C (Charlez, 1997; as cited in van Oort, 2007) and 5 psi/°C to 15 psi/°C in water injection wells in sandstones (Hettema, 2005; as cited in van Oort, 2007). An example of change in fracture gradient caused by temperature has been shown by van Oort (2007): when a formation at 20,000 ft with natural temperature of 200 °F comes in contact with drilling mud heated to 150 °F, with the thermal effect assumed to be 10 psi/°C, the fracture gradient equivalent decreases from 14.5 ppg to 14.23 ppg. The difference of 0.27 ppg seems to be small, however, in deepwater drilling environment, failure to recognize such small difference in fracture gradient can lead to lost circulation and rig non-productive times.

External temperature profile along the well path significantly affects mud density and mud viscosity, especially with WBM. When drilling in deepwater environments, drilling mud often gets cooled down in the risers and gets warmed up as it enters the formation. Because the temperature in a drilling riser can get to as low as the normal freezing point of water, drillers often warm the mud to compensate the cooling effect (Rezmer-Cooper, 2000). The density and viscosity of the mud reacts to change in temperature in the same fashion; they both increase as the mud cool down and decrease as the mud warm up. The cooling effect makes it possible to have a higher effective mud density at a casing shoe than the recorded mud density at the drill floor. This effect can lead to miscalculation of leak-off gradients if the change in mud density is not recognized. Figure 2.15 shows the typical drilling fluid temperature profiles for both deepwater wells and land rigs, note the decrease in temperature from the surface to BOP for the deepwater case. In addition, Figure 2.16 shows the mud density profiles corresponding to temperature profiles for both deepwater wells and land rigs.

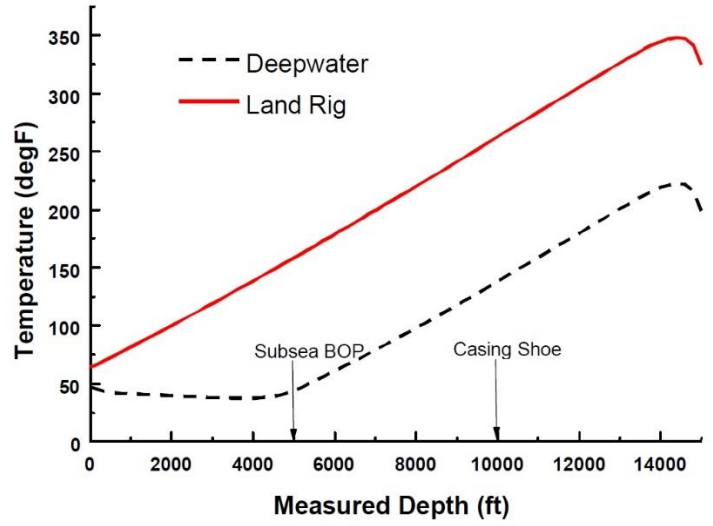

Figure 2.15 Typical drilling fluid temperature profiles for both deepwater wells and land rigs (Rezmer-Cooper, 2000)

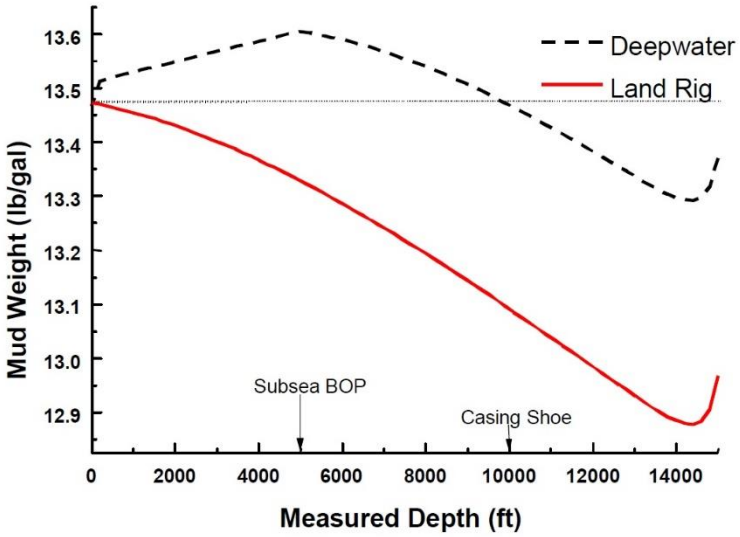

Figure 2.16 Mud density profiles corresponding to temperature profiles for both deepwater wells and land rigs (Rezmer-Cooper, 2000)

Temperature also causes change in mud compressibility, thermal effect, and gel strength of the mud. Changes in leak-off behavior due to mud compressibility and thermal

effect have been discussed in previous sections. Changes in leak-off behavior due to mud gel strength is considered when comparing surface data with downhole data, which will be discussed in section 2.5.

2.3.5 Variation in Time

The shoe strength of a particular casing after LOT may not stay the same over time. Fracture healing effect is observed when LOT is conducted using WBM. However, OBM does not allow fracture healing in the same way (Økland, 2002; Aadnoy, 2009; van Oort, 2007). Many believe the rock around the wellbore loses some of its strength during a LOT as fractures are created, the magnitude of the lost strength is characterized by the rock tensile strength. In the case when WBM is used for a LOT/XLOT, as water comes in contact with clay rocks, clay particles absorbs water and expands. Over time, this allows the rock to regain some of its lost strength. Therefore, the casing shoe strength may increase over time due to this fracture healing effect.

2.3.6 Location of Cementing Unit

Majority of the LOT are performed by recording pressure readings at the cementing unit. In most cases, the cementing unit is located on a deck lower than the rig floor, or the top of the mud column (van Oort, 2007). Figure 2.17 illustrates an example of surface equipment connection for LOT; note the elevation difference between the pumps and the rig floor.

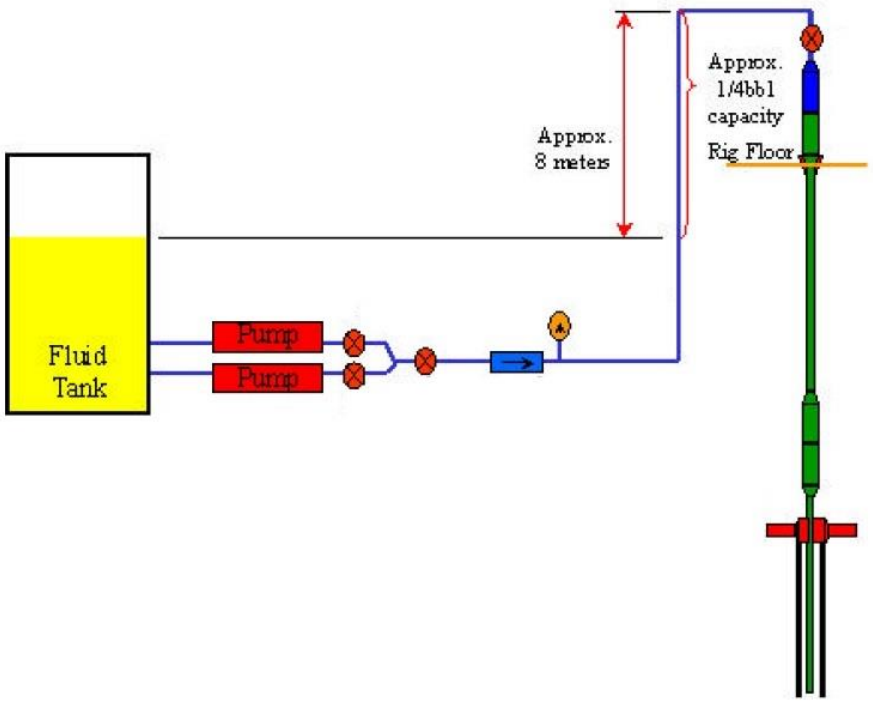

Figure 2.17 Example surface equipment connection for LOT (Modified after Lee, 2004)

It is possible to overestimate the LOP if the elevation difference and the volume of mud in the pipes are not recognized. Therefore, it is important to calculate the hydrostatic pressure difference generated between the two points of interest mentioned above.

2.3.7 Fluid Viscosity

Viscosity of the fluid used during a LOT has significant impact on crack stability and crack extension (Postler, 1997). As previously discussed in section 2.2.3, most pressure loss and fluid loss occur along the length of the fracture during stable fracture growth. Higher fluid viscosity results in higher pressure drop. Therefore, the fracture tip is temporarily protected from the full hydraulic force of the mud. Even if the pressure in the wellbore is well beyond fracture initiation pressure or fracture propagation pressure, the

fracture will not propagate due to the viscosity effect. Thus, higher pressure in the wellbore is required to deliver sufficient force to the fracture tip. As a result, a delay between fracture initiation and fracture propagation can be observed and a higher propagation pressure is expected when pumping using viscous fluid (Ishijima, 1983). However, this delay is not significant when pumping using fluids with low viscosities, such as water.

2.3.8 Fluid Penetration

Most LOTs are performed with WBM, OBM, or SBM. Among the three types of muds, WBM is considered to be non-penetrating, OBM and SBM are considered to be penetrating.

It was found that LOTs performed with a penetrating fluid exhibit lower fracture initiation pressures than LOTs performed with non-penetrating fluid (Postler, 1997; Altun, 1999). This is because of the reduction in formation strength due to the temporary increase in pore pressure caused by the penetration of higher pressure fluid. In addition, penetrating fluids can also cause the temporary reduction in matrix stress (Altun, 1999). Figure 2.18 shows the difference in pore fluid distributions for a penetrating fluid and a non-penetrating fluid.

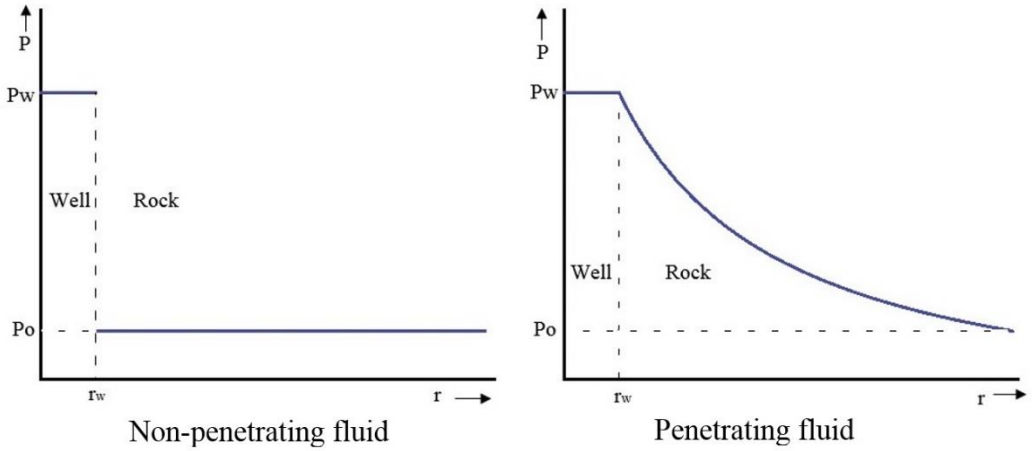

Figure 2.18 Penetrating fluid vs. non-penetrating fluid (Modified after Haimson, 1967)

Whether a fluid can penetrate or not also depends on the size of the interconnected pore sizes, in other words, the permeability of the rock. The same logic can be applied here as well: the affected pore-pressure region from fluid penetration is larger for a permeable rock than for an impermeable rock. In the case for an impermeable rock, the highly pressured fluid can only penetrate along the length of the crack and the near wellbore region, which causes the fluid pressure to be constant for the majority portion of the crack. Thus, the FIP and FPP are higher. Whereas in the case of a permeable rock, highly pressured fluids can penetrate much deeper in the formation, which causes the pore pressure to be equal to the fluid pressure. Therefore, lowered FIP and FPP are expected.

2.3.9 Pre-Existing Crack

It is common for any section of the wellbore to intersect pre-existing cracks, faults, or joints (Altun, 1999). This situation reduces the fracture initiation pressure and narrows the drilling mud window. In the downhole environment, most of the pre-existing cracks are closed due to the naturally occurring compressive stresses of the formation. Therefore, the tensile strength of the rock can be assumed to be zero. The pressure required to initiate a fracture should be lower than the pressure needed with an intact rock. Most field observations have confirmed this theory (Postler, 1997). Ishijima (1983) studied the effect of crack length on initiation pressure and breakdown pressure in detail by numerically modelling a hydraulic fracture test and concluded that the pre-existing flaw size relative to well radius alters leak-off behavior and the magnitude of breakdown pressure. The results of this study can be seen in Figure 2.19.

Pre-existing cracks can also alter the orientation of the generated fractures. Studies have found that in shallower marine sediments, horizontal fractures can be generated rather than vertical fractures (Altun, 1999).

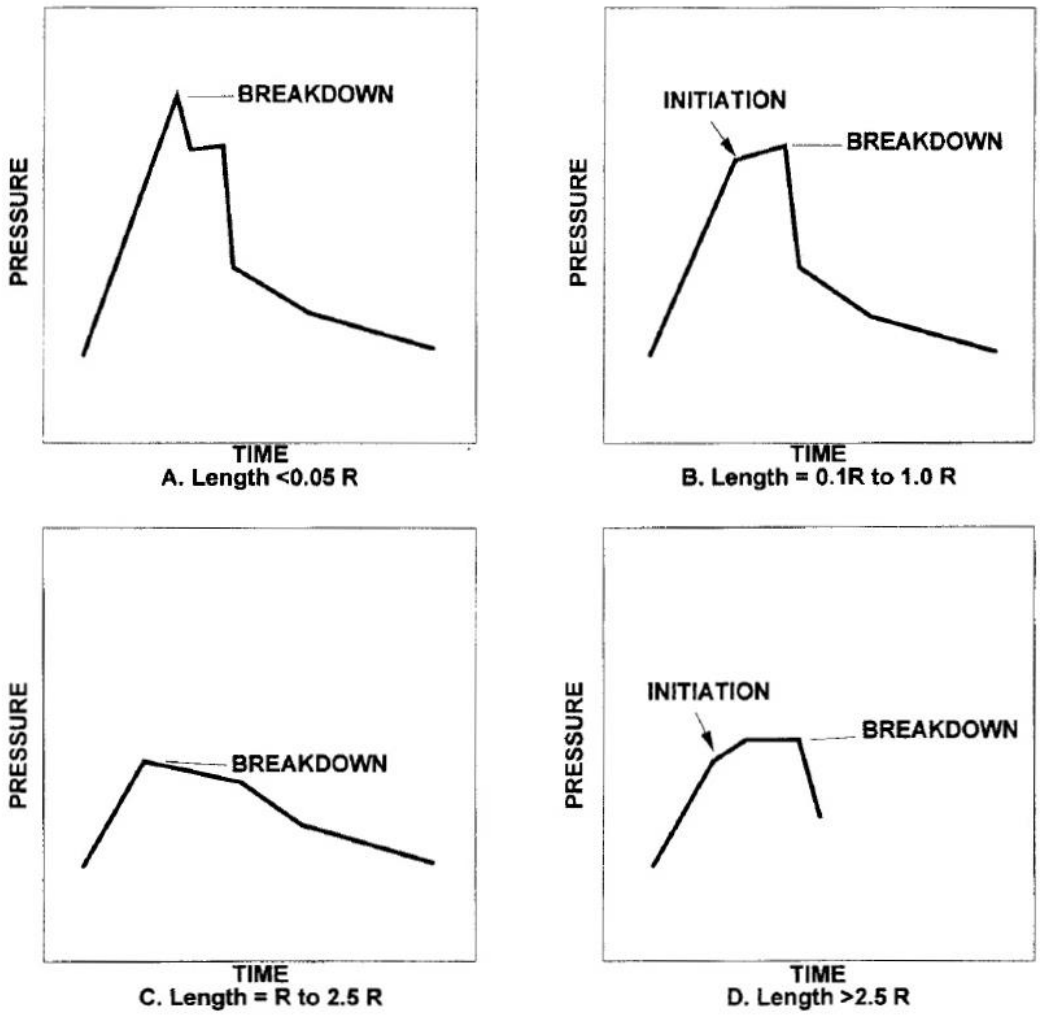

Figure 2.19 Effect of pre-existing cracks on breakdown pressure (Postler, 1997; Modified from Ishijima, 1983)

2.3.10 Pump Rate

The effects of injection rate on fracturing have been studied by many in the past. Postler (1997) and Ishijima (1983) suggest that both FIP and FPP increase as the pump rate increases. A field example is shown in Figure 2.20. It clearly shows the effect of pump rate on the magnitude of breakdown pressure. The breakdown pressure and LOP obtained from a test performed at high pump rate may not necessarily reflect the actual strength of the

rock as pressurizing at low pump rate can still fracture the rock over time. Therefore, it is recommended to use the LOP obtained using the slowest pump rate (Postler, 1997).

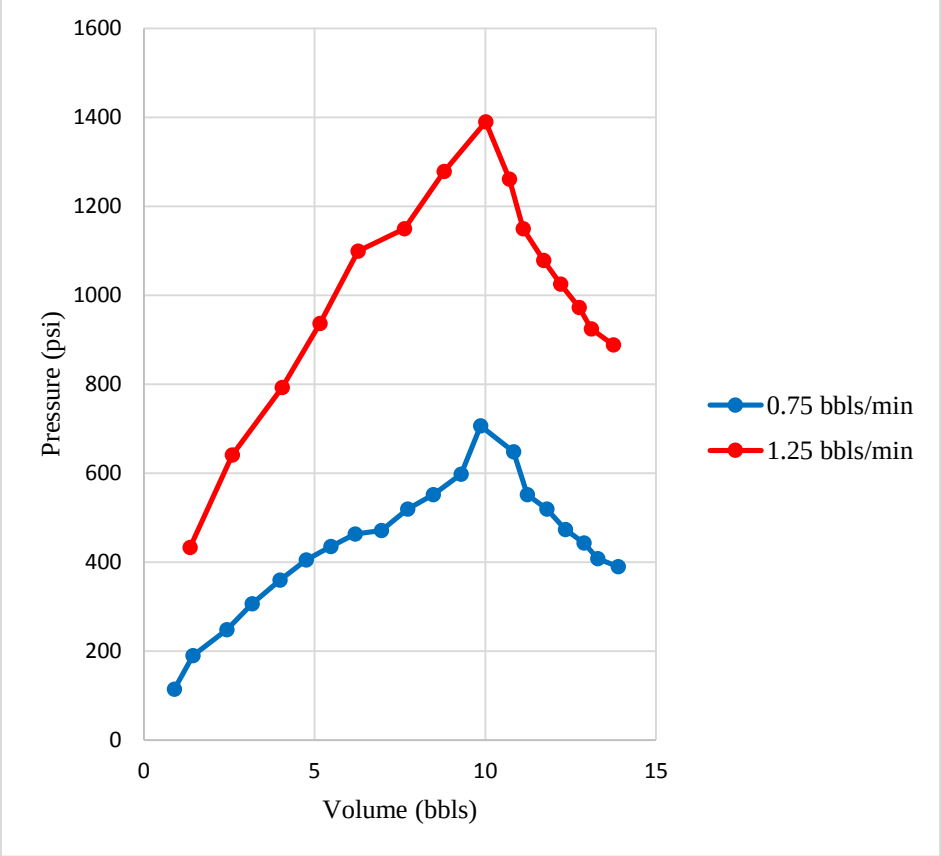

Figure 2.20 Effect of pump rate (Modified after Postler, 1997)

2.3.11 Cement Channels

Postler (1997) and Altun (1999) suggested that cement channel is the leading cause of unusual leak-off behaviors in the field. Cement channels of concern during a LOT are those that provide hydraulic communication between rock layers with different pressure regimes. Generally, a fluid path generated during a LOT will connect the casing shoe to a shallower zone with lower fracture pressure.

The effect of a large open cement channel on leak-off behavior can be seen in Figure 2.21. It is clear that the LOP is significantly lower than the predicted leak-off line,

this suggests that direct hydraulic communication is established immediately as fluid and pressure are lost to the weaker formation. A large cement channel can be confirmed if the actual LOP is more than ½ ppg EMW below the EMW at predicted leak-off value (Postler, 1997).

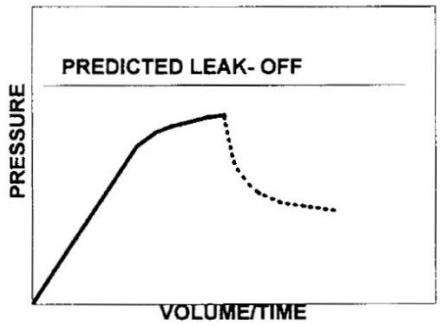

Figure 2.21 Effect of a large open cement channel (Postler, 1997)

Figure 2.22 shows the effect of a small open cement channel on leak-off behavior. Unlike a large open channel, the small open channel only provides limited fluid flow to the weaker zone. Therefore, pressure buildup still occurs in the wellbore. Two distinctive LOPs exist on the pressure vs. volume plot. LOP 1 is much lower than the predicted leak-off value and it represents fracture initiation in the weaker zone. On the contrary, LOP 2 represents fracture initiation of the stronger formation at the open hole.

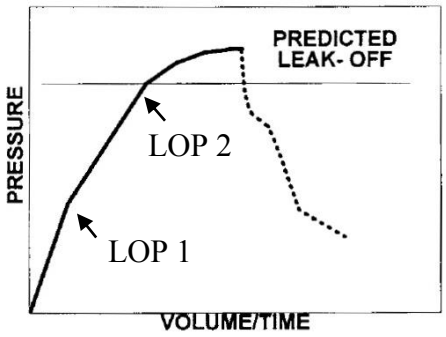

Figure 2.22 Effect of a small open cement channel (Modified after Postler, 1997)

A cement channel can be plugged with gelled mud. When pressurized, the plugged material prevents immediate hydraulic communication. However, as pressure increases with pumping, the plugging material will be forced out of the cement channel and a slight change in the pressure vs. volume slope can be observed. It can be seen from Figure 2.23 that the pressure achieved when the plugging material is forced out of the cement channel can be as high as the predicted leak-off value, which can result in misinterpretation of the LOT if plugged cement channel is not recognized.

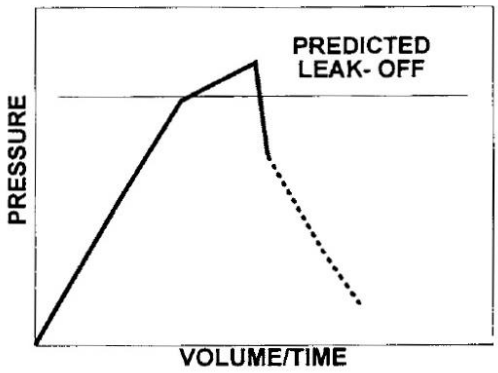

Figure 2.23 Effect of a plugged cement channel (Postler, 1997)

2.3.12 Magnitude of Far-field Stresses

The magnitude of far-field stresses directly influence the shape of the LOT plot prior to formation breakdown (Ishijima, 1983). Figure 2.24 shows the pressure vs. time plot for three different far-field stress regimes. It can be seen that as the magnitude of far-field stress decreases, the slope of the pressure vs. time plot between LOP and breakdown pressure decreases, which indicates a flatter stable fracture growth. However, the breakdown pressures for different far-field stress regimes remain scattered (Haimson, 1974; as cited in Ishijima, 1983).

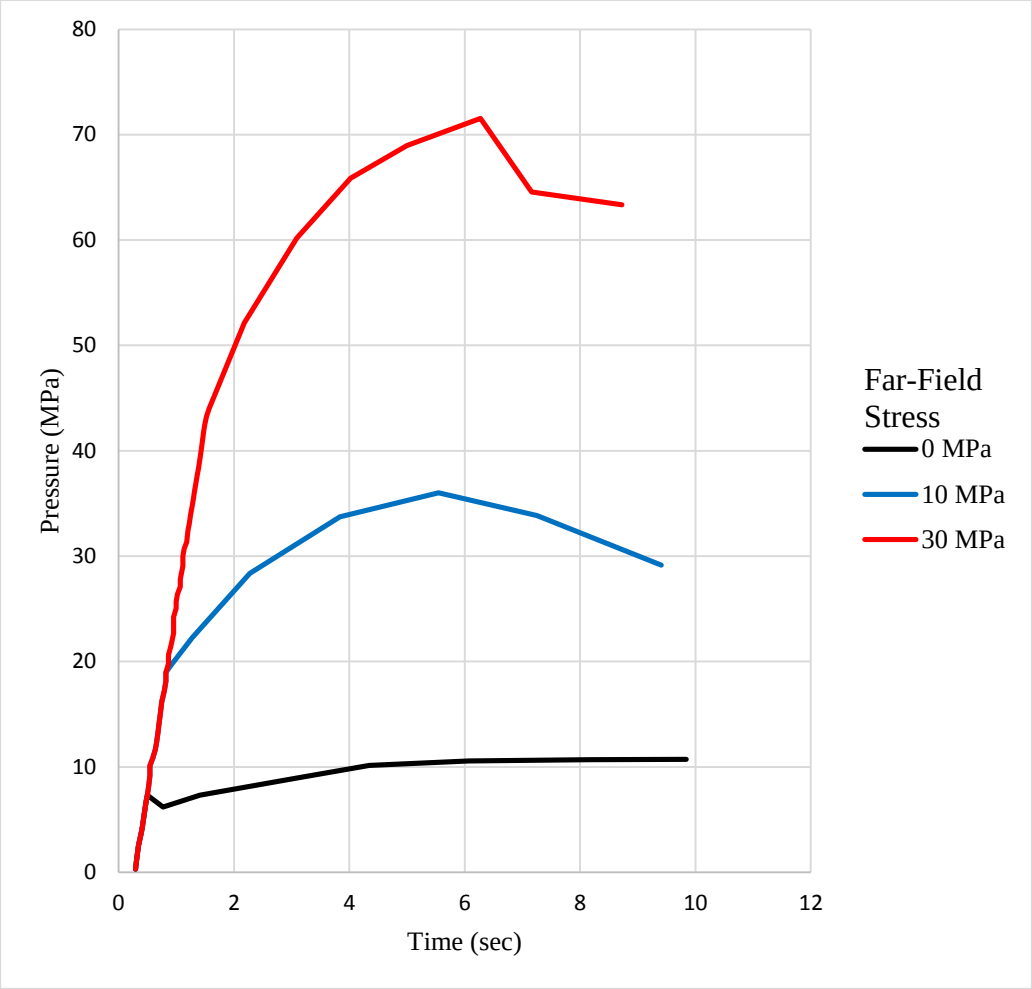

Figure 2.24 Effect of far-field stresses (Modified after Ishijima, 1983)

2.4 NON-LINEAR LOT INTERPRETATION

Most LOTs exhibit a linear trend between the pump pressure and the pumped volume. However, non-linear LOTs are not uncommon, especially in shallow marine sediments (SMS). Conventional LOT interpretation relies on determining the failure point where the pressure buildup curve departs from linear trend by bending to the right. However, recorded LOTs in SMS give non-linear trend with no obvious point of deflection to indicate the beginning of failure.

SMS are defined as deposits below the sea floor to a depth of about 3,000 ft (Wojtanowicz, 2001), but some have been found as deep as 3,500 ft (Rezmer-Cooper, 2000). The mechanisms that cause shallow water flows have been studied by Alberty et al. (1999). The four identified mechanisms are induced fractures, induced storage, geopressured sands in conductor intervals, and transmission of geopressure through cement channels.

Paknejad et al. (2007) suggested that using log-log plots helps to identify the point of deflection on LOT plots in SMS. Figure 2.25 and Figure 2.26 shows an example of using log-log plot to identify leak-off pressure presented in Paknejad's work.

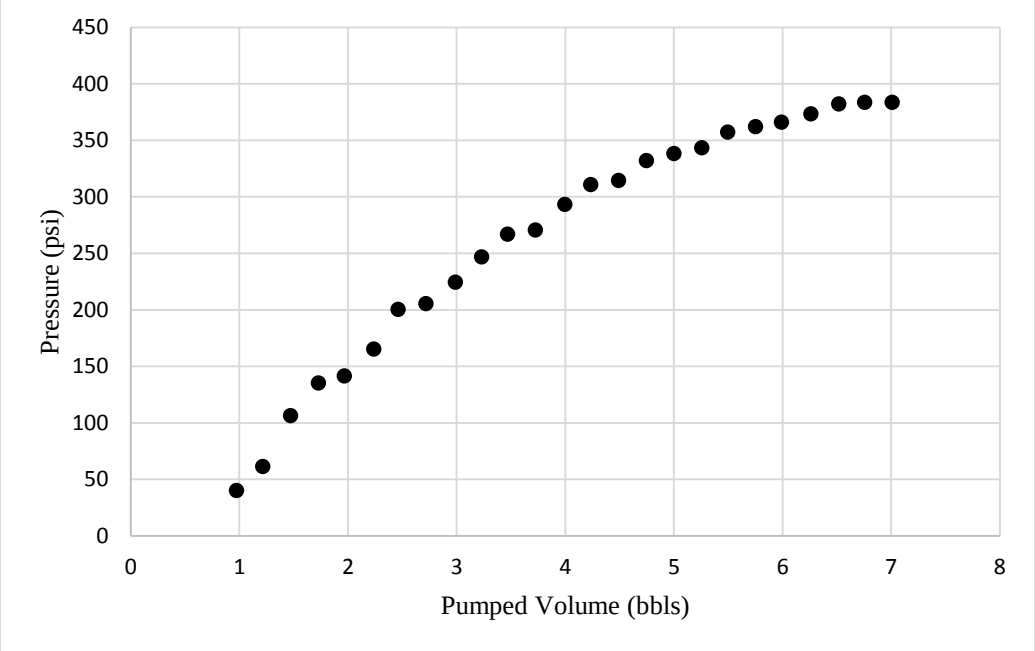

Figure 2.25 Non-linear LOT with conventional interpretation (Modified after Paknejad, 2007)

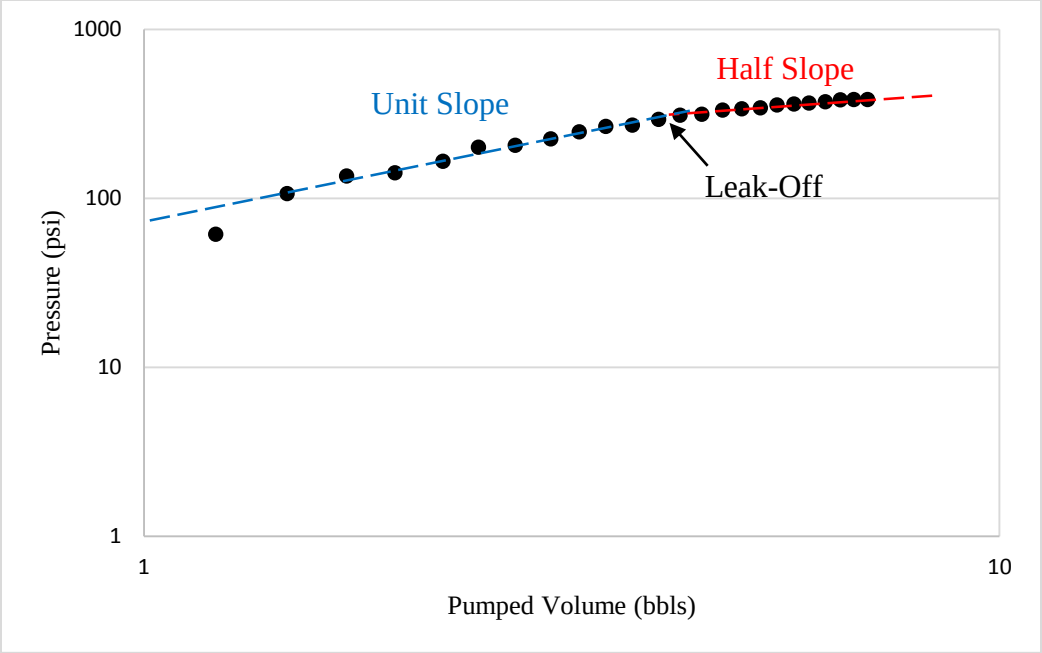

Figure 2.26 Using log-log plot to identify leak-off pressure (Modified after Paknejad, 2007)

Figure 2.25 shows that conventional LOT plots do not offer a clear deflection point, making it impossible to identify leak-off pressure. However, using log-log plot, a clear deflection point can be pinpointed as the slope changes from unit slope to half slope.

Wojtanowicz et al. (2001) suggests another theoretical method to help analyze LOTs in SMS. In this work, pumping continues until the system yields and pressure no longer increases as shown in Figure 2.27.

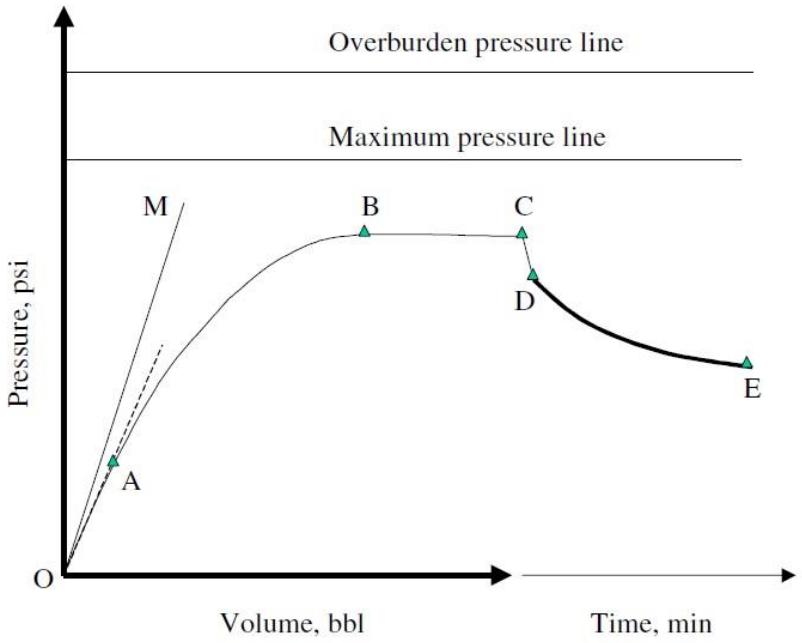

Figure 2.27 Conceptual leak-off test plot from shallow marine sediment (Wojtanowicz, 2001)

Point O represents the starting of pumping and point A represents the initial departure from linearity. However, point A is often hard to distinguish since the entire OAB section is likely to exhibit non-linear behavior for a LOT in SMS. Point B represents the beginning of pressure stabilization and it is usually the highest pressure achieved during a LOT in SMS. Pumps are stopped at point C and a sharp pressure drop can be observed from C to D. Section DE represents the pressure fall-off stage as fluid can be lost to rock matrix, cement channels, or rock fractures (Wojtanowicz, 2001). The maximum pressure line is identified as the difference between the maximum hydrostatic pressure during cementing and the hydrostatic mud pressure before the LOT.

Wojtanowicz et al. (2001) suggested that using the stabilized portion of the LOT curve (B to C) can help to determine the cause of the non-linear behavior. If the stabilized LOT pressure, pressure at point B is close to the overburden pressure line, horizontal

fractures are likely generated during the LOT. If the stabilized pressure is situated between the overburden pressure line and the maximum pressure line, cement-rock parting is the likely cause of the non-linear LOT. In addition, if the stabilized pressure is below the maximum pressure line, cement-rock parting and fluid loss to rock matrix can both cause the non-linear behavior with the later one being the most likely cause.

2.5 SURFACE AND DOWNHOLE LOT DATA COMPARISON

Recent technology advancement has enabled the real-time downhole measurement of pressure during a LOT/FIT. Shell (1998-1999) conducted a real-time FIT using wireline while drilling services on the Auger platform, installed in the GOM with water depth of 2,862 ft (Rezmer-Cooper, 2000). The FIT was conducted after drilling out of the casing shoe at 8,050 ft. Both downhole pressure and temperature were measured by the wireline operated LWD inductive coupling tool, which enables real-time data transfer to the surface without relying on the traditional mud pulse method. Surface and downhole pressure data were plotted against each other to show the difference, shown in Figure 2.28.

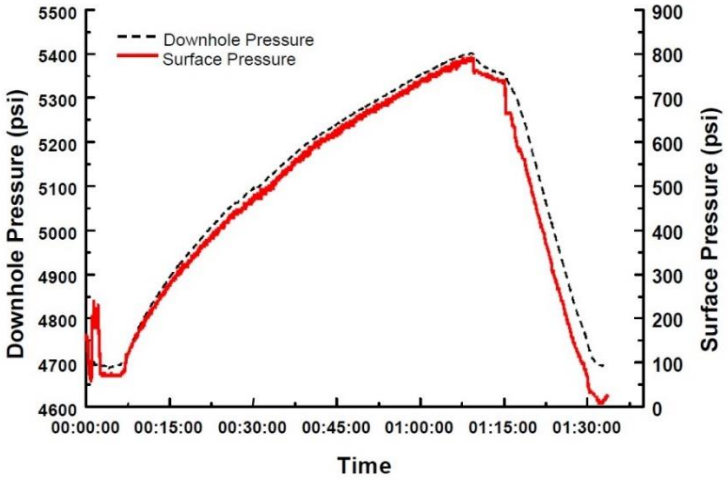

Figure 2.28 Auger FIT surface vs. downhole pressure (Rezmer-Cooper, 2000)

After calculating the EMWs based on both surface and downhole pressure measurements, it was concluded that the EMW resulting from surface measurement is 12.7

ppg whereas the EMW derived from downhole measurement is 12.9 ppg (Rezmer-Cooper, 2000). The difference 0.2 ppg may seem insignificant, but it is unacceptable in drilling deepwater wells with tight margins.

Although Rezmer-Cooper attributed most of the difference in surface and downhole measurement to mud compressibility effect, van Oort (2007) suggested that mud gel strength effect can also help to explain the difference:

The equation to estimate the change in pressure due to mud gelation is:

$$\Delta P_{gel} = \frac{L_{mud} \times G_{10\,\min}}{300 \times (D_o - D_i)} \tag{2.1}$$

Where,

ΔP_{gel} = magnitude of mud gelation

L_{mud} = the length of the mud column

$G_{10\,\min}$ = the 10 min gel strength of the mud

D_o = outer diameter of the casing

D_i = inner diameter of annulus

Chapter 3 Previous LOT Models

3.1 ALTUN, G. (1999)

The Altun model was developed in 1999 to better analyze LOT results in formations that give non-linear relationships between the pumped volume and the observed pump pressure. This section discusses the sub-systems, the mathematic solutions, the volume predictions, and the deficiencies of the Altun LOT model.

3.1.1 Altun Model Sub-systems

The model consists of 4 sub-systems: fluid expansion, casing expansion, borehole expansion, and fluid leakage (filtration). The behavior of each sub-system is investigated independently and combined together to show the total system behavior. Figure 3.1 shows the sub-systems for the Altun model.

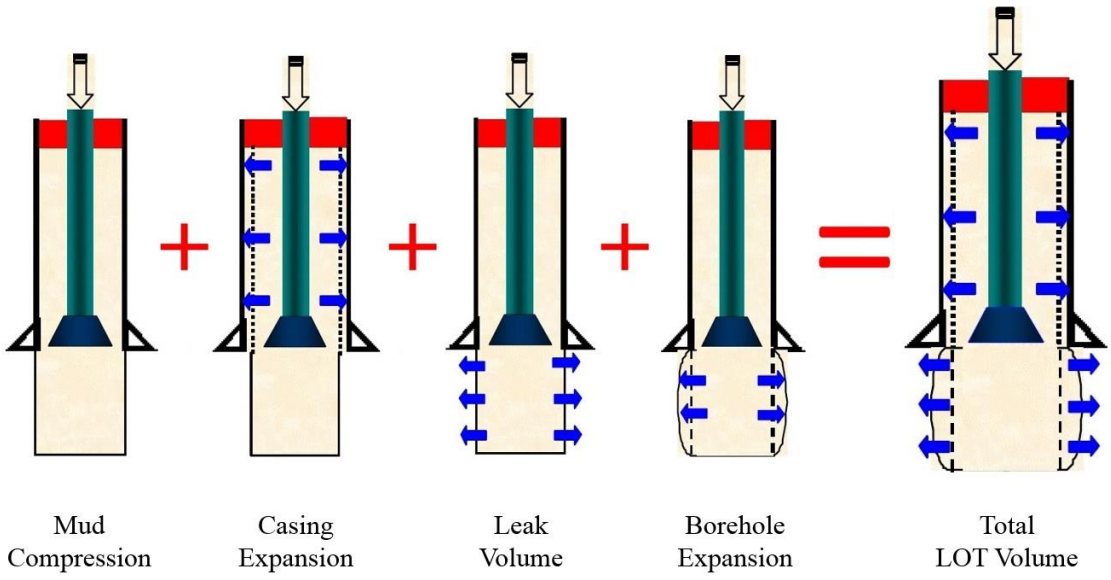

Figure 3.1 Altun model sub-systems (Modified after Altun, 2001)

3.1.2 Mathematic Solutions

The mathematic solutions to Altun's leak-off sub-systems are presented in this section.

3.1.2.1 Mud Compression (Altun, 2001)

The system boundary for fluid compression is assumed to be fixed throughout the LOT and the system would only allow drilling fluid compression in the well. The pumped volume to compress mud is then derived to be:

$$V_m = c_{mud} V_o P \tag{3.1}$$

Where,

V_m = volume to mud compression

c_{mud} = mud compressibility

V_o = original volume of mud in the system

P = pump pressure

3.1.2.2 Casing Expansion (Altun, 2001)

The volume required for the casing expansion system is further divided into the volume pumped to expand the casing and volume pumped to compress the casing expansion volume. Figure 3.2 shows the diagram for casing expansion.

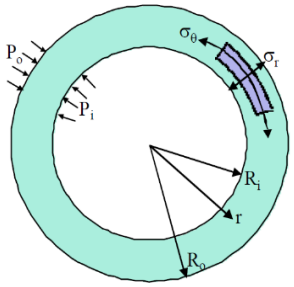

Figure 3.2 Casing expansion (Altun, 2001)

The equation for the volume pumped to expand the casing is:

$$V_{ce} = 2\pi h_{csg} R_i^2 \frac{P}{E_{csg}} \left[-\frac{\left(R_o^2 + R_i^2\right)}{R_o^2 - R_i^2}(1-\nu^2) - (\nu + \nu^2) \right] \tag{3.2}$$

Where,

V_{ce} = volume pumped to expand casing

h_{csg} = length of the casing string

R_i = inner radius of the casing string

E_{csg} = casing Young's modulus

P = pump pressure

R_o = outer radius of the casing string

ν = casing Poisson's ratio

And the volume pumped to compress the casing expansion volume can be described as:

$$V_{cce} = 2\pi h_{csg} c_{mud} R_i^2 \frac{P^2}{E_{csg}} \left[-\frac{\left(R_o^2 + R_i^2\right)}{R_o^2 - R_i^2}(1-\nu^2) - (\nu + \nu^2) \right] \tag{3.3}$$

Where,

c_{mud} = compressibility of drilling mud

3.1.2.3 Borehole Expansion (Altun, 2001)

The system boundary for borehole expansion is not fixed. The overall system volume V_o changes with time during loading and increases to a new volume of $V_o + V_e$. The volume increment V_e is the volume increment or the variable volume of the system due to borehole expansion caused by pump pressure. Like the sub-system for casing expansion, the volume pumped for the borehole expansion system is also further divided into volume pumped to expand the borehole and volume pumped to compress the borehole expansion volume.

The volume pumped to expand the borehole is:

$$V_{be} = 2\pi h_{fmn} r_o^2 \left[\frac{P}{E_{fmn}} + \left(\frac{P}{E_{fmn}} \right)^2 \right] \tag{3.4}$$

And the volume pumped to compress the borehole expansion volume is:

$$V_{cbe} = 2\pi h_{fmn} r_o^2 c_{mud} P \left[\frac{P}{E_{fmn}} + \left(\frac{P}{E_{fmn}} \right)^2 \right] \tag{3.5}$$

Where,

V_{be} = volume pumped to expand the borehole

h_{fmn} = length of Openhole

r_o = radius of borehole

E_{fmn} = formation Young's Modulus

P = pump pressure

V_{cbe} = volume pumped to compress the borehole expansion volume

c_{mud} = mud compressibility

3.1.2.4 Leak Volume (Altun, 2001)

The leak volume in Altun's model is described using Poiseuille's flow in channels. The general relationship for the leak volume is given as:

$$V_l = D\Delta P t \tag{3.6}$$

Where,

V_l = leak volume

D = leak constant

ΔP = the pressure difference between the tip of the channel and the bottom of the channel

t = time

If the channel shape is assumed to have a rectangular shape, then the leak constant D becomes:

$$D = 8.7 \times 10^{9} \frac{W^{2} A_{x-s}}{\mu L} \tag{3.7}$$

Where,

W = channel width

A_{x-s} = cross-sectional area of the fracture

μ = mud viscosity

L = channel length

Then the volume pumped to compress the leak volume becomes:

$$V_{cl} = Dc_{mud} \Delta P t \tag{3.8}$$

Where,

V_{cl} = volume to compress leak volume

3.1.2.5 Altun Model Total System Solution

The total pumped volume is the sum of volumes for the 4 sub-systems and can be described as:

$$\text{Volume Pumped} = \begin{cases} \text{Volume to Compress Mud } (V_m) \\ + \\ \text{Volume to Expand Casing } (V_{ce}) \\ + \\ \text{Volume to Compress Casing Expansion Volume } (V_{cce}) \\ + \\ \text{Volume to Expand Borehole } (V_{be}) \\ + \\ \text{Volume to Compress Borehole Expansion Volume } (V_{cbe}) \\ + \\ \text{Volume to Leaks } (V_l) \\ + \\ \text{Volume to Compress Leaks Volume } (V_{cl}) \end{cases}$$

And the total system equation is:

$$
\begin{aligned}
V &= c_{mud} V_o P + 2\pi h_{csg} R_i^{\,2} \frac{P}{E}\left[-\frac{R_o^{\,2}+R_i^{\,2}}{R_o^{\,2}-R_i^{\,2}}(1-\nu^2)-(\nu+\nu^2)\right] \\
&+ c_{mud} P\left(\pi h_{csg} R_i^{\,2} \frac{P}{E_{csg}}\left[\frac{R_o^{\,2}+R_i^{\,2}}{R_o^{\,2}-R_i^{\,2}}(1-\nu^2)+(\nu+\nu^2)\right]\right)^2 \\
&+ 2\pi h_{fmn} r_o^2 \frac{P}{E_{fmn}}\left[1+\frac{P}{E_{fmn}}\right] + c_{mud} P\left[2\pi h_{fmn} r_o^2 \left(\frac{P}{E_{fmn}}\right)\left(1+\frac{P}{E_{fmn}}\right)\right] \\
&+ \left[c_{mud} V_o \left(\frac{D}{q}\right) P^2 + c_{mud} V_o \left(\frac{D}{q}\right)^2 P^3 + c_{mud} V_o \left(\frac{D}{q}\right)^3 P^4 + \ldots\right]
\end{aligned}
\tag{3.9}
$$

However, Altun concluded that the following types of volume are negligible: the volume to expand casing expansion volume, volume to expand borehole, volume to compress borehole expansion volume, and volume to compress leaks volume. Therefore, the total system behavior becomes:

$$
V = \frac{V_o\left(e^{c_{mud}P}-1\right)}{1-\frac{D}{q}P} + 2\pi h_{csg} R_i^{\,2} \frac{P}{E_{csg}}\left[\frac{R_o^{\,2}+R_i^{\,2}}{R_o^{\,2}-R_i^{\,2}}(1-\nu^2)-(\nu+\nu^2)\right] \tag{3.10}
$$

3.1.3 Results

Three wells were studied in Altun's published paper in 2001. Volumes are calculated from each of the sub-system described above and combined to predict the overall leak-off volume. The three tested wells are A-2 in GOM, U-2 in Montana, and U-3 in Trinidad respectively. Figure 3.3, Figure 3.4, and Figure 3.5 show the results from the Altun model for GOM A-2, Montana U-2, and Trinidad U-3.

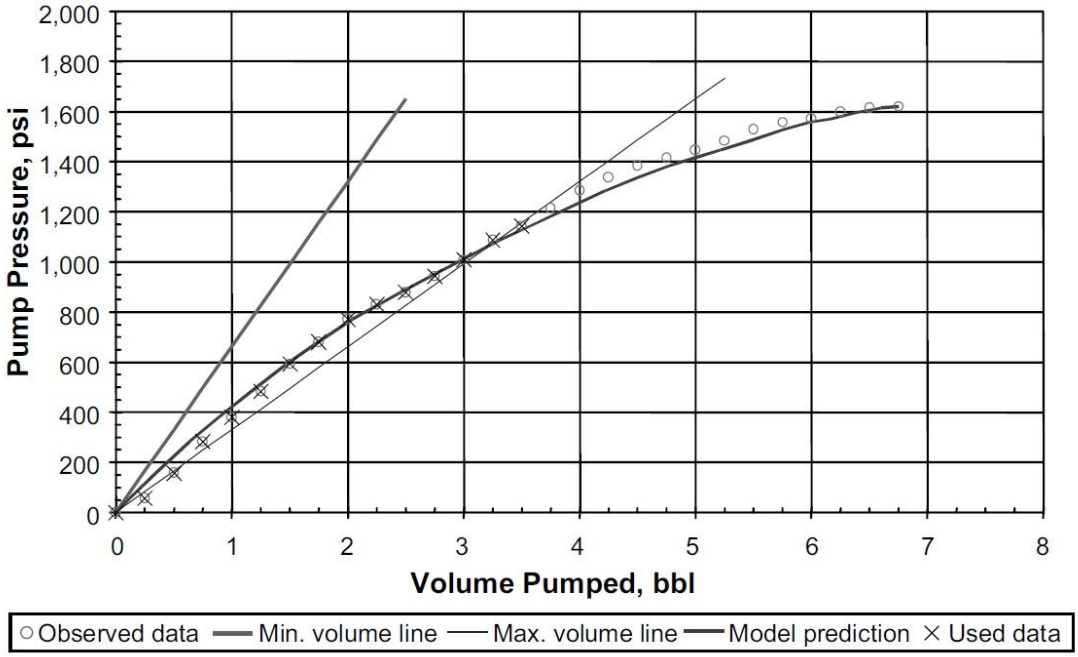

Figure 3.3 GOM U-2 Altun model results (Altun, 2001)

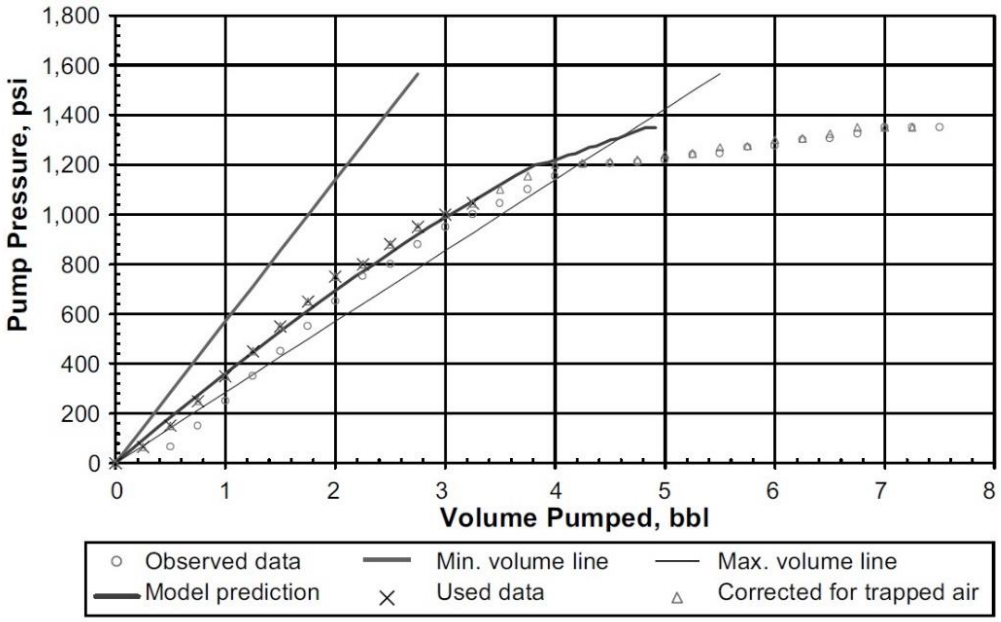

Figure 3.4 Montana U-2 Altun model results (Altun, 2001)

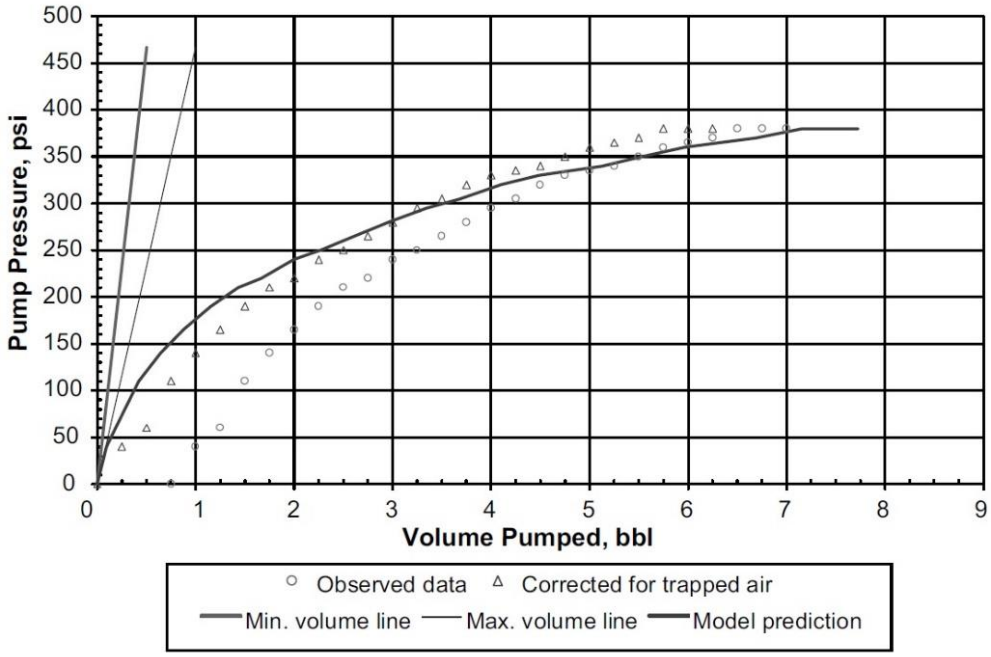

Figure 3.5 Trinidad U-3 Altun model results (Altun, 2001)

3.1.4 Deficiencies of Altun's LOT Model

Altun's LOT model considers the volumes generated by casing expansion, borehole expansion, fluid filtration, and mud compression. Upon close inspection of Altun's calculations, it was concluded that only pump pressure is used for all the sub-systems volume calculations. This means that all the calculations are solely based on the pressure inside the wellbore, not including the far field stresses. In reality, casing is bonded by layers of cement, other casing strings, and the formation rock. The behaviors of these layers were ignored in Altun's model.

Altun's leak model is based on Poiseuille's flow in channels. In the original reference, Craft and Hawkins (1991) stated that change in pressure should be defined by the pressure difference between the tip of the flow channel and the mouth of the crack. However, Altun did not account for the pressure difference in his calculations. In addition,

Altun assumed that the pre-existing crack has the length of 15 ft. With this length, the crack would have extended well beyond the near wellbore stress region. However, questions remain regarding the validity of this assumption because many believe that the cracks cannot extend that long during a LOT.

3.2 PAKNEJAD, A. (2007)

Paknejad presented a new method to evaluate LOT in shallow marine sediments in 2007. This section discusses Paknejad's LOT model.

3.2.1 Sub-systems

Paknejad's LOT model consists of two large components. The first component represents the volume change in a closed system, which consists of fluid compression, casing expansion, and open hole expansion. The second component is the fluid leakage to fractures assuming linear flow.

3.2.2 Mathematic Solutions (Paknejad, 2007)

Paknejad's mathematic solutions to fluid compression, casing expansion, and open hole expansion are identical to Altun's mathematic solutions. However, the fluid leakage model differs from Altun's and assumes linear flow through created fractures during a LOT, and it is described as:

$$\Delta P = \frac{4.064qB}{h_f x_f}\sqrt{\frac{\mu t}{k\phi c_t}} \tag{3.11}$$

Where,

ΔP = change in pressure

B = formation volume factor

h_f = fracture height

k = permeability

q = injection rate

t = time

x_f = fracture half length

3.2.3 Results

Six wells were studied in Paknejad's SPE paper in 2007. However, none of his model predictions were published. Instead, conventional Cartesian plots and log-log plots of non-linear LOT data were compared.

3.2.3 Deficiencies of Paknejad's Model

Because Paknejad's model follows Altun's casing expansion, borehole expansion, and mud compression models, the deficiencies for Altun's model also apply to Paknejad's model.

The fluid leakage term in Paknejad's model assumes linear flow through created fractures, and the equation is derived from hydraulic fracturing theories. Conventional hydraulic fracturing equations are derived based on elastic behavior of rocks. However, in shallow marine sediments, the applied stress loads cause the rocks to display plastic behavior rather than elastic behavior. Therefore, it is theoretically inconsistent to use conventional hydraulic fracturing theories to describe fracturing in shallow marine sediments.

Chapter 4 Wider Windows LOT Models

4.1 Concentric Cylinder Concept

The algorithm and derivations for the concentric cylinder concept has been developed by Norris (2013) and it is the basis for the software program Concyl. Both the algorithm and the software are authorized for use in the Wider Windows research program. The algorithm and derivation for single cylinder solution and multi-cylinder solution are presented in this section.

4.1.1 Single Cylinder Solution by Norris (2003)

The stress distribution for a single unconstrained thick-walled cylinder under pressure loading from both inside and outside is shown below. The linear solution to this problem is known as the Lame's equations. Figure 4.1 shows a single cylinder with external pressure and internal pressure.

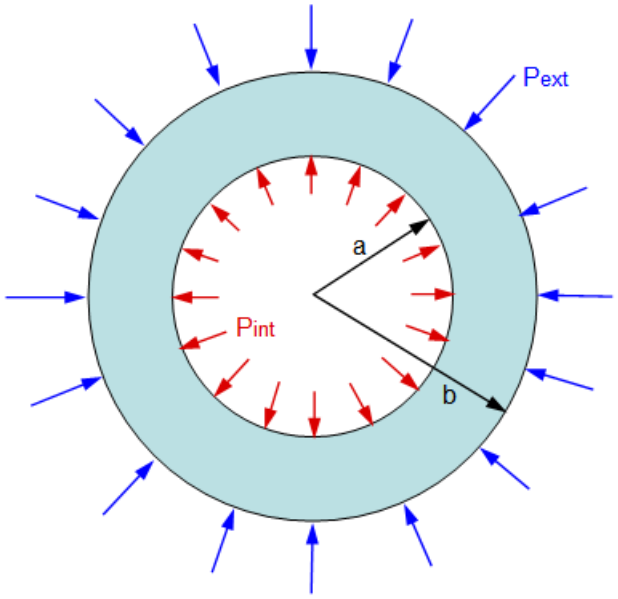

Figure 4.1 Single Cylinder Solution (Norris, 2003)

According to Lame's equations, the radial and hoop stresses at any radial location, r, are given by the following formulas:

$$\sigma_r = \frac{P_i a^2 - P_o b^2 - (P_i - P_o)(a^2 b^2 / r^2)}{b^2 - a^2} \tag{4.1}$$

$$\sigma_\theta = \frac{P_i a^2 - P_o b^2 + (P_i - P_o)(a^2 b^2 / r^2)}{b^2 - a^2} \tag{4.2}$$

Where,

σ_r = radial stress

σ_θ = hoop stress

a = inner radius of the cylinder

b = outer radius of the cylinder

P_i = internal pressure

P_o = external pressure

r = any radial location

And if the cylinder is fully or partially constrained axially then a uniform axial stress also develops which is given by:

$$\sigma_z = E\varepsilon_z + \nu(\sigma_r + \sigma_\theta) \tag{4.3}$$

Where,

ν = cylinder Poisson's ratio

σ_z = axial stress

ε_z = axial strain

E = cylinder Young's modulus

If the cylinder is unconstrained then Equation 4.3 equals to zero and the induced axial strain can be defined as:

$$\varepsilon_z = \frac{-\nu(\sigma_r + \sigma_\theta)}{E} \tag{4.4}$$

The linear strain displacement relations in polar coordinates for a generalized plain strain axisymmetric problem are:

$$\varepsilon_r = \frac{\partial u}{\partial r} \tag{4.5}$$

$$\varepsilon_r = \frac{u}{r} \tag{4.6}$$

$$\varepsilon_z = const. \tag{4.7}$$

$$\frac{\partial u}{\partial z} = \frac{\partial v}{\partial z} = \frac{\partial w}{\partial z} = 0 \tag{4.8}$$

$$\frac{\partial u}{\partial \theta} = \frac{\partial v}{\partial \theta} = \frac{\partial w}{\partial \theta} = 0 \tag{4.9}$$

Where,

ε_r = radial strain

u = radial deflection

v = hoop deflection

w = axial deflection

r = radial direction

θ = hoop direction

z = axial direction

The 3D constitutive relations for an isotropic Hookean material can be expressed as:

$$\varepsilon_r = \frac{1}{E}\left[\sigma_r - v\left(\sigma_\theta + \sigma_z\right)\right] + \alpha T \tag{4.10}$$

$$\varepsilon_\theta = \frac{1}{E}\left[\sigma_\theta - v\left(\sigma_r + \sigma_z\right)\right] + \alpha T \tag{4.11}$$

$$\varepsilon_z = \frac{1}{E}\left[\sigma_z - v\left(\sigma_r + \sigma_\theta\right)\right] + \alpha T \tag{4.12}$$

Where,

α = coefficient of thermal expansion

T = temperature difference relative to T_o

T_o = stress-free temperature

Equation 4.12 can be rearranged as

$$\sigma_z = E\varepsilon_z + v\left(\sigma_r + \sigma_\theta\right) - E\alpha T \tag{4.13}$$

The radial displacement can be expressed as:

$$u = r\varepsilon_\theta = \frac{1}{E}\left[\sigma_\theta - v\left(\sigma_r + \sigma_\theta\right)\right] + r\alpha T \tag{4.14}$$

$$u = \frac{r}{E}\left[\sigma_\theta\left(1-v^2\right) - v\sigma_r\left(1+v\right) - vE\varepsilon_z\right] + r\left(1+v\right)\alpha T \tag{4.15}$$

The radial displacements at the inner and outer surfaces of the cylinder are:

$$u_a = \frac{a}{E}\left\{\frac{2P_o b^2(v^2-1) + P_i\left[a^2\left(1-v-2v^2\right) + b^2\left(1+v\right)\right]}{b^2-a^2} - vE\varepsilon_z\right\} + a\left(1+v\right)\alpha T \tag{4.16}$$

$$u_b = \frac{b}{E}\left\{\frac{2P_i a^2(v^2-1) - P_o\left[b^2\left(1-v-2v^2\right) + a^2\left(1+v\right)\right]}{b^2-a^2} - vE\varepsilon_z\right\} + b\left(1+v\right)\alpha T \tag{4.17}$$

Where,

u_a = inner radial deflection

u_b =outer radial deflection

4.1.2 Multi-Cylinder Solution by Norris (2003)

Extension of the single cylinder solution to a system of concentric cylinders begins by enforcing the kinematic compatibility constraint at the interface between each cylinder. The outer radial deflection of any cylinder must equal the inner radial deflection of the cylinder that is bonded to its outer surface. This statement can be expressed in the following equation:

$$u_b{}^i = u_a{}^{i+1} \tag{4.18}$$

Where,

i=1:N-1

For each pair of bonded cylinders, *i* is the cylinder number, starting at 1 for the innermost cylinder and ending at *N* for the outermost cylinder. Figure 4.2 shows the cylinder and interface numbering scheme for a system of 5 cylinders.

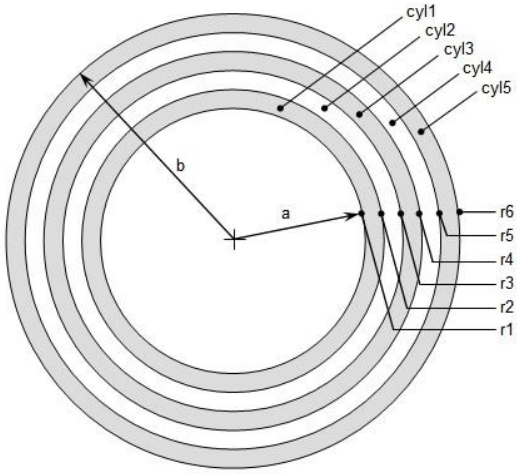

Figure 4.2 Multi-Cylinder System (Norris, 2003)

Consider a system with only two bonded cylinders. The interfaces will then be numbered from 1 to 3, and the cylinders numbered from 1 to 2. The system of cylinders can be represented with only 1 single equation. Substituting Equation 4.16 and 4.17 into Equation 4.18 and collecting similar terms, the resulting equation can be expressed in terms of:

$$Ap_1 + Bp_2 + Cp_3 = D \tag{4.19}$$

The subscripts denote the interface numbers. Since the interface pressures on interface 1 and 3 are known, only p_2 is unknown. Therefore, Equation 4.19 can be readily solved. The values of A, B, C, and D in Equation 4.19 are as follows:

$$A_i = \frac{2r_{i-1}^{\,2}\left(v^2_{\,i-1}-1\right)}{E_{i-1}\left(r_i^2 - r_{i-1}^{\,2}\right)} \tag{4.20}$$

$$B_i = \frac{r_i^2\left(1-v_i-2v_i^{\,2}\right)+r^2_{\,i+1}\left(1+v_i\right)}{E_i\left(r_{i+1}^{\,2}-r_i^{\,2}\right)} + \frac{r_i^2\left(1-v_{i-1}-2v_{i-1}^{\,2}\right)+r^2_{\,i-1}\left(1+v_{i-1}\right)}{E_{i-1}\left(r_i^2 - r_{i-1}^{\,2}\right)} \tag{4.21}$$

$$C_i = \frac{2r_{i+1}^{\,2}\left(v_i^{\,2}-1\right)}{E_i\left(r_{i+1}^{\,2}-r_i^2\right)} \tag{4.22}$$

$$D_i = (v_i - v_{i-1})\varepsilon_z + (1+v_{i-1})\alpha_{i-1}T_{i-1} - (1+v_i)\alpha_i T_i \tag{4.23}$$

with *i* ranging from 2 to *N*, where *N* is the total number of cylinders. The *i* subscript on the radius denotes the radial interface number, and the *i* on the material properties denotes the cylinder number.

Extending the solution to an arbitrary number of cylinders results in the following system of equations with one row for each interface:

$$\begin{bmatrix} 1 & 0 & 0 & 0 & 0 & 0 \\ A & B & C & 0 & 0 & 0 \\ 0 & A & B & C & 0 & 0 \\ 0 & 0 & A & B & C & 0 \\ 0 & 0 & 0 & A & B & C \\ 0 & 0 & 0 & 0 & 0 & 1 \end{bmatrix} \begin{bmatrix} p_1 \\ p_2 \\ p_3 \\ p_4 \\ p_5 \\ p_N \end{bmatrix} = \begin{bmatrix} D_1 = p_{\text{int}} \\ D_2 \\ D_3 \\ D_4 \\ D_5 \\ D_N = p_{ext} \end{bmatrix} \tag{4.24}$$

The first and last rows have the internal and external pressure boundary conditions. This system of equations can be solved using Gauss Elimination to obtain all of the unknown interface pressures between the cylinders. Once the interface pressures are solved, then they can be substituted back into Lame's Equation 4.15 to determine the corresponding radial displacements.

4.2 OBTAINED FIELD LOT DATA

Three sets of LOT data were digitized from Altun's published paper in 2001. Additional parameters were obtained from Altun's dissertation at Louisiana State University in 1999. The three LOTs were performed on offshore well U-1 in Alaska,

onshore well U-2 in Montana, and offshore well U-3 in Trinidad respectively. This section presents the digitized data and the additional parameters required for model calculations.

4.2.1 Digitized Well Data

Three LOT plots are obtained from Altun's dissertation and Altun's published paper. The plots are digitized and shown in this section.

4.2.1.1 Alaska U-1

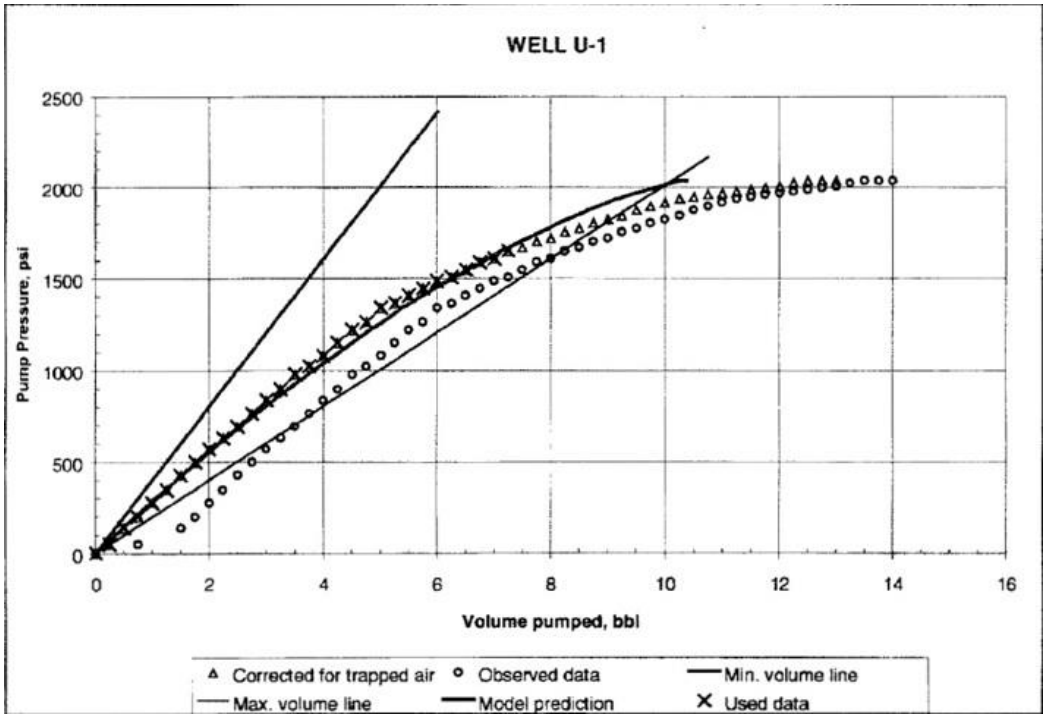

Figure 4.3 Original LOT Plot for Alaska U-1

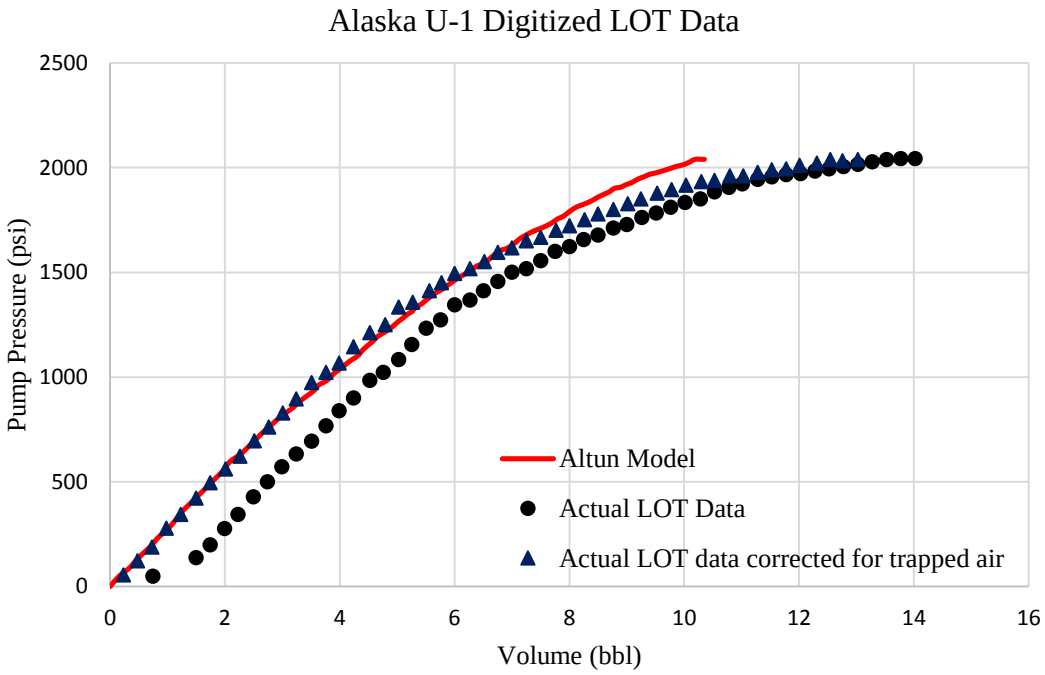

Figure 4.4 Digitized LOT Data for Alaska U-1

4.2.1.2 Montana U-2

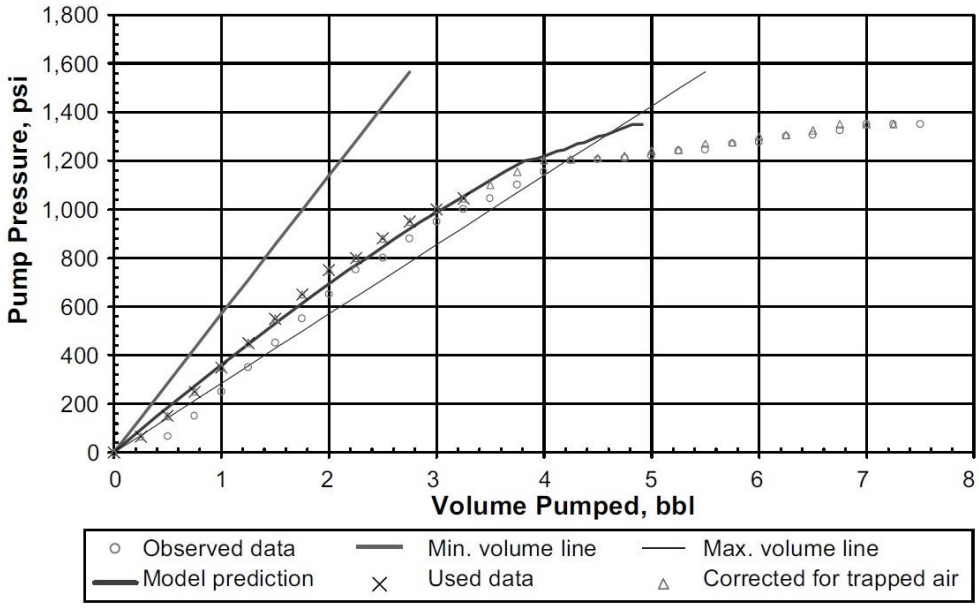

Figure 4.5 Original LOT Plot for Montana U-2

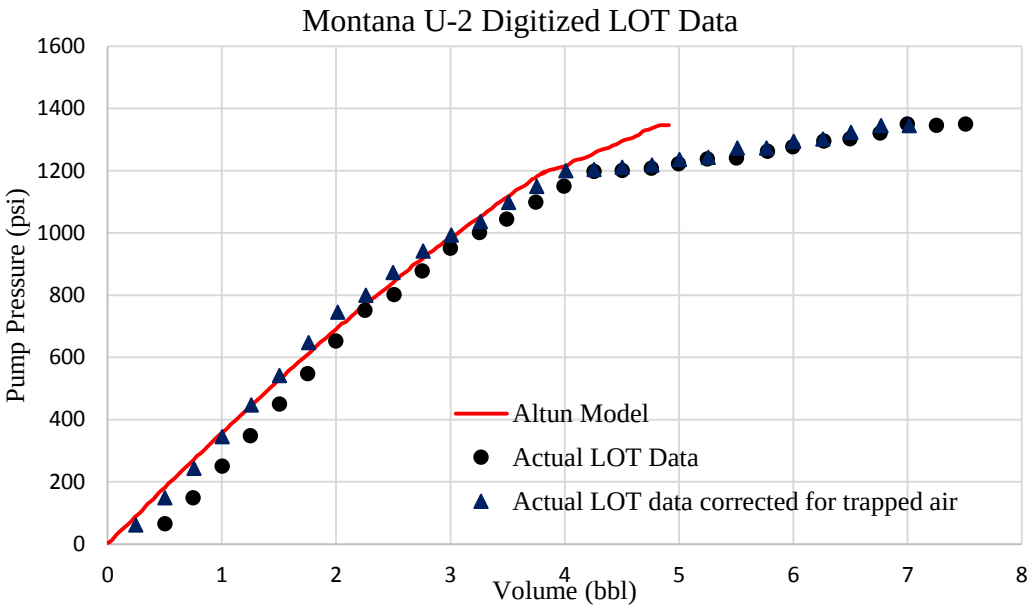

Figure 4.6 Digitized LOT Data for Montana U-2

4.2.1.3 Trinidad U-3

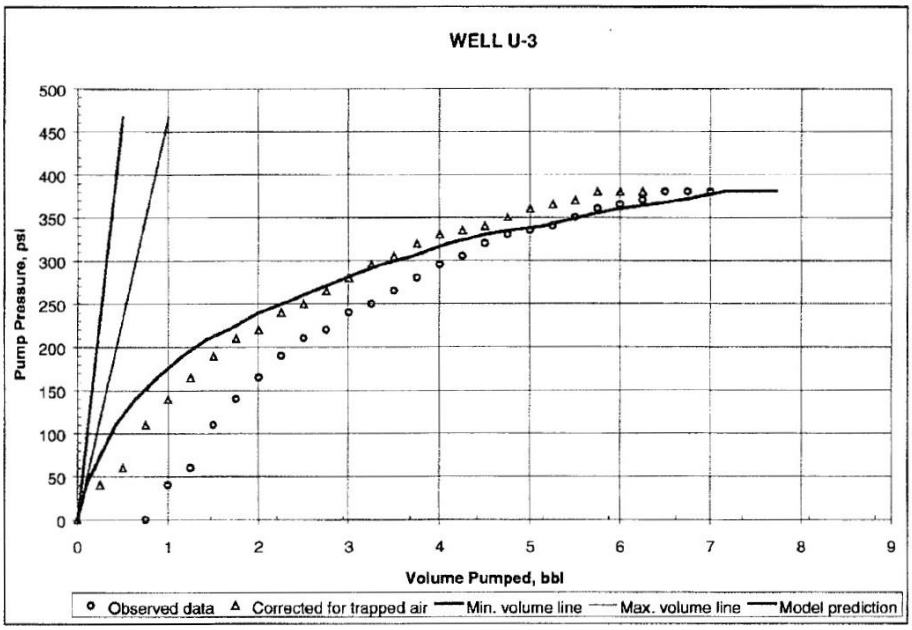

Figure 4.7 Original LOT Data for Trinidad U-3

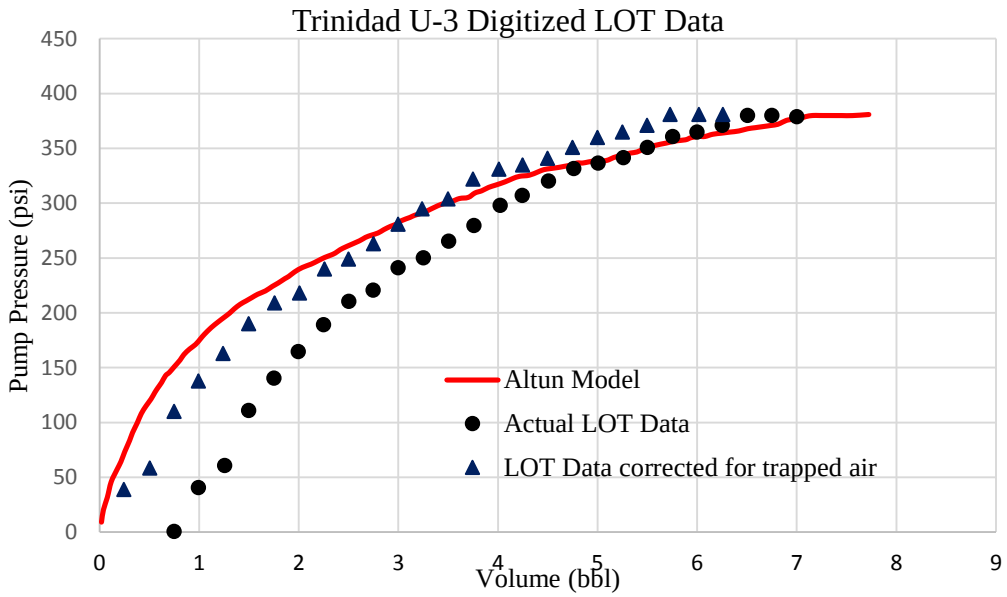

Figure 4.8 Digitized LOT Data for Trinidad U-3

4.2.2 Additional Parameters Obtained from Altun (1999)

Basic well data are obtained from Altun's dissertation and are shown in Table 4.1

Table 4.1 Basic well data (Altun, 1999)

Well ID	Date	Mud Weight (ppg)	Pump Rate (bpm)	Casing Size (in)	Water Depth (ft)	RKB
U-1	Dec-93	9.2	0.25	20	102	118
U-2	Nov-88	8.45	0.25	20	0	30*
U-3	N/A	8.8	0.25	20	196	86

*assumed

Additional Well data extracted from Altun's dissertation are shown in Table 4.2

Table 4.2 Additional well data (Altun, 1999)

Well ID	TVD Casing (ft)	Openhole Length (ft)	MD (ft)	TVD (ft)
U-1	5869	15*	5884	5884
U-2	1765	15*	1780	1780
U-3	1029	15*	1044	1044

*assumed

Some other input data that are necessary to implement the model were also extracted from Altun's dissertation and are shown in Table 4.3.

Table 4.3 Additional input data necessary to implement the model

Parameter	Value	Unit
Compressibility of water	3.00E-6	1/psi
Compressibility of oil	5.00E-6	1/psi
Casing Young's modulus	3.00E+7	1/psi
Mud viscosity	30*	cp
Channel Length	30*	ft
Channel length in lateral plane	1*	Fraction
Overburden gradient	1*	psi/ft

*assumed

The formation Young's modulus, mud compressibility, and other parameters related to leak volume calculations are also obtained from Altun's dissertation, shown in Table 4.4 and Table 4.5.

Table 4.4 Formation Young's Modulus and mud compressibility (Altun, 1999)

Well ID	Formation Young's Modulus (psi)	Mud Compressibility (1/psi)
U-1	1.14E+06	2.78E-06
U-2	8.51E+05	2.78E-06
U-3	6.40E+05	2.89E-06

Table 4.5 Parameters necessary to leak modeling (Altun, 1999)

Well ID	Wellbore Volume (bbl)	Equivalent Channel Width (in)	Equivalent Channel Area (sq in)	Leak Constant D
U-1	895	0.0136	0.5702	3.40E-05
U-2	632	0.0121	0.7529	3.50E-05
U-3	371	0.0333	2.0913	7.50E-04

Assumed data and other input parameters for concentric cylinder calculations are shown in Table 4.6.

Table 4.6 Assumed parameters necessary to implement the Wider Windows model

Parameter	Value	Unit
Casing Young's Modulus	3E+07	Psi
Casing Poisson's Ratio	0.3*	Fraction
Cement Young's Modulus	6E+06*	psi
Cement Poisson's Ratio	0.25*	Fraction
Formation Young's Modulus	Different for each well	psi
Formation Poisson's Ratio	0.3*	Fraction

*assumed

4.3 ALTUN MODEL WITH CEMENT SHEATH EXPANSION AND FORMATION EXPANSION

Previous LOT models by Altun (2001) and Paknejad (2007) do not include the expansion volume of the cement sheaths and formation rock outside of the casing. However, the additional volumes are not trivial and should not be neglected. This section discusses the sub-systems and mathematic solutions of the Altun model with consideration of cement and formation expansion.

4.3.1 Sub-systems

The enhanced Altun model consists of casing expansion, borehole expansion, mud compression, volume to leak (filtration), cement sheath expansion, and formation expansion. Therefore, the improved mathematic model becomes:

$$
\begin{aligned}
\text{Volume Pumped} = \Big[& \text{Volume to Compress Mud } (V_m) \\
& + \\
& \text{Volume to Expand Casing } (V_{ce}) \\
& + \\
& \text{Volume to Compress Casing Expansion Volume } (V_{cce}) \\
& + \\
& \text{Volume to Expand Borehole } (V_{be}) \\
& + \\
& \text{Volume to Compress Borehole Expansion Volume } (V_{cbe}) \\
& + \\
& \text{Volume to Leaks } (V_l) \\
& + \\
& \text{Volume to Compress Leaks Volume } (V_{cl}) \\
& + \\
& \textit{Volume to Cement Sheath} \\
& + \\
& \textit{Volume to Compress Cement Sheath Expansion Volume} \\
& + \\
& \textit{Volume to Expand Formation Rock} \\
& + \\
& \textit{Volume to Compress Formation Rock Expansion Volume} \Big]
\end{aligned}
$$

4.3.2 Mathematic Solutions

The mathematic solutions to the sub-systems of the enhanced Altun model are discussed in this section.

4.3.2.1 Casing Expansion by Altun (2001)

The mathematic solutions to the casing expansion system has been discussed in section 3.1.2.2. The equation for the volume pumped to expand the casing is:

$$V_{ce} = 2\pi h_{csg} R_i^2 \frac{P}{E_{csg}} \left[-\frac{\left(R_o^2 + R_i^2\right)}{R_o^2 - R_i^2}(1-v^2) - (v+v^2) \right] \tag{4.25}$$

and the volume pumped to compress the casing expansion volume is:

$$V_{cce} = 2\pi h_{csg} c_{mud} R_i^2 \frac{P^2}{E_{csg}} \left[-\frac{\left(R_o^2 + R_i^2\right)}{R_o^2 - R_i^2}(1-v^2) - (v+v^2) \right] \tag{4.26}$$

4.3.2.2 Borehole Expansion by Altun (2001)

The mathematic solution to the borehole expansion system has been discussed in section 3.1.2.3. The volume pumped to expand the borehole is:

$$V_{be} = 2\pi h_{\,fmn} r_o^2 \left[\frac{P}{E_{fmn}} + \left(\frac{P}{E_{fmn}} \right)^2 \right] \tag{4.27}$$

and the volume pumped to compress the borehole expansion volume is:

$$V_{cbe} = 2\pi h_{fmn} r_o^2 c_{mud} P \left[\frac{P}{E_{fmn}} + \left(\frac{P}{E_{fmn}} \right)^2 \right] \tag{4.28}$$

4.3.2.3 Mud Compression by Altun (2001)

The pumped volume to compress mud is given by:

$$V_m = c_{mud} V_o P \tag{4.29}$$

4.3.2.4 Volume to Leak by Altun (2001)

The leak volume in Altun's model is described using Poiseuille's flow in channels. The general relationship for the leak volume is given as:

$$V_l = D\Delta P t \tag{4.30}$$

Where,

D = leak constant

ΔP = the pressure difference between the tip of the channel and the bottom of the channel

t = time

If the channel shape is assumed to have a rectangular shape, then the leak constant D becomes:

$$D = 8.7 \times 10^9 \frac{W^2 A_{x-s}}{\mu L} \tag{4.31}$$

Where,

W = channel width

A_{x-s} = cross-sectional area of the fracture

μ = mud viscosity

L = channel length

The volume pumped to compress the leak volume becomes:

$$V_{cl} = Dc_{mud} \Delta P t \tag{4.32}$$

4.3.2.5 Cement Sheath Expansion

The cement expansion volume can be calculated using the single cylinder solution of the concentric cylinder theory. If only mechanical expansion is considered for a perfectly uniform cement sheath cylinder, under plain strain conditions, the radial displacement at the inner surface can be calculated as:

$$u_a = \frac{a}{E}\left\{\frac{2P_o b^2(v^2-1) + P_i\left[a^2\left(1-v-2v^2\right)+b^2\left(1+v\right)\right]}{b^2-a^2}\right\} \tag{4.33}$$

and the radial displacement at the outer surface can be obtained by:

$$u_b = \frac{b}{E}\left\{\frac{2P_i a^2(v^2-1) - P_o\left[b^2\left(1-v-2v^2\right)+a^2\left(1+v\right)\right]}{b^2-a^2}\right\} \tag{4.34}$$

The pressures acting on the inner and outer surfaces of the cement sheath can be obtained by solving the multi-cylinder concentric cylinder system using Gauss Elimination:

$$\begin{bmatrix} p_1 \\ p_2 \\ p_3 \\ p_4 \\ p_5 \\ p_N \end{bmatrix} = \begin{bmatrix} 1 & 0 & 0 & 0 & 0 & 0 \\ A & B & C & 0 & 0 & 0 \\ 0 & A & B & C & 0 & 0 \\ 0 & 0 & A & B & C & 0 \\ 0 & 0 & 0 & A & B & C \\ 0 & 0 & 0 & 0 & 0 & 1 \end{bmatrix}^{-1} \begin{bmatrix} D_1 = p_{\text{int}} \\ D_2 \\ D_3 \\ D_4 \\ D_5 \\ D_N = p_{ext} \end{bmatrix} \tag{4.35}$$

The incremental volume with respect to the radial displacement at the inner surface can then be readily calculated.

4.3.2.6 Formation Expansion

Similar to the cement sheath expansion calculation, the incremental volume due to formation expansion can also be obtained by calculating the radial displacement at the inner surface of the formation cylinder. Unlike the cement sheath cylinder with known outer radius, the outer radius of the formation cylinder is assumed to be the inner radius plus six times the wellbore radii. This is to insure that the stress acting on the outer surface of the formation cylinder is undistorted by the wellbore.

4.3.3 Results and Discussion

The results obtained from the enhanced Altun model are discussed in this section.

4.3.3.1 Displacement of Cement Cylinder and Formation Cylinder

The displacements at the inner surfaces of both the cement sheath cylinder and the formation rock cylinder are calculated based on the pressures acting on the interfaces. Figure 4.9, Figure 4.10, and Figure 4.11 show the displacements for Alaska U-1, Montana U-2, and Trinidad U-3, respectively.

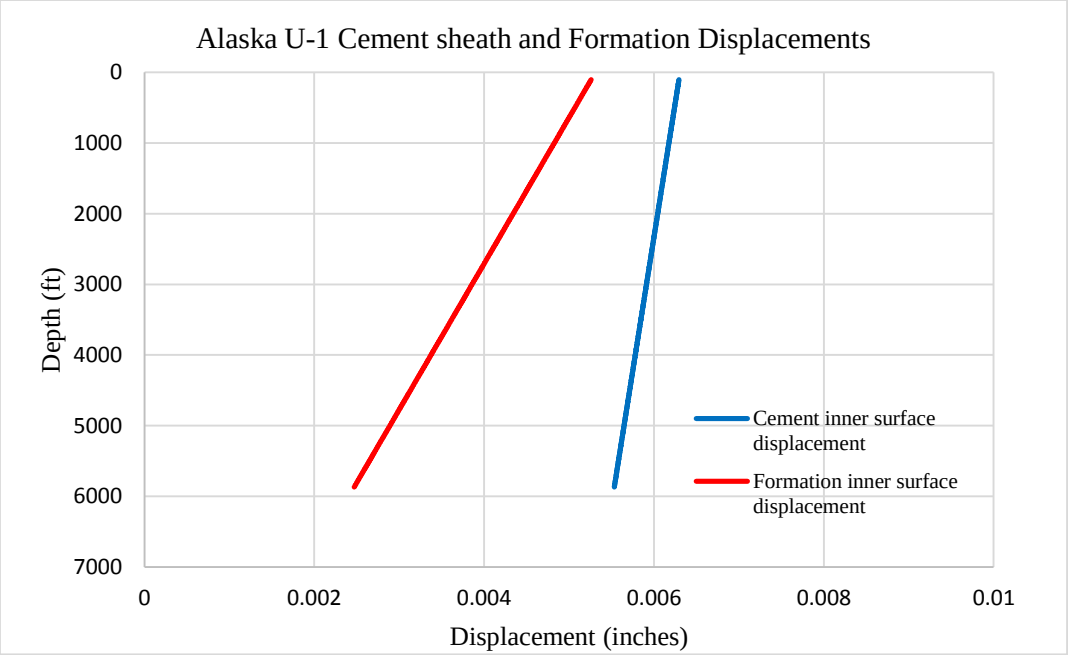

Figure 4.9 Alaska U-1 cement and formation displacements

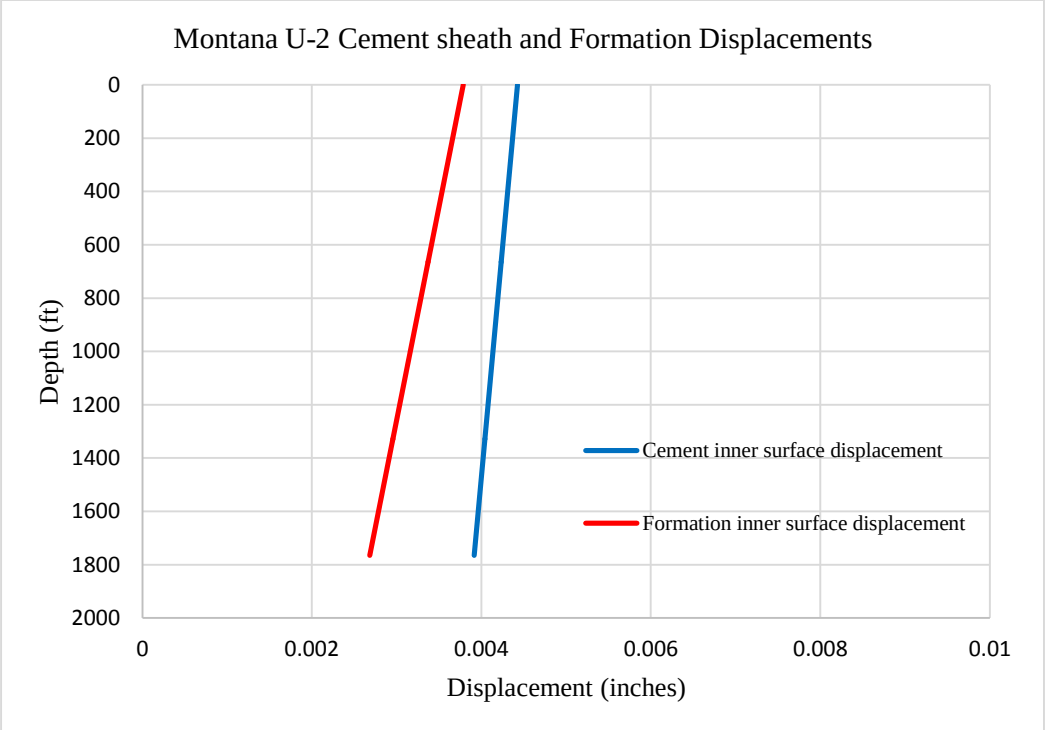

Figure 4.10 Montana U-2 cement and formation displacements

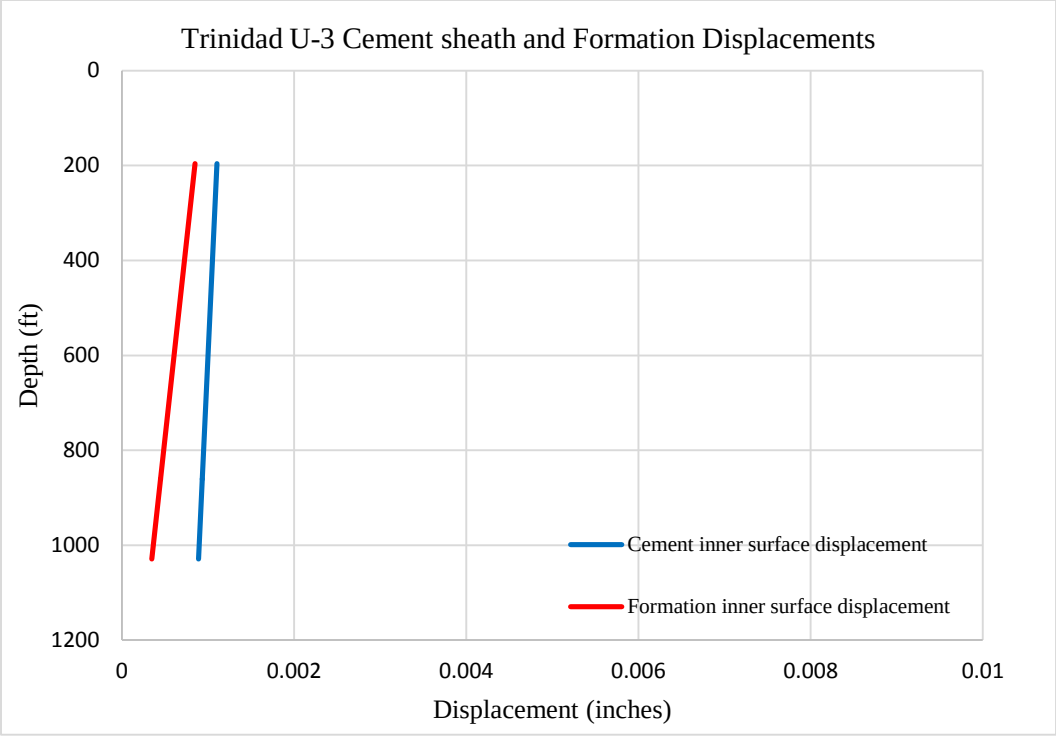

Figure 4.11 Trinidad U-3 cement and formation displacements

The above three plots show that displacement decreases as depth increases. In all three cases, the horizontal stress is assumed to be one-third of overburden. Therefore, as depth increases, the pressure inside the wellbore becomes less than the pressure acting from the outside. However, if the horizontal to vertical stress ratio changes, the displacement profile would change accordingly.

4.3.3.2 Volume Contributions of Each Sub-system

The volume contributions from sub-systems in the enhanced Altun model are calculated and plotted, the results are shown in Figure 4.12, Figure 4.13, and Figure 4.14.

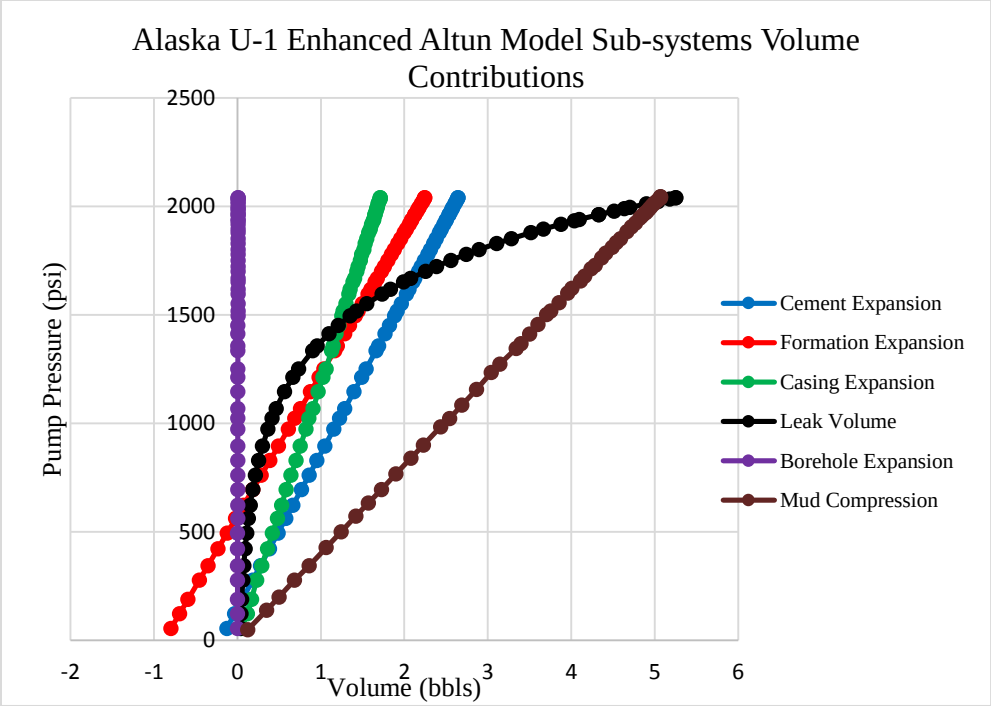

Figure 4.12 Alaska U-1 enhanced Altun model sub-systems volume contributions

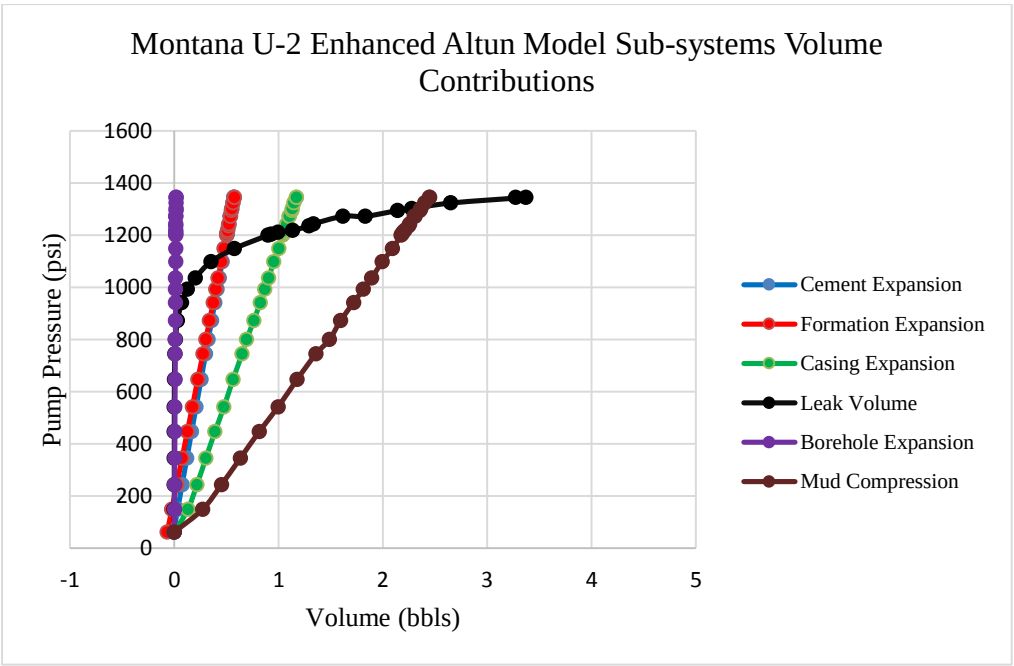

Figure 4.13 Montana U-2 enhanced Altun model sub-systems volume contributions

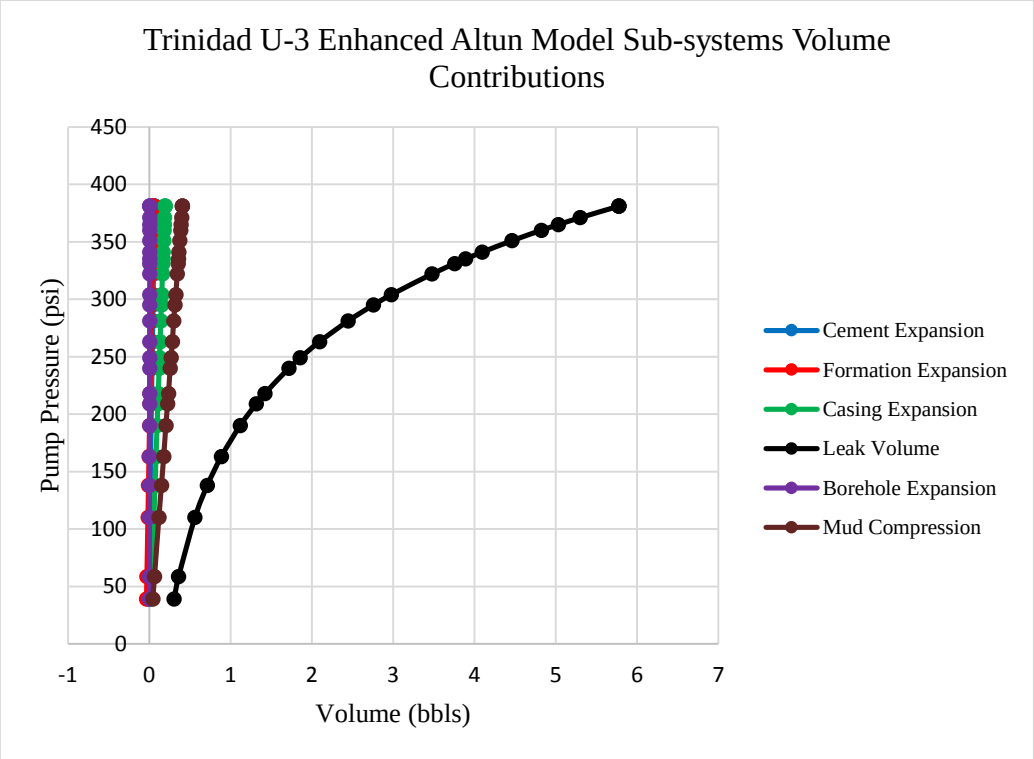

Figure 4.14 Trinidad U-3 enhanced Altun model sub-systems volume contributions

The sub-system volume contribution plots show that borehole expansion volumes are small in all three cases. Therefore, borehole expansion is neglected from total volume calculation. Figure 4.14 illustrates that leak volume dominates all other sub-systems from the beginning for Trinidad U-3. However, such dominance in volume contribution is not observed for the other two tested wells.

4.3.3.3 Combined Volume Results

The volume contributions from sub-systems in the enhanced Altun model are combined and plotted to compare with the actual LOT data. Figure 4.15, Figure 4.16, and Figure 4.17 show the results from Alaska U-1, Montana U-2, and Trinidad U-3, respectively.

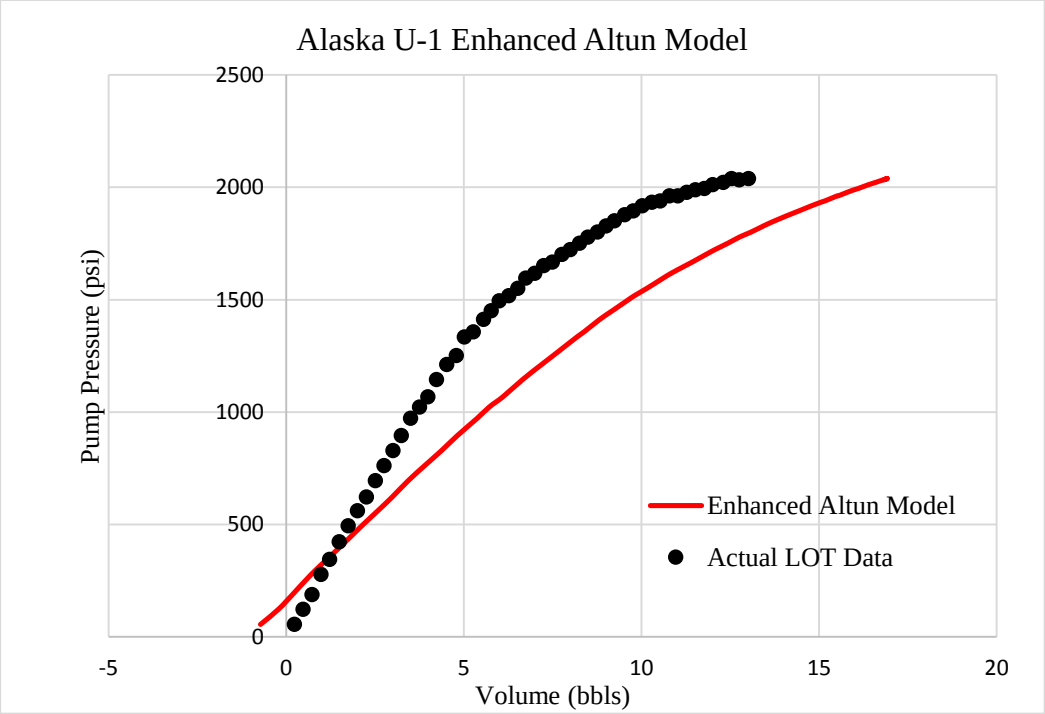

Figure 4.15 Alaska U-1 enhanced Altun model volume prediction

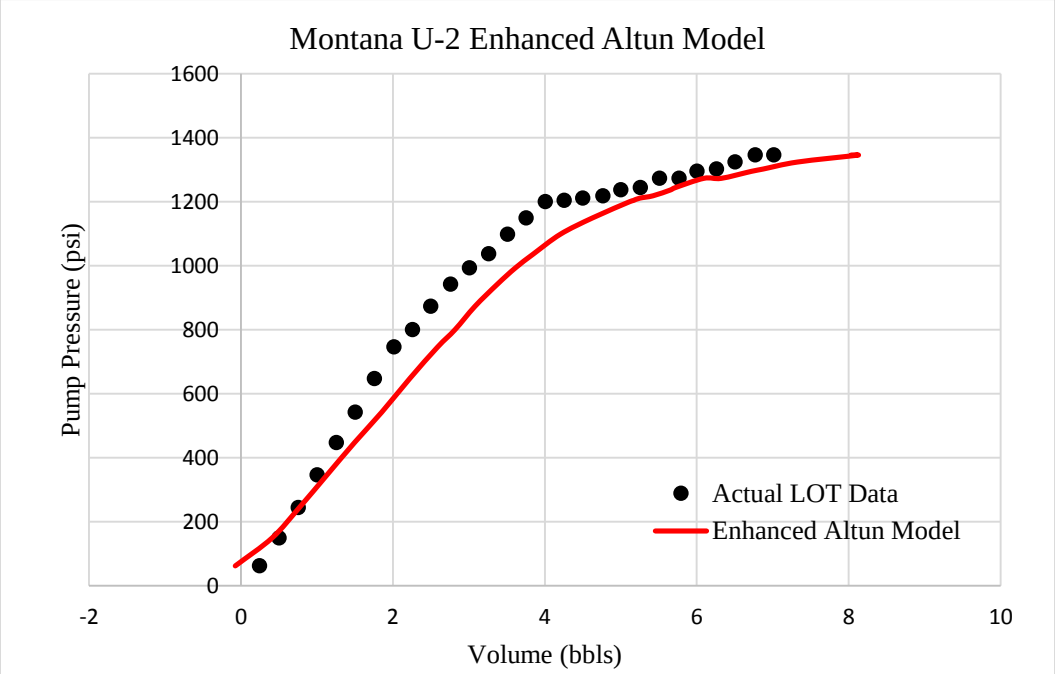

Figure 4.16 Montana U-2 enhanced Altun model volume prediction

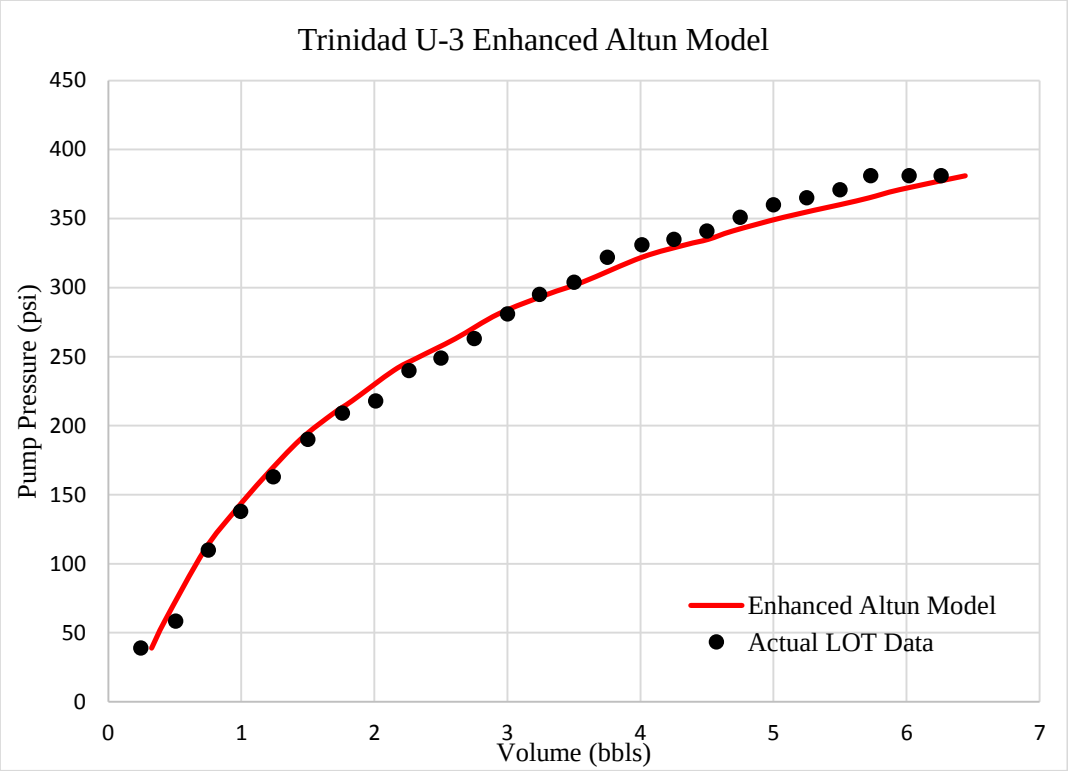

Figure 4.17 Trinidad U-3 enhanced Altun model volume prediction

All three figures above clearly show the trend in estimating LOT volume responses using the enhanced Altun model. Figure 4.15 and Figure 4.16 show that the model overestimates leak-off volumes for Alaska U-1 and Montana U-2. However, the model volume prediction provides good estimation for Trinidad U-3 because the leak volume makes up the majority of the total volume. Therefore the overall model prediction is significantly affected by the magnitude of leak volume and the shape of the leak sub-system.

4.3.3.4 Relative Error Analysis

The results from enhanced Altun model predictions are compared with the actual LOT data by calculating the absolute relative error at each data point. Figure 4.18, Figure 4.19, and Figure 4.20 show the results from Alaska U-1, Montana U-2, and Trinidad U-3, respectively.

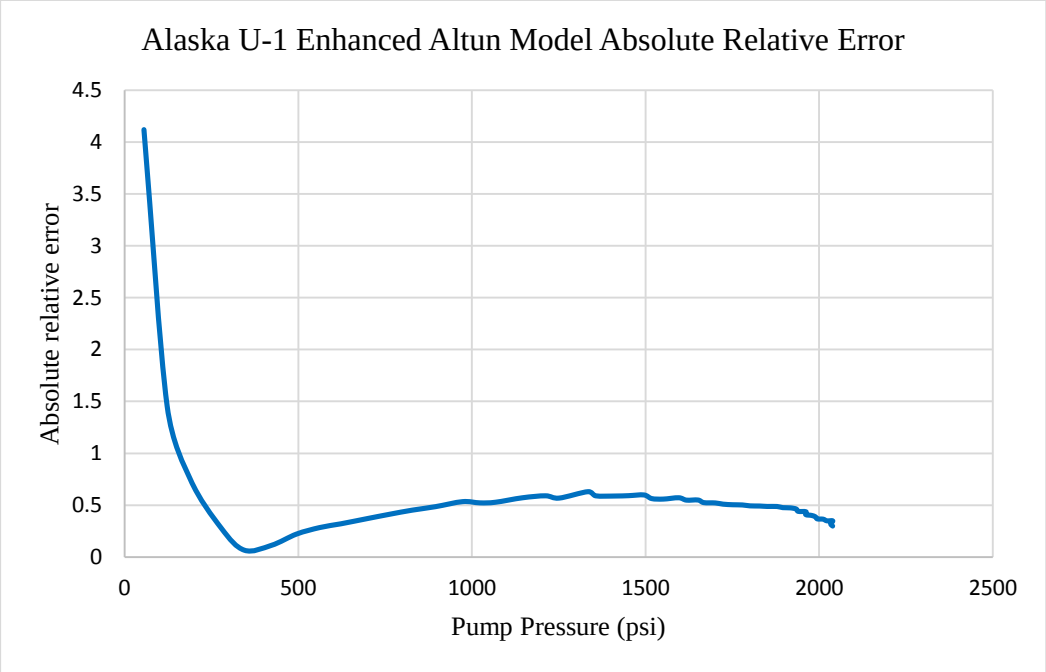

Figure 4.18 Alaska U-1 enhanced Altun model absolute relative error

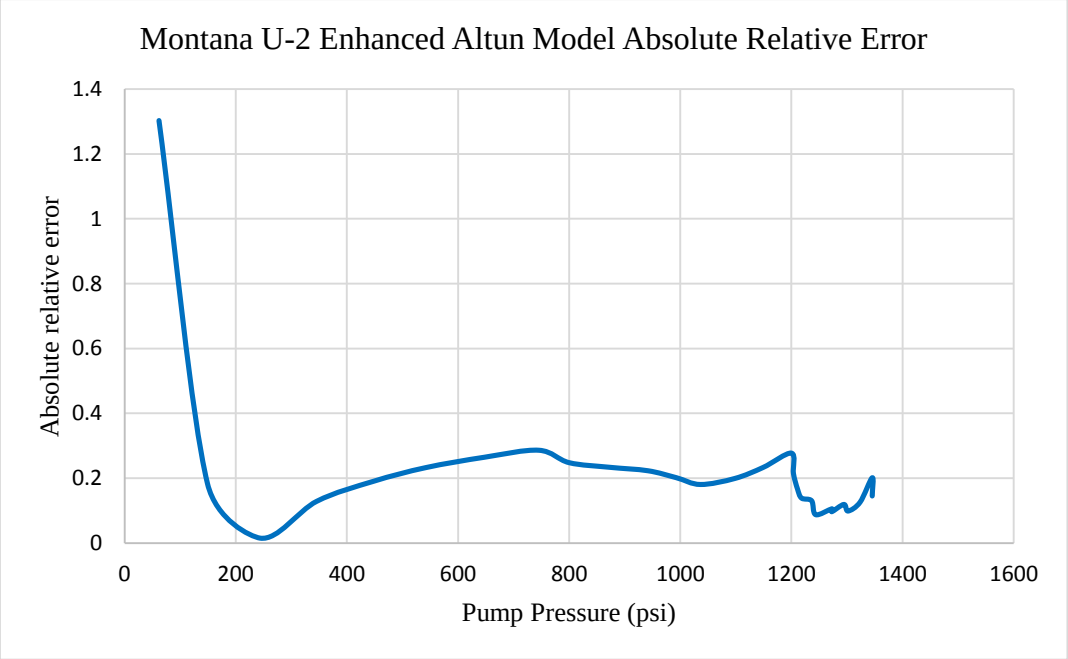

Figure 4.19 Montana U-2 enhanced Altun model absolute relative error

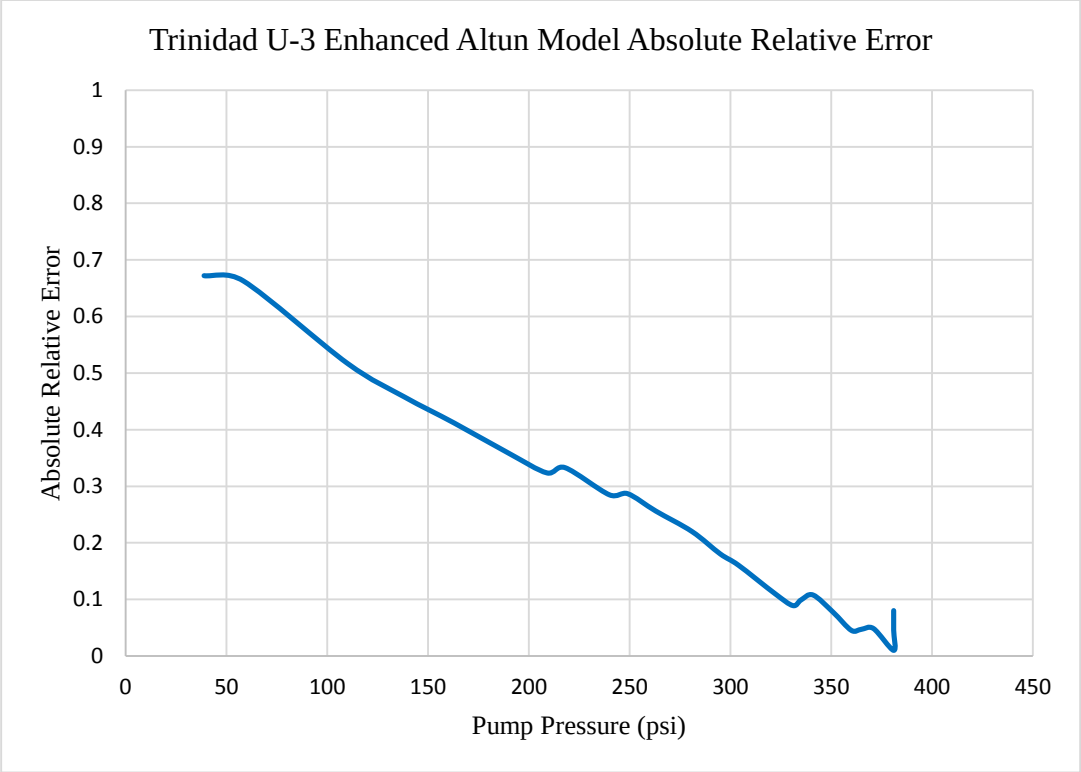

Figure 4.20 Trinidad U-3 enhanced Altun model absolute relative error

Figure 4.18 through Figure 4.20 illustrate that the enhanced Altun model generates a greater margin of error at low pump rate. However, the error tends to decrease as pump pressure increases. For Alaska U-1 and Montana U-2, the error drops rapidly within 200 psi of pump pressure increase. Table 3.1 shows the magnitude of average absolute relative errors and the standard deviations for all three cases. A decreasing trend in average error can be observed as the length of casing under loading decreases.

Table 4.7 Average absolute relative error for enhanced Altun Model

Well ID	Casing length (ft)	Average absolute relative error %	Standard deviation
Alaska U-1	5767	54.80	0.539
Montana U-2	1765	21.53	0.22
Trinidad U-3	833	7.39	0.06

4.4 WIDER WINDOWS MECHANICAL EXPANSION MODEL

Two LOT models are developed based on the concentric cylinder theory developed by Norris (2003). The first Wider Windows (WW) model considers the compounded expansion effect of the 20" casing, cement sheath, and formation rock without the influence of the conductor casing. The second model is also based on concentric cylinder theory and assumes that a conductor casing is placed outside of the 20" surface casing. Because the conductor casing sizes and shoe depths are not provided, the conductor casing is assumed to be 36" and the casing shoes are placed between 100 ft to 600 ft TVD/MD. The results from two wider windows models are presented in this section.

4.4.1 Sub-systems

Wider Windows mechanical expansion model utilizes the multi-cylinder solution developed by Norris (2003) to calculate the incremental volume generated from the combined effect of casing, cement sheath, and formation rock expansion along the cased hole. The calculated volume is then added with volume from the leak model and volume from the borehole expansion model developed by Altun (2001). The combined effect can be summarized as:

$$
\begin{aligned}
\text{Volume Pumped} = \Big[& \text{Volume to Expand Casing } (V_{ce}) \\
& + \\
& \text{Volume to Compress Casing Expansion Volume } (V_{cce}) \\
& + \\
& \text{Volume to Cement Sheath} \\
& + \\
& \text{Volume to Compress Cement Sheath Expansion Volume} \\
& + \\
& \text{Volume to Expand Formation Rock} \\
& + \\
& \text{Volume to Compress Formation Rock Expansion Volume} \Big] \quad \text{Volume to Concentric Cylinders} \\
& + \\
& \text{Volume to Compress Mud } (V_m) \\
& + \\
& \text{Volume to Expand Borehole } (V_{be}) \\
& + \\
& \text{Volume to Compress Borehole Expansion Volume } (V_{cbe}) \\
& + \\
& \text{Volume to Leaks } (V_l) \\
& + \\
& \text{Volume to Compress Leaks Volume } (V_{cl})
\end{aligned}
$$

4.4.2 Mathematic Solutions

The mathematic solutions to the sub-systems of the wider windows model are discussed in this section.

4.4.2.1 Volume to Concentric Cylinders

The volume to centric cylinders can be modeled by the multi-cylinder solution developed by Norris (2003). Unlike the enhanced Altun model, the WW model calculates the incremental volume based on a compounded effect of casing, cement, and formation rock expansion because many layers of concentric cylinders can exist in oil wells.

The algorithm to calculate the incremental volume generated by concentric cylinders are as follows:

1. Recognize layers of concentric layers from wellbore schematic drawings

2. Identify radius profile for each concentric cylinder

3. Calculate interface pressure profiles for each of the concentric cylinder layer

4. Calculate inner surface displacement for the innermost cylinder (usually casing)

5. Calculate incremental volume resulted from each of the concentric cylinder layer

4.4.2.2 Mud Compression by Altun (2001)

The mud compression calculation is identical Altun's calculation. The equation to calculate pumped mud volume to compress mud is given in section 4.3.2.3.

4.4.2.3 Borehole Expansion by Altun (2001)

The borehole expansion model is also identical to the borehole expansion model described in section 4.3.2.2

4.4.2.4 Volume to Leak by Altun (2001)

The leak volume model is identical to the leak volume developed by Altun (2001), the equations can be found in section 4.3.2.4.

4.4.3 Wider Windows Mechanical Expansion Model without Conductor

In this study, the concentric cylinder system consists of the 20" casing, the cement sheath, and the formation rock. Therefore, there are three cylinders for each of the tested wells included in this study.

4.4.3.1 Displacement

The displacement at the inner surface of the 20" casing is calculated based on the interface pressures obtained from the multi-cylinder solution. The results are shown in Figure 4.21, Figure 4.22, and Figure 4.23.

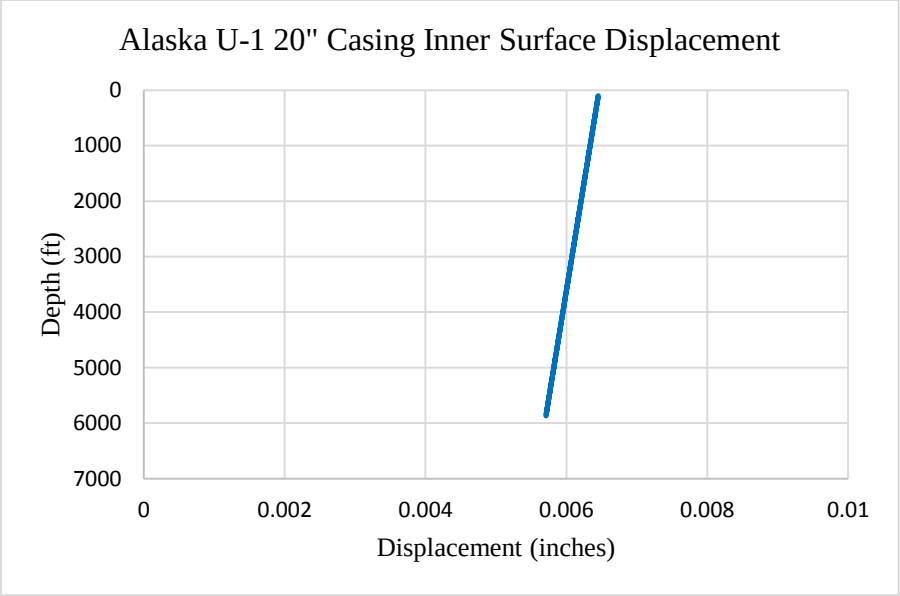

Figure 4.21 Alaska U-1 20” casing inner surface displacement

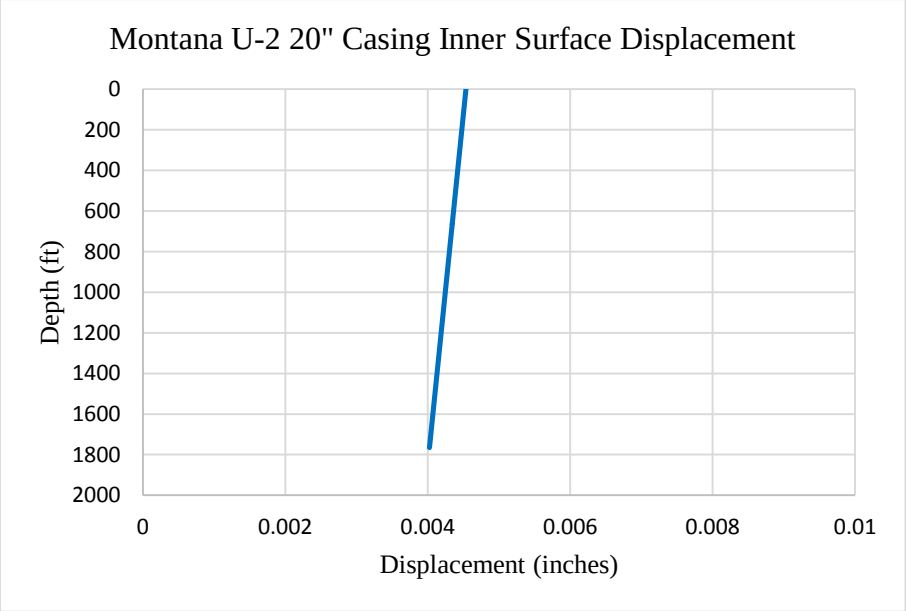

Figure 4.22 Montana U-2 20” casing inner surface displacement

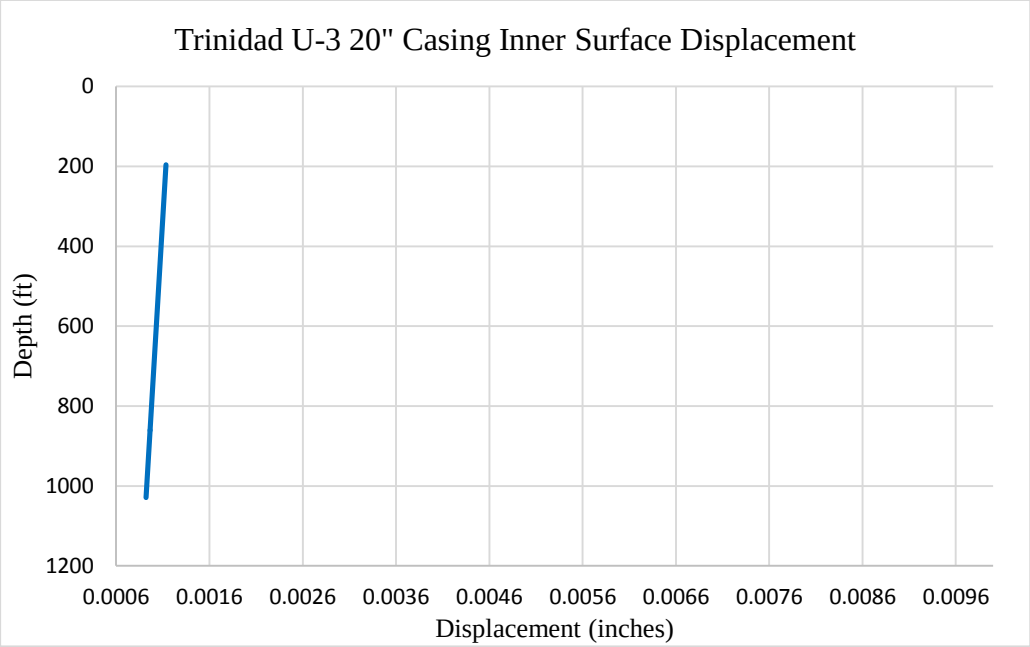

Figure 4.23 Trinidad U-3 20" casing inner surface displacement

The above graphs show that the displacement of Alaska U-1 is larger than that of the Montana U-2. Also, the displacement of Montana U-2 is larger than that of Trinidad U-3. The findings are consistent with Figures 4.9 through 4.11.

4.4.3.2 Volume Contributions of each sub-system

The volume produced by concentric cylinder expansion is calculated based on displacement shown in the previous section and plotted together with volume due to leak effect, borehole expansion, and mud compression. The results are shown in Figure 4.24 through 4.26.

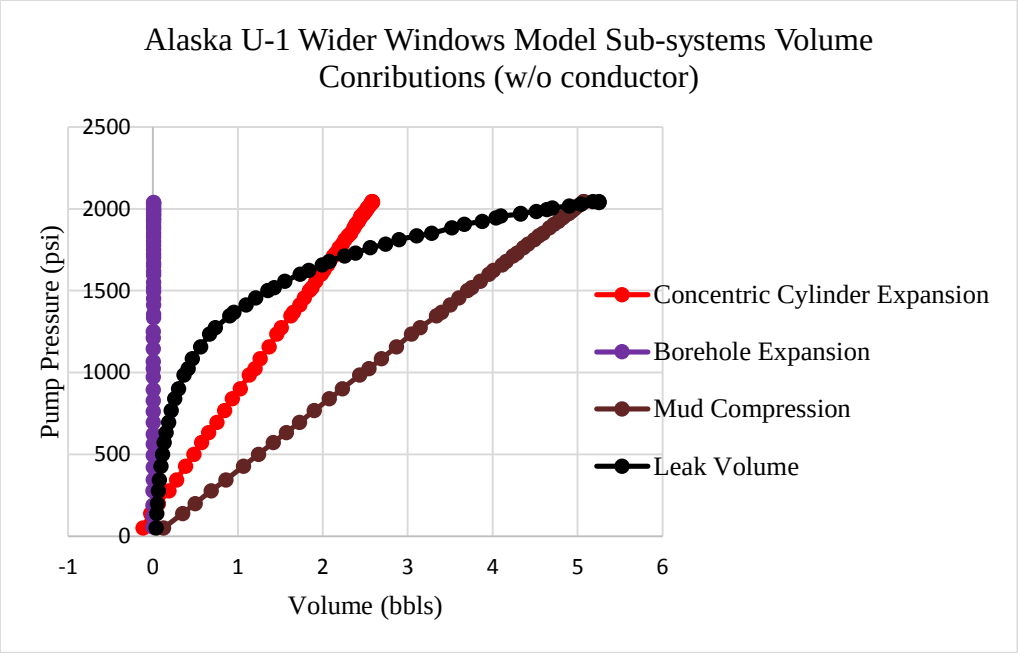

Figure 4.24 Alaska U-1 Wider Windows model sub-systems volume contributions

Figure 4.24 shows that all sub-systems generate significant volumes except borehole expansion. Mud compression dominates for the majority of the LOT.

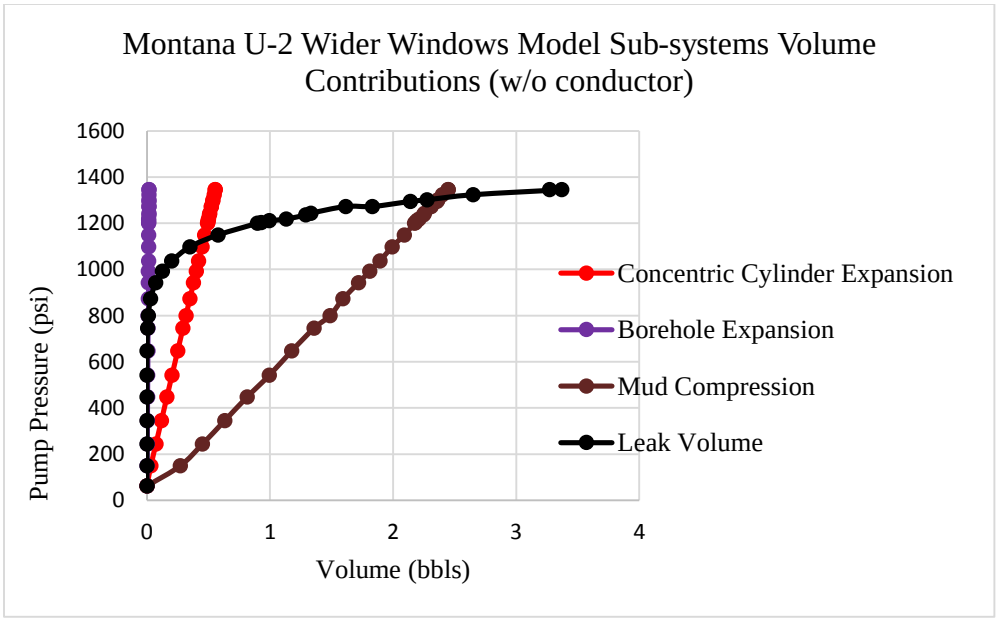

Figure 4.25 Montana U-2 Wider Windows model sub-systems volume contributions

Compared to Alaska U-1, the volume contribution from concentric cylinder is greatly reduced because the length of casing is shortened. Due the length of the well, mud compression still makes up majority of the leak-off volume until it is surpassed by leakage at near 1300 psi.

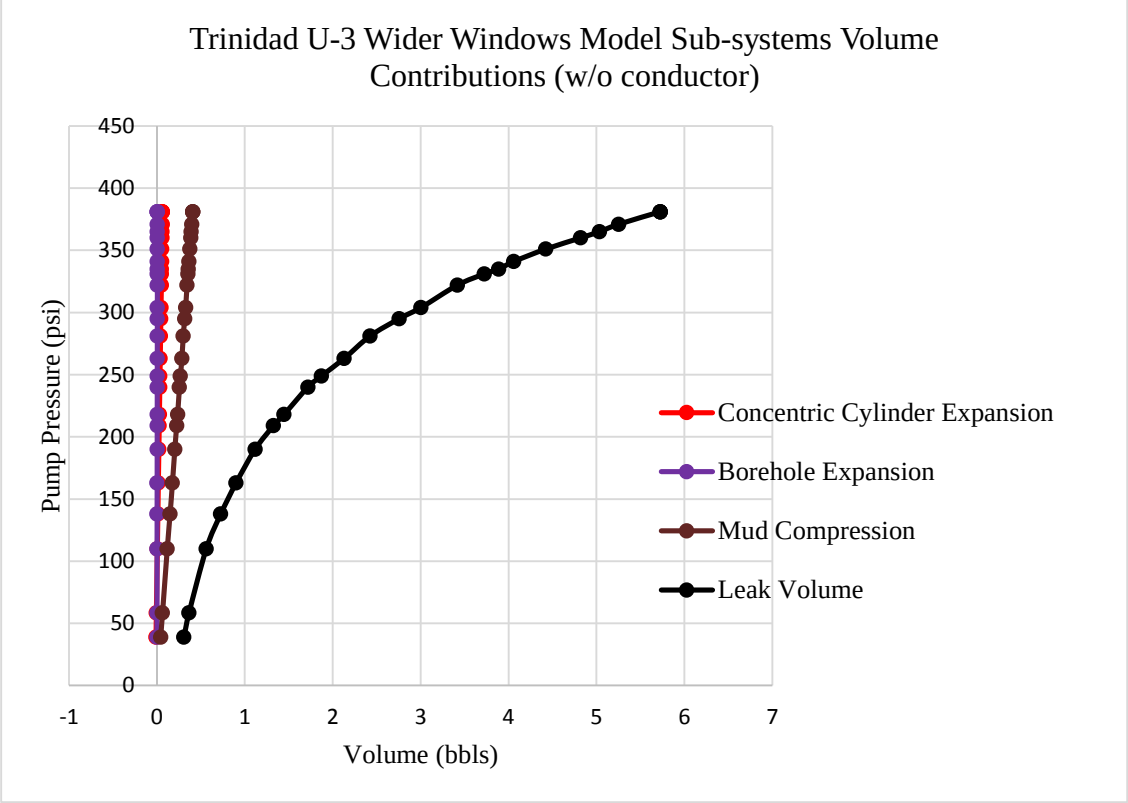

Figure 4.26 Trinidad U-3 Wider Windows model sub-systems volume contributions

Figure 4.26 illustrates that the leak volume dominates throughout the LOT, this observation is consistent with Figure 4.14. Volumes generated by the other systems only account for a small amount in total volume behavior for Trinidad U-3.

4.4.3.3 Total Volume

The volumes from concentric cylinder expansion, mud compression, and leak volume are combined and plotted to compare with the actual LOT data. The total volumes

predicted for Alaska U-1, Montana U-2, and Trinidad U-3 are shown in Figure 4.27, Figure 4.28, and Figure 4.29 respectively.

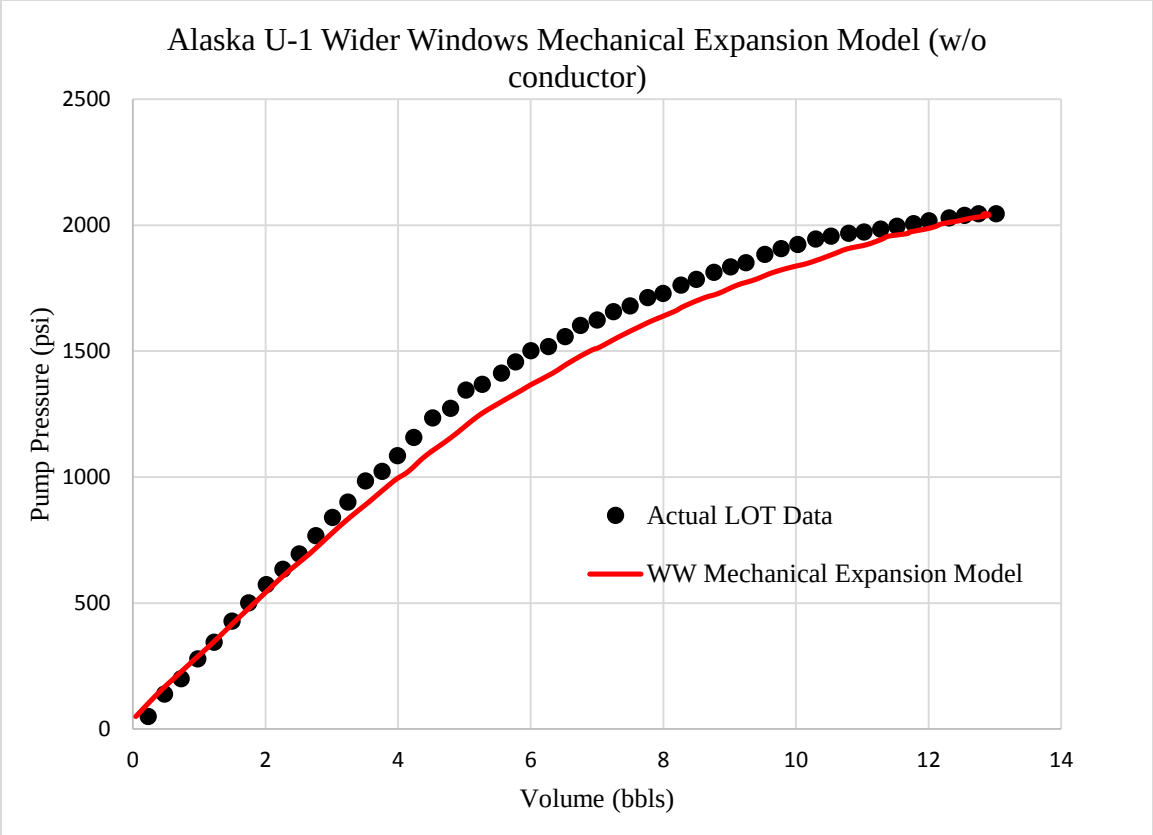

Figure 4.27 Alaska U-1 Wider Windows mechanical model volume prediction

Figure 4.27 reflects that the WW model provides good volume predictions from the beginning to approximately 750 psi of pump pressure. As pressure exceeds 750 psi, the WW model slightly overestimates leak-off volume. However, the difference between model prediction and the actual leak-off volume decreases toward the end of the LOT. As pump pressure passes 2000 psi, the difference becomes less than 0.2 barrels.

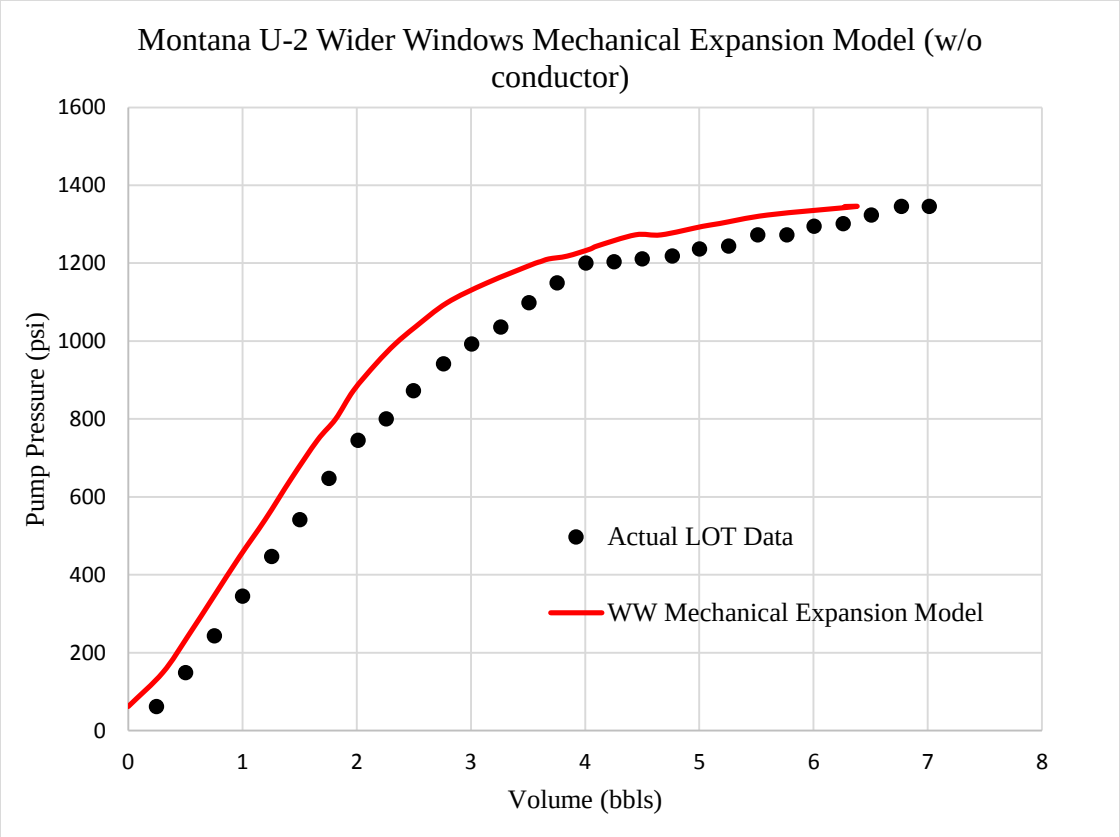

Figure 4.28 Montana U-2 Wider Windows mechanical model volume prediction

For Montana U-2, WW model underestimates leak-off volume throughout the LOT. The difference between actual LOT data and model prediction is approximately 0.2-0.25 barrels from the beginning to 400 psi. The gap widens from 400 psi to 1200 psi with the largest difference near 0.7-0.9 barrels at 1000 psi. The difference decreases after pump pressure surpasses 1200 psi.

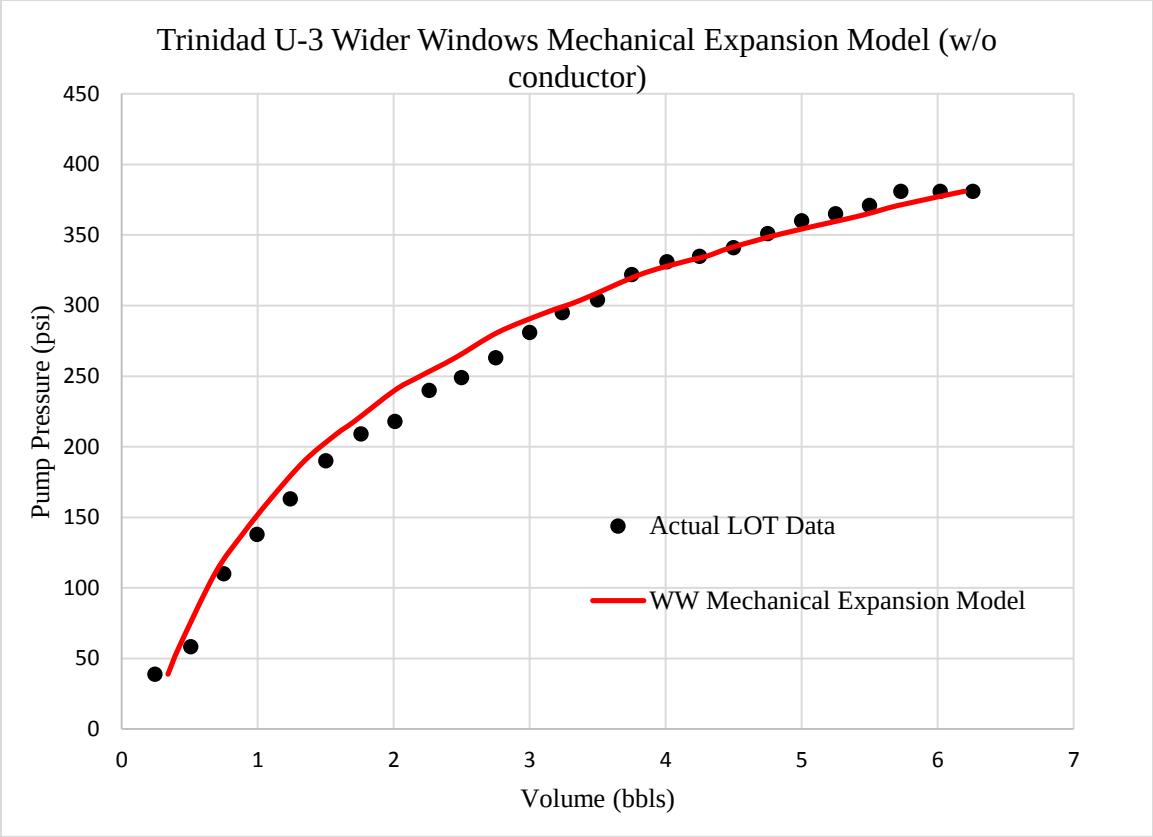

Figure 4.29 Trinidad U-3 Wider Windows mechanical model volume prediction

For Trinidad U-3, WW model provides excellent predictions of leak-off behavior overall. The model slightly underestimates leak-off volume from the beginning to approximately 300 psi. After 350 psi pump pressure, model prediction slightly over estimates leak-off volume. However, the largest difference between model prediction and actual LOT data is only about 0.1-0.2 barrels throughout the entire LOT.

4.4.3.4 Sub-systems Volume Contributions as Percentages of Total Volume

The overall shape of the LOT can be explained by the sub-system volume contributions. When the non-linearly behaved system (leakage) contributes little to the overall leak-off volume, the LOT plot tends to demonstrate a linear trend between pump pressure and pumped volume. However, when the leakage volume becomes significant,

the overall LOT tends to exhibit non-linear behaviors. Figure 4.30, Figure 4.31, and Figure 4.32 show the sub-systems volume contributions plotted as percentages of total volume.

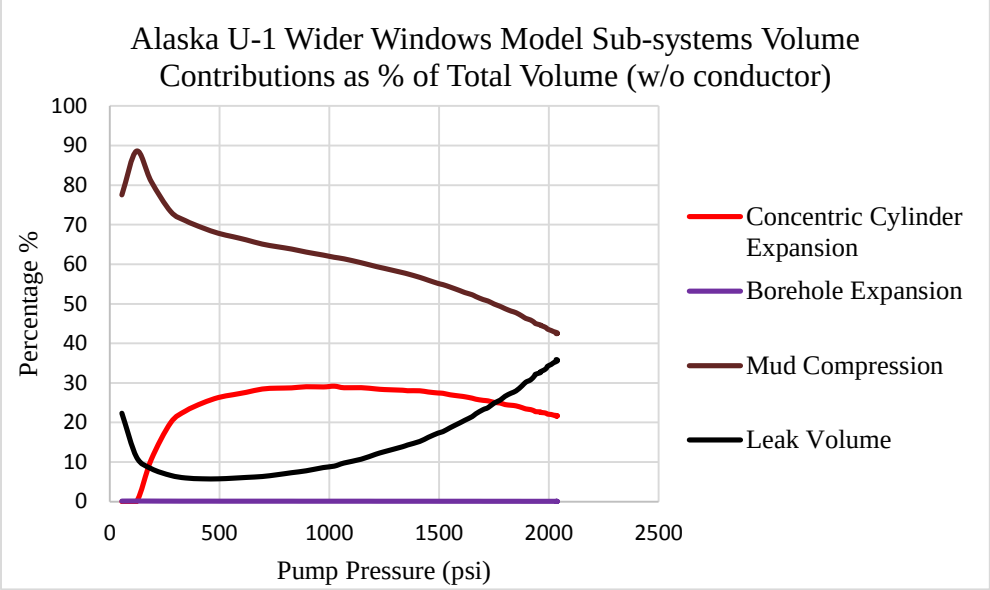

Figure 4.30 Alaska U-1 Wider Windows model sub-systems volume contributions as percentages of total volume

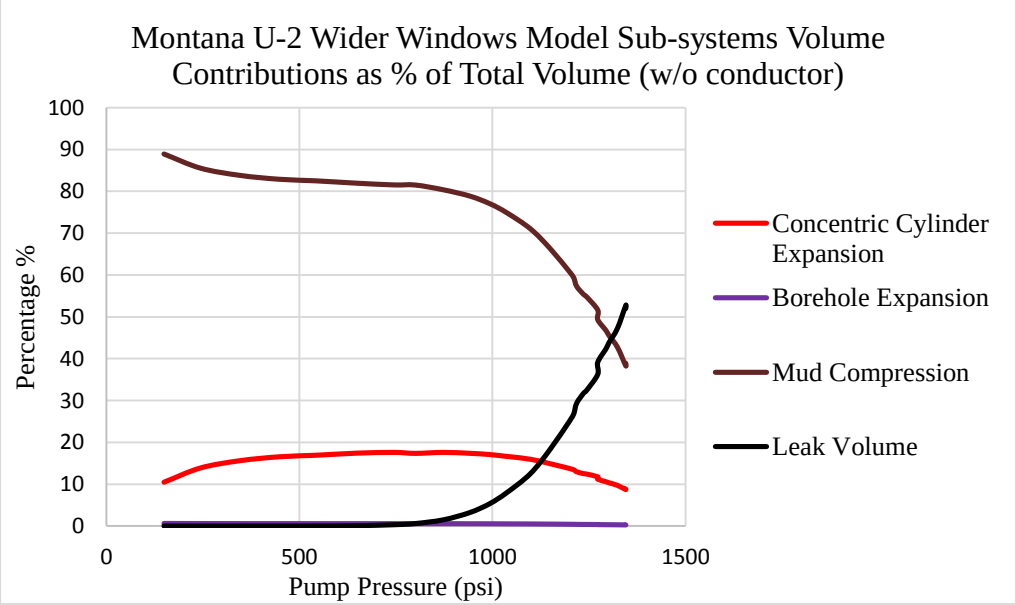

Figure 4.31 Montana U-2 Wider Windows model sub-systems volume contributions as percentages of total volume

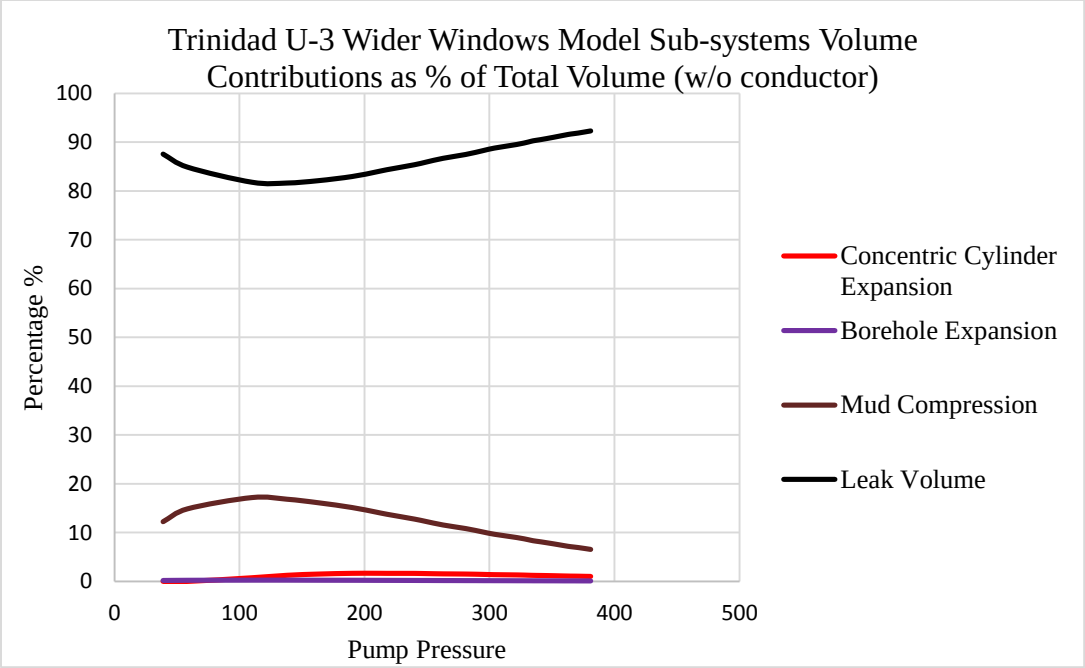

Figure 4.32 Trinidad U-3 Wider Windows model sub-systems volume contributions as percentages of total volume

For Alaska U-1 and Montana U-2, the leakage volumes become significant when pump pressure reaches 1000 psi. On the overall volume plot shown in Figure 4.27 and 4.28, it can be seen that the pressure buildup curve remains linear up until 1000 psi and becomes non-linear afterwards. However, for Trinidad U-3, because the leakage volume dominates throughout the LOT, the overall leak-off volume curve behaves non-linearly throughout the LOT as well.

4.4.3.5 Relative Errors

The results from WW mechanical expansion model predictions are compared with the actual LOT data by calculating the absolute relative errors. Figure 4.33, Figure 4.34, and Figure 4.35 show the results from Alaska U-1, Montana U-2, and Trinidad U-3, respectively.

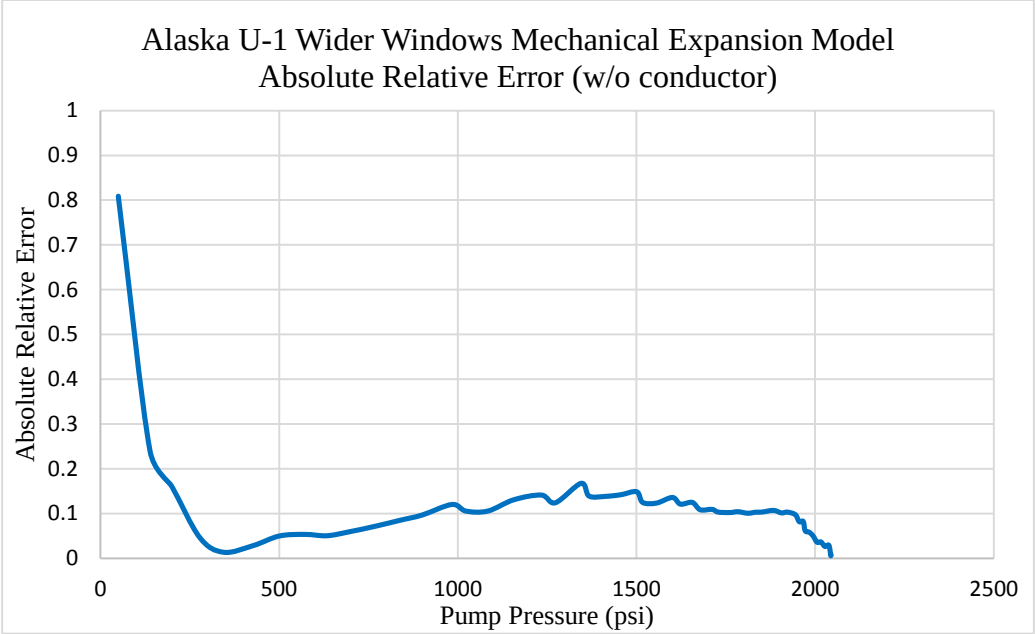

Figure 4.33 Alaska U-1 Wider Windows mechanical expansion model absolute relative error

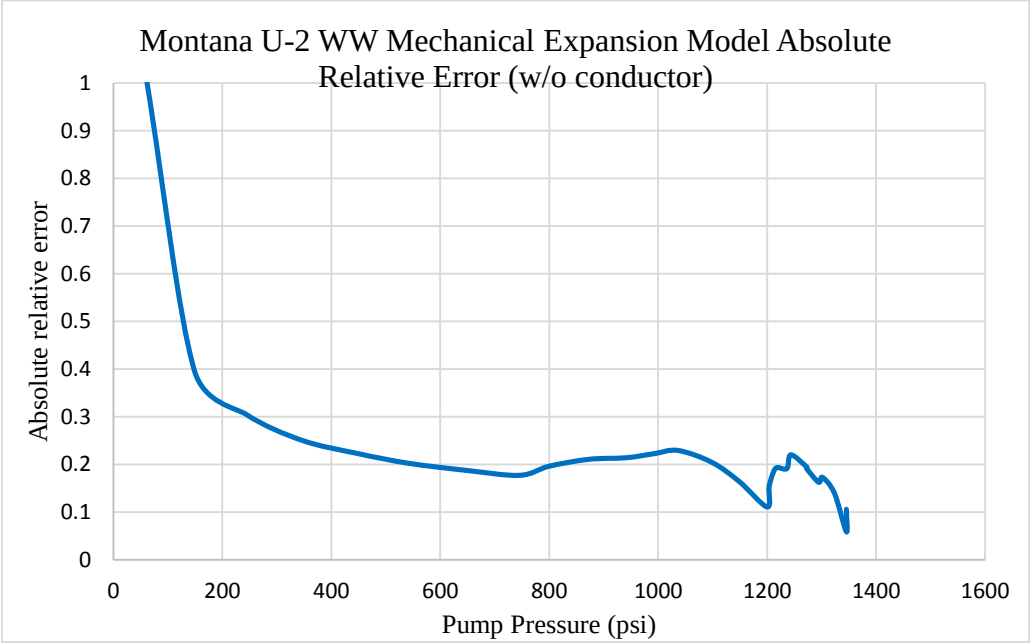

Figure 4.34 Montana U-2 Wider Windows mechanical expansion model absolute relative error

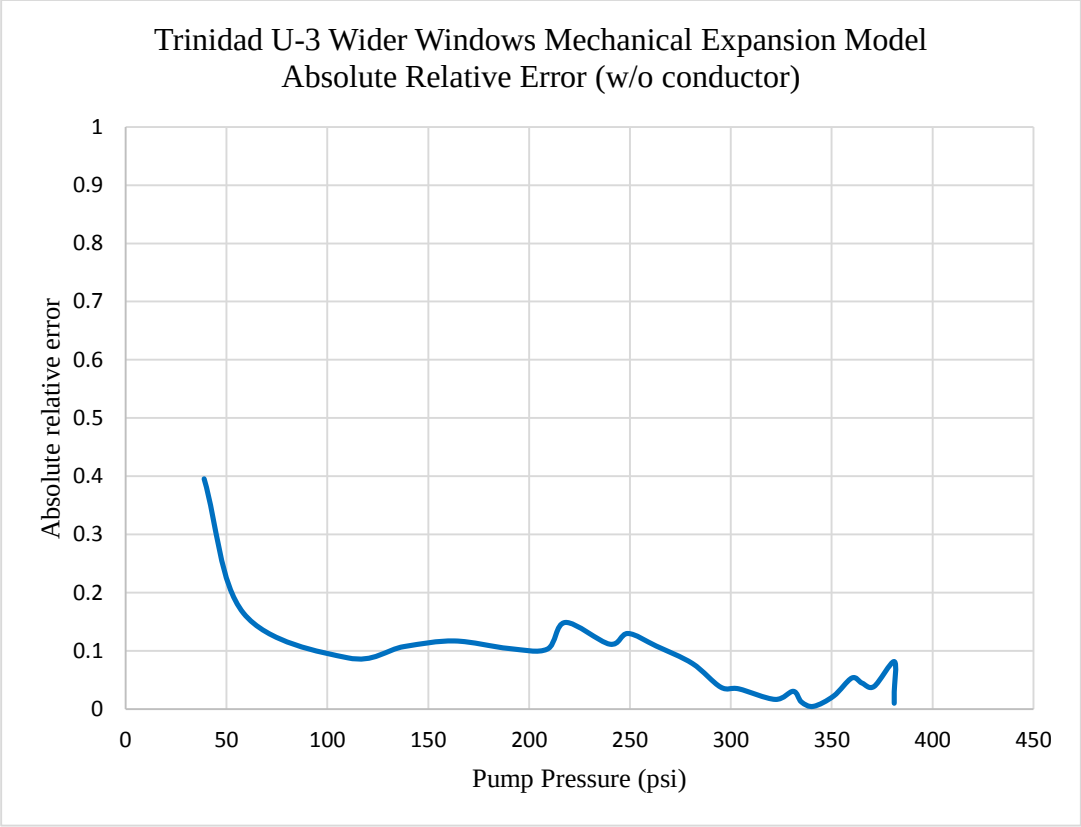

Figure 4.35 Trinidad U-3 Wider Windows mechanical expansion model absolute relative error

All three plots above show that the WW model generates significant errors at the beginning of pumping. However, the errors drop rapidly after the first few data points. It is important to notice the decrease in average absolute relative error for Alaska U-1 between the enhanced Altun model and the WW mechanical model, as the results are shown in Table 4.8.

Table 4.8 Wider Windows mechanical expansion model average absolute relative errors

Well ID	Casing length (ft)	Average absolute relative error %	Standard deviation
Alaska U-1	5767	10.71	0.109
Montana U-2	1765	22.34	0.164
Trinidad U-3	833	8.29	0.080

4.4.4 Wider Windows Mechanical Expansion Model with Conductor Casing

In this study, a 36” conductor casing is placed outside of the 20” surface casing, the depth of the 36” casing shoe varies from 100 ft to 500 ft below the seafloor. The results are discussed and shown in this section.

4.4.4.1 Wellbore Schematics

Figure 4.36, Figure 4.37, and Figure 4.38 show the wellbore schematics for Alaska U-1, Montana U-2, and Trinidad U-3 respectively. There are no cement layers outside of the 36” conductor casing for Alaska U-1 and Trinidad U-3 because conductor casings are assumed to be jetted.

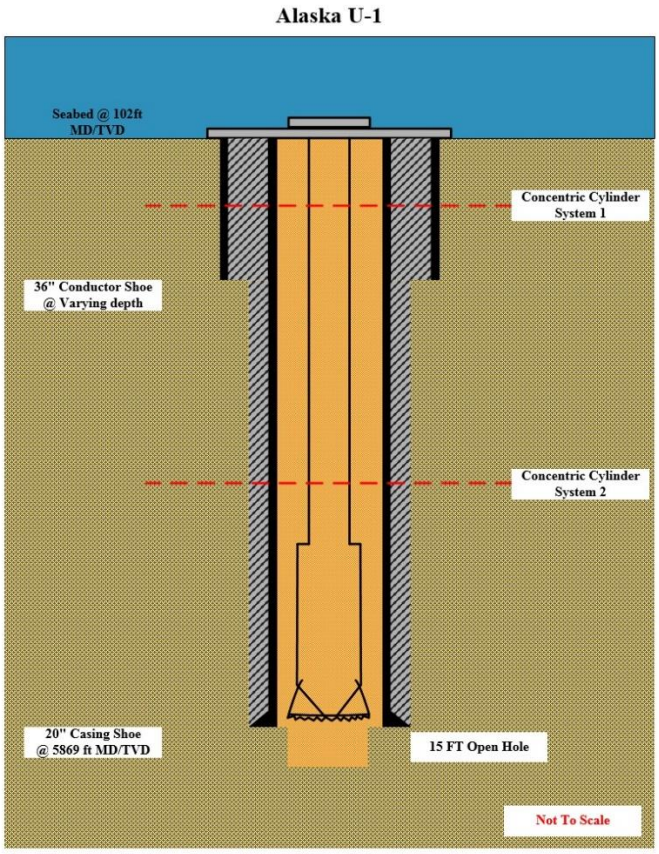

Figure 4.36 Alaska U-1 wellbore schematic

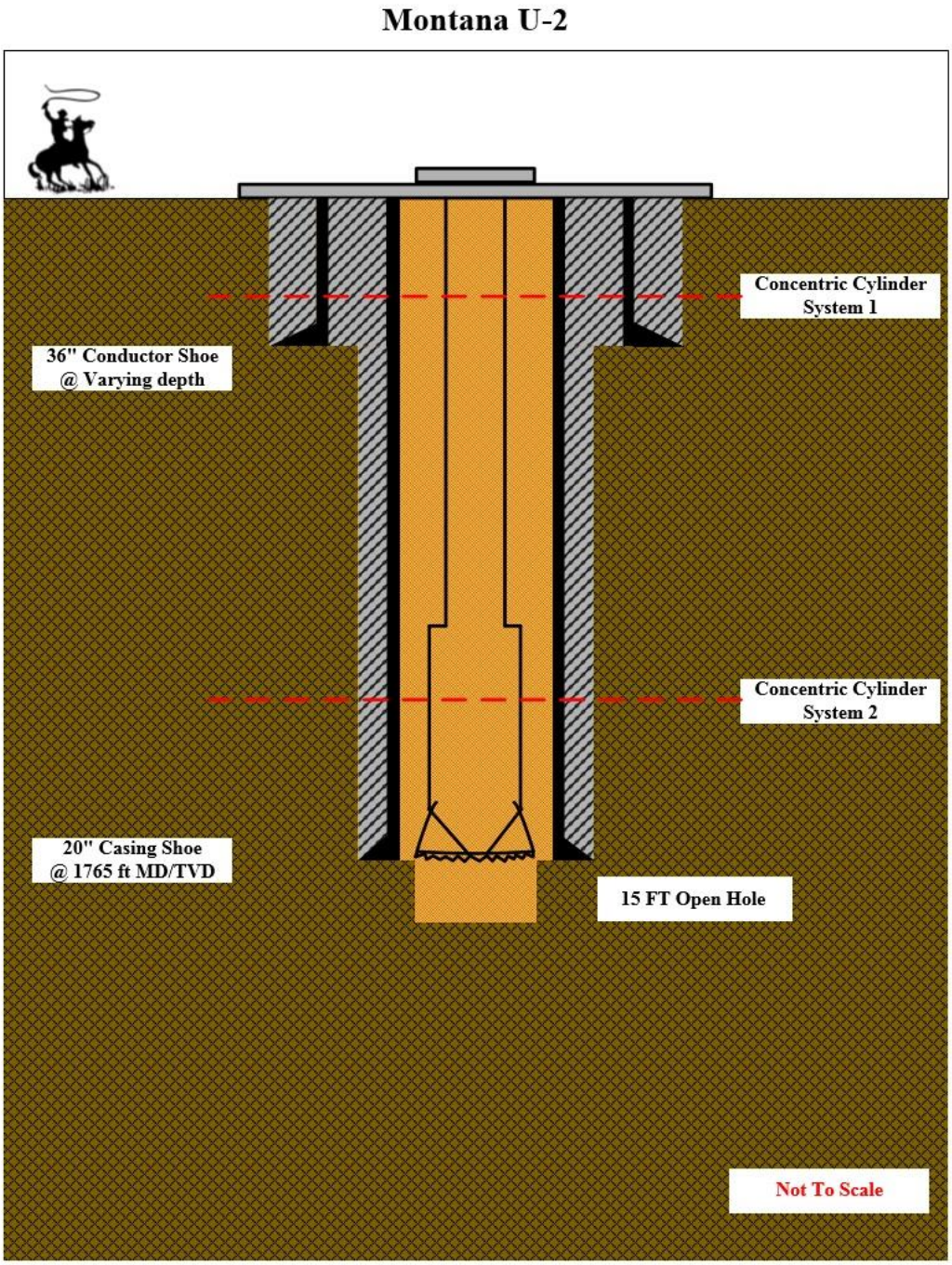

Figure 4.37 Montana U-2 wellbore schematic

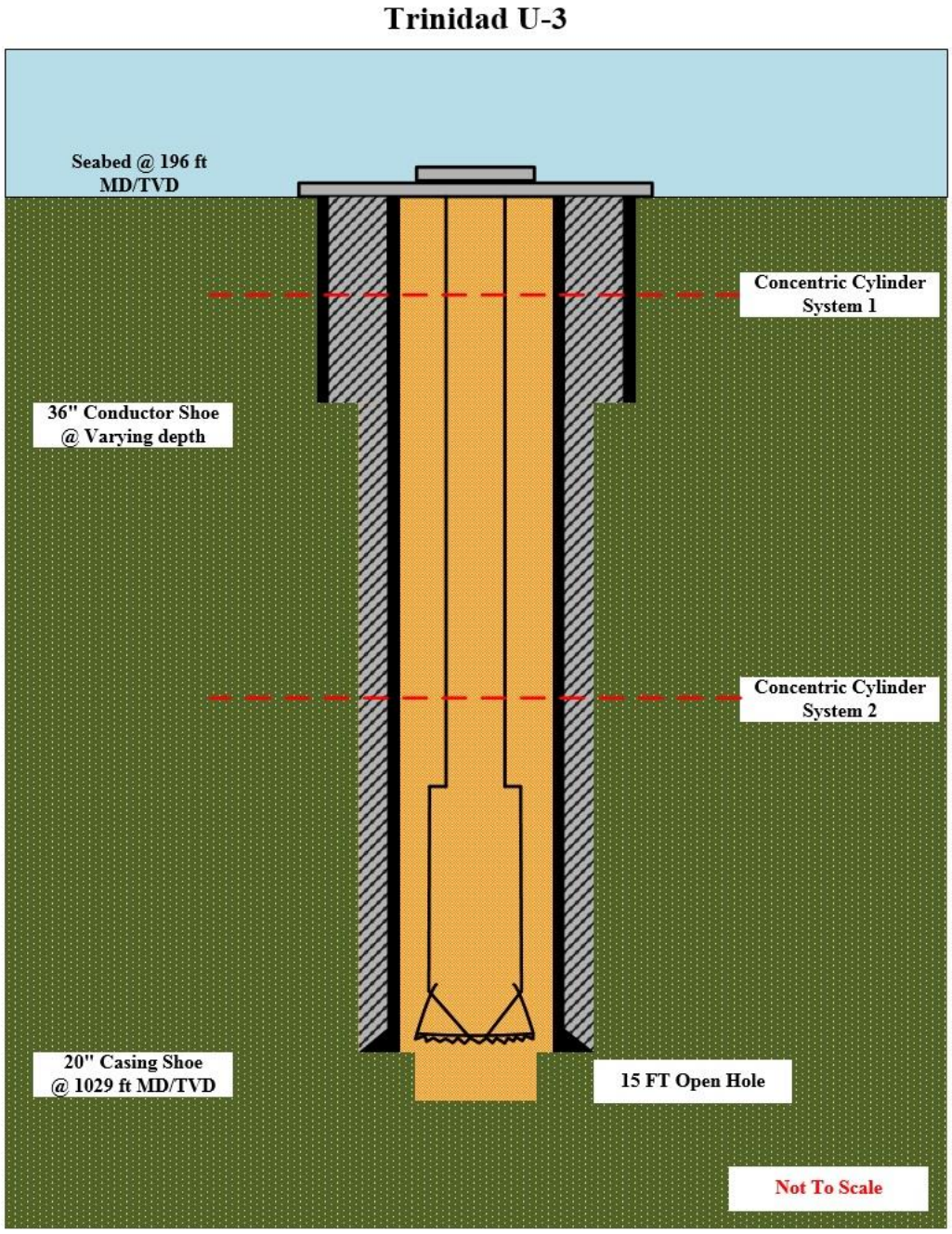

Figure 4.38 Trinidad U-3 wellbore schematic

4.4.4.2 Displacement

The displacements at the inner surfaces of the 20” casing and the 36” conductor casing are calculated based on the interface pressures obtained from multi-cylinder solutions. Figure 4.39, Figure 4.40, and Figure 4.41 show the displacement profiles for Alaska U-1, Montana U-2, and Trinidad U-3 respectively.

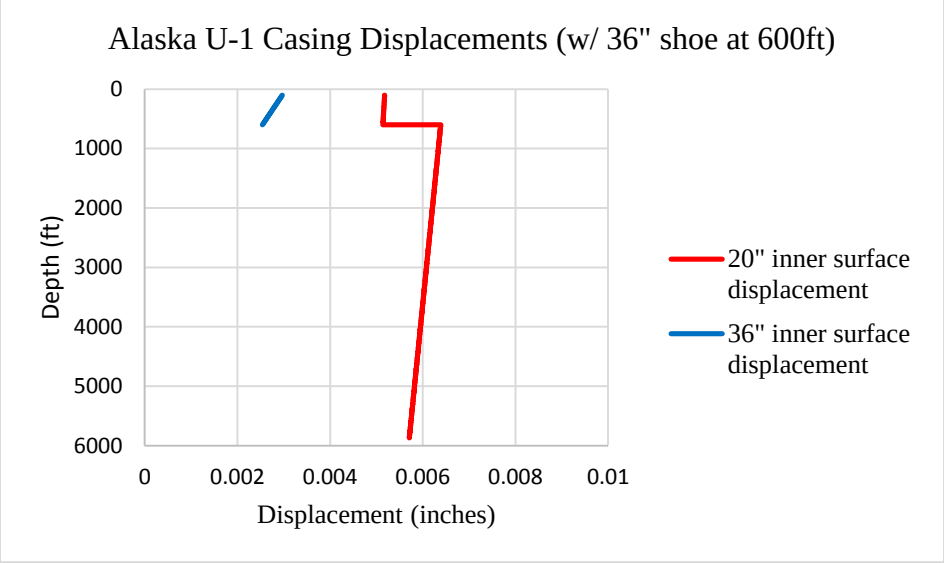

Figure 4.39 Alaska U-1 casing displacement profiles

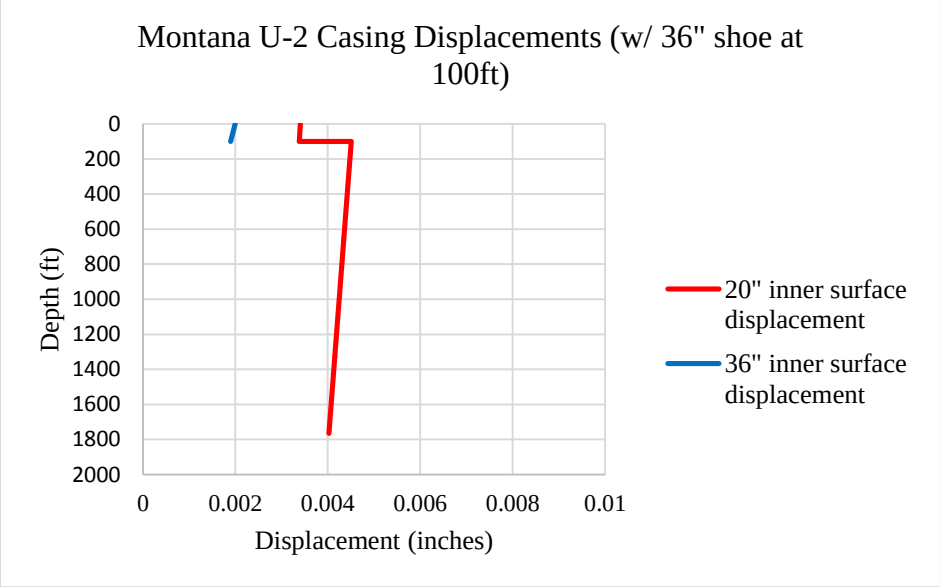

Figure 4.40 Montana U-2 casing displacement profiles

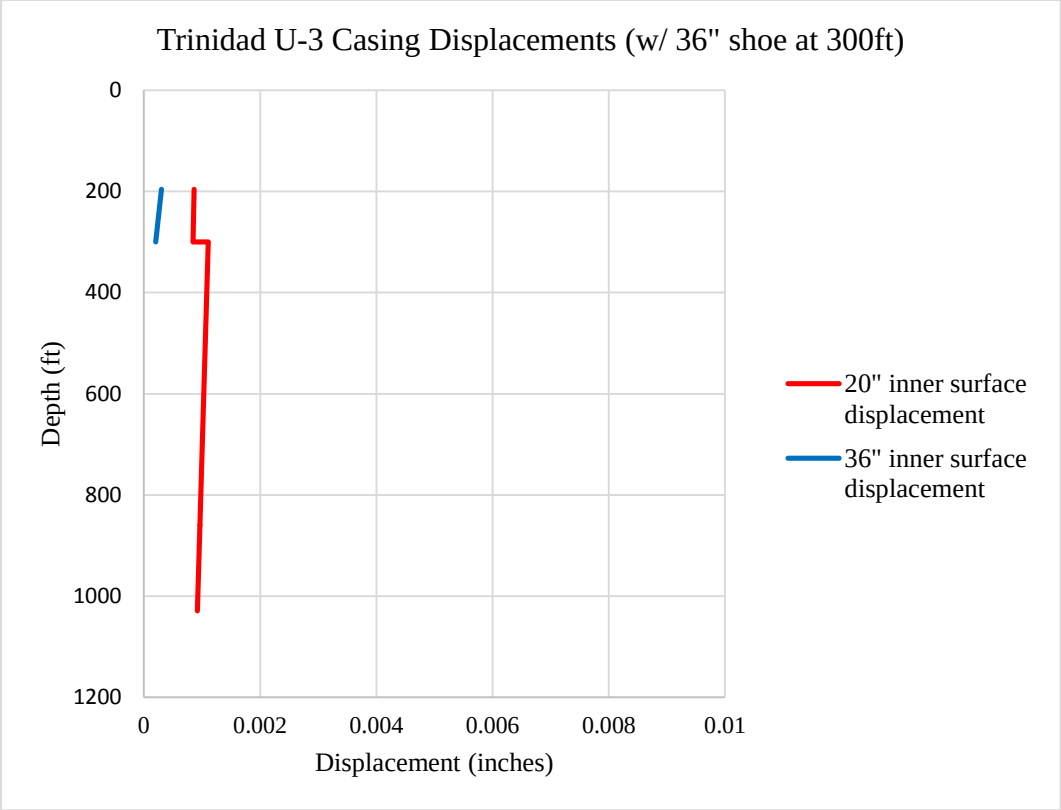

Figure 4.41 Trinidad U-3 casing displacement profiles

The above figures clearly demonstrate the discontinuities in 20” casing displacements at 36” conductor casing shoes. However, in field drilling operations, the inner casing has to be intact at outer casing shoes. The WW model uses concentric cylinder theory developed by Norris, which is based on Lame’s 2D solutions. The model can only calculate displacements based on properties of each concentric cylinder system. Therefore, discontinuities in inner casing displacements are observed at outer casing shoes, which are the boundaries for different concentric cylinder systems. However, the discontinuities are considered to be local effects because of the magnitudes of displacements and the length of the casing strings under pressure.

4.4.4.3 Volume Contributions of Each Sub-system

The volumes generated from sub-systems for the three tested wells are shown in Figure 4.42, Figure 4.43, and Figure 4.44.

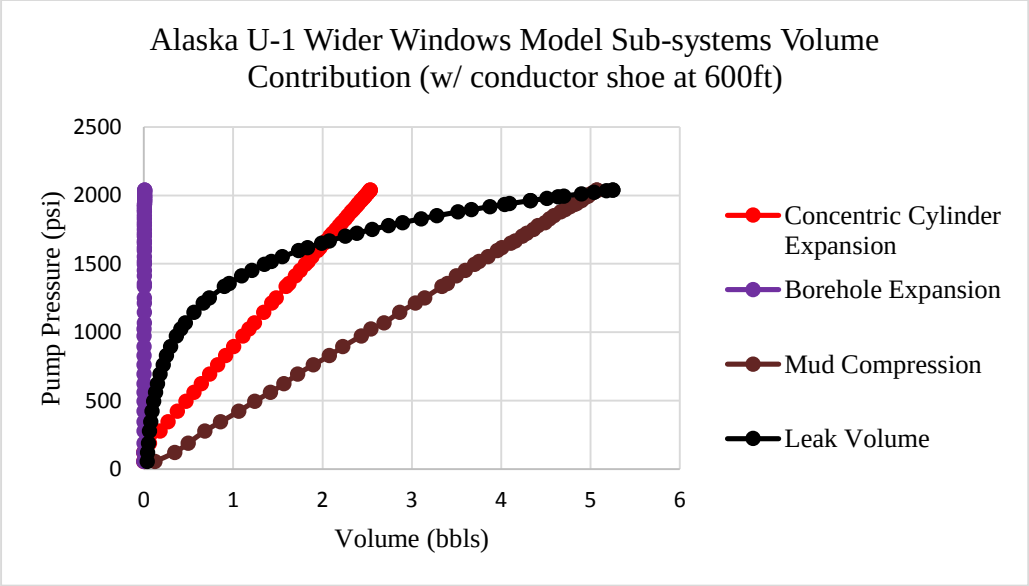

Figure 4.42 Alaska U-1 Wider Windows model sub-systems volume contributions (with conductor casing shoe at 600 ft)

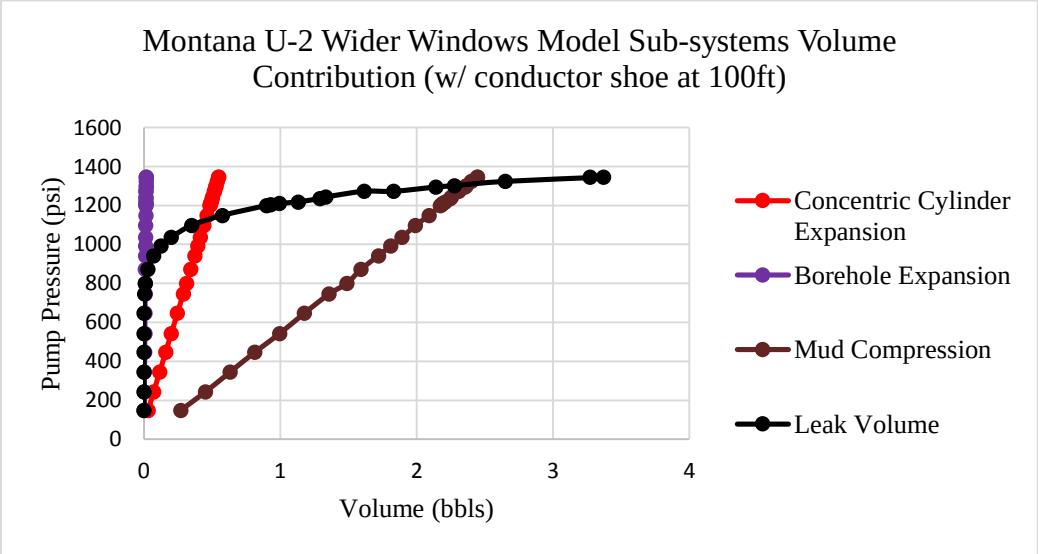

Figure 4.43 Montana U-2 Wider Windows model sub-systems volume contributions (with conductor casing shoe at 100 ft)

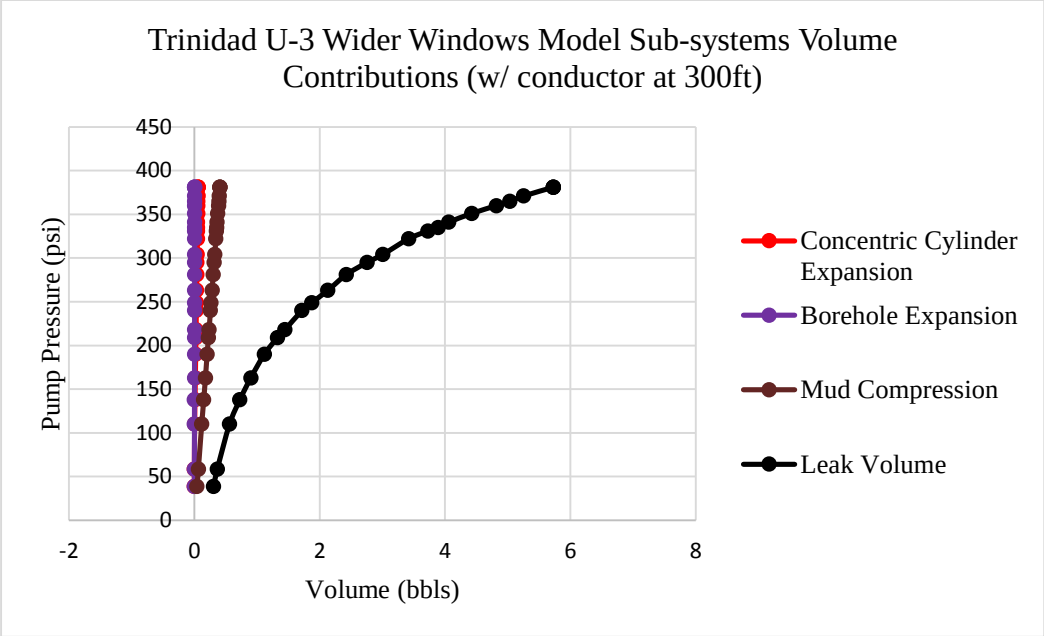

Figure 4.44 Trinidad U-3 Wider Windows model sub-systems volume contributions (with conductor casing shoe at 300 ft)

4.4.4.4 Total Volume Plots with Conductor Casing

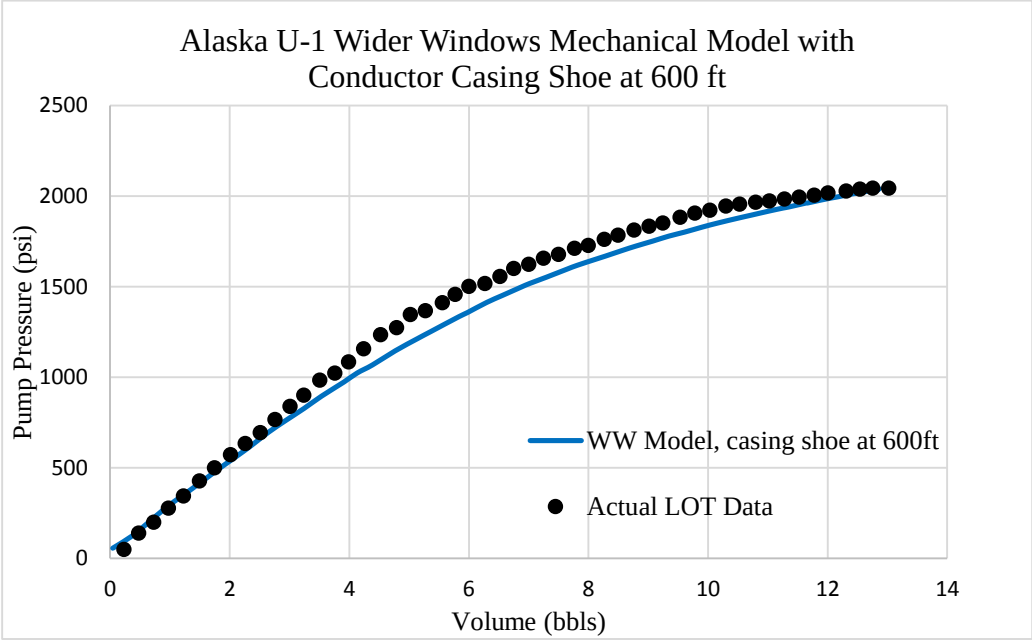

Figure 4.45 Alaska U-1 Wider Windows mechanical model with conductor casing volume prediction

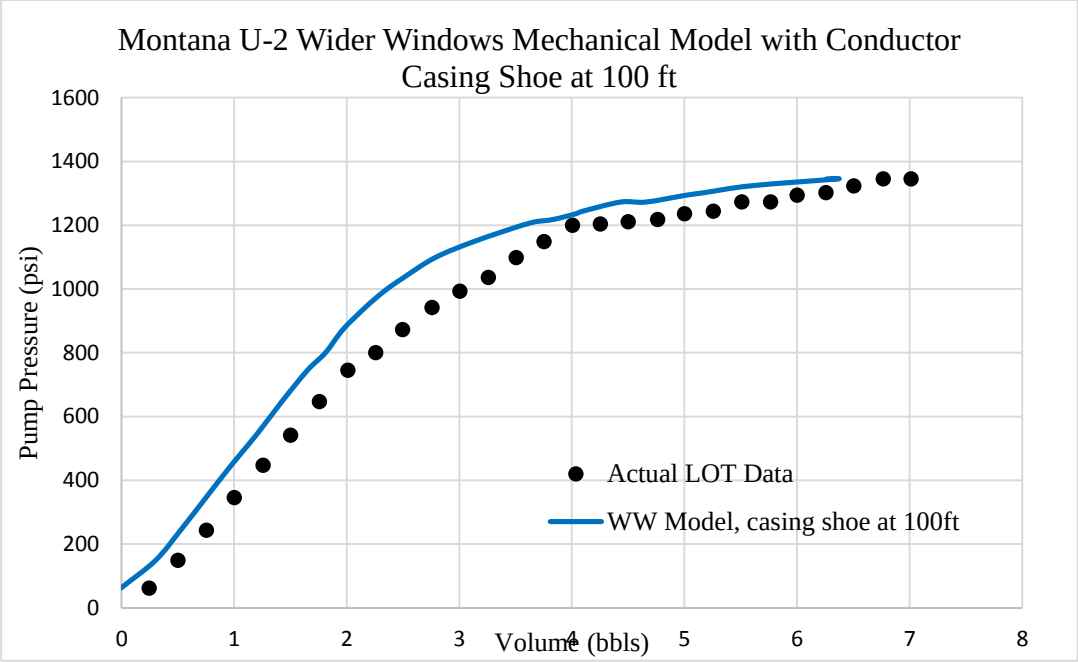

Figure 4.46 Montana U-2 Wider Windows mechanical model with conductor casing volume prediction

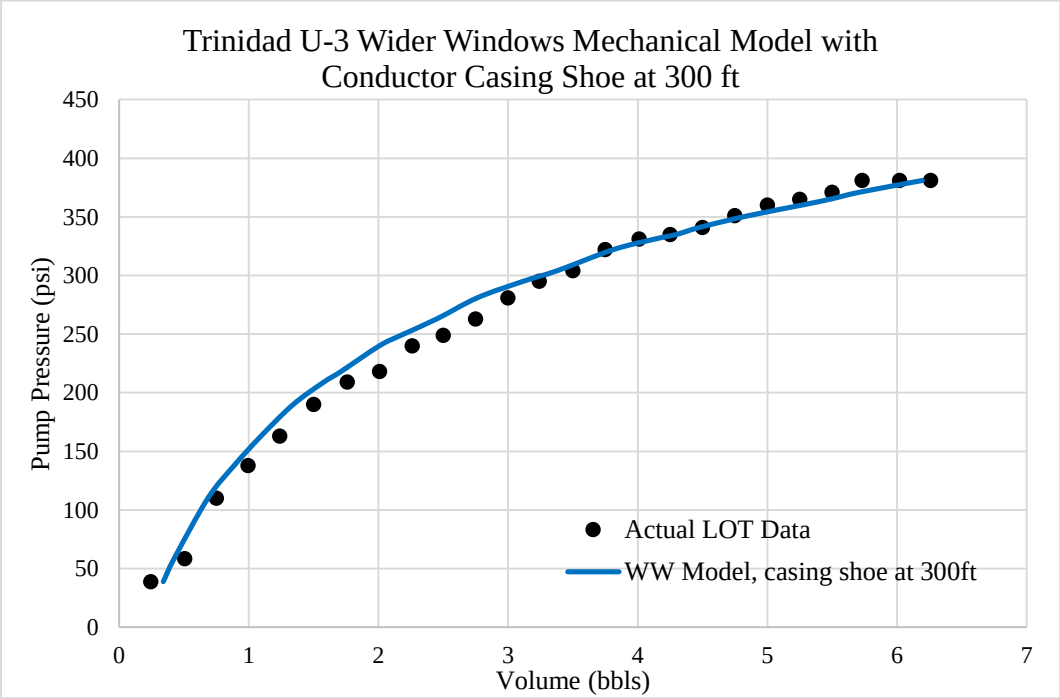

Figure 4.47 Trinidad U-3 Wider Windows mechanical model with conductor casing volume prediction

4.4.4.5 Sub-systems Volume Contributions as Percentages of Total Volume

The volumes generated from sub-systems for the three tested wells are shown in Figure 4.48, Figure 4.49, and Figure 4.50.

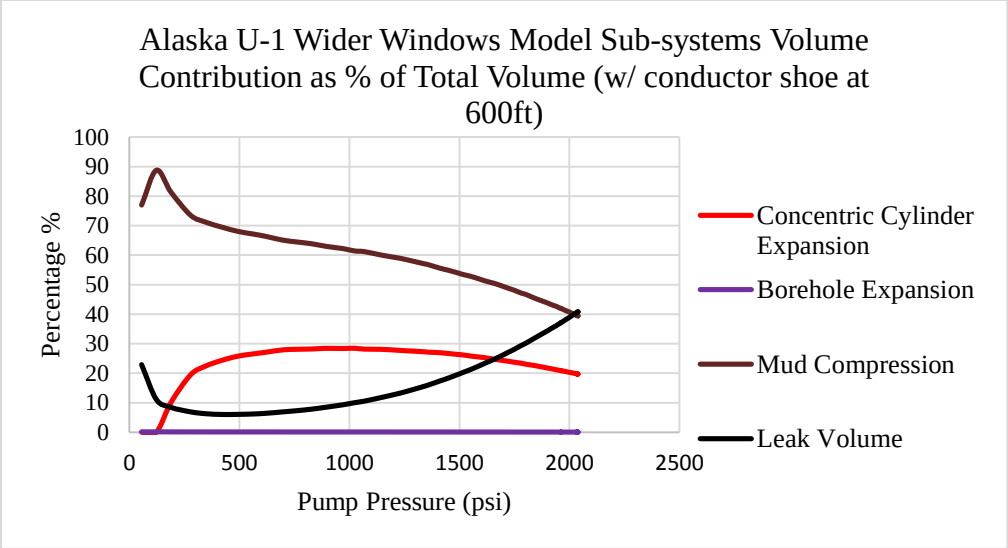

Figure 4.48 Alaska U-1 Wider Windows model sub-systems volume contributions as percentages of total volume (with conductor casing shoe at 600 ft)

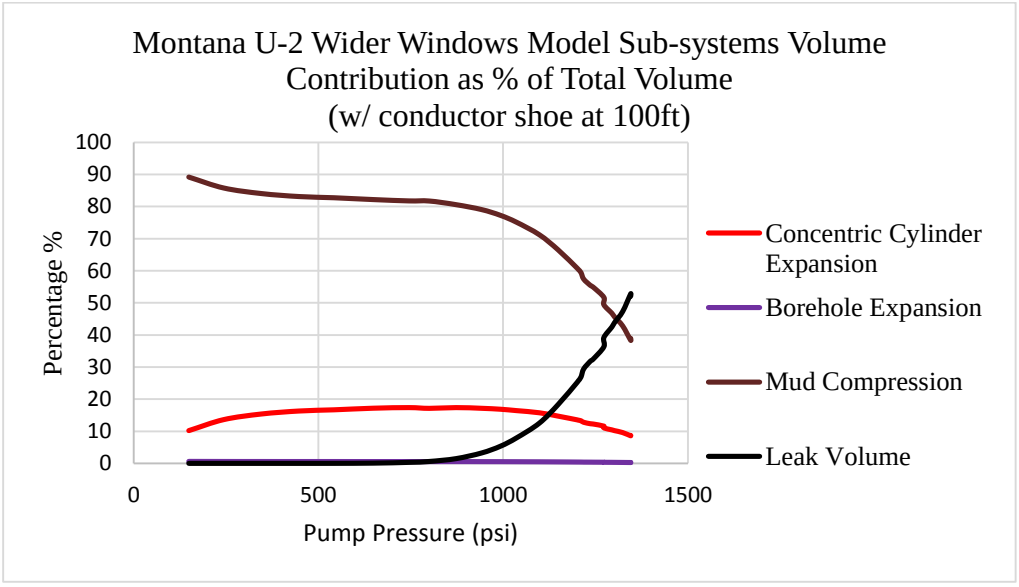

Figure 4.49 Montana U-2 Wider Windows model sub-systems volume contributions as percentages of total volume (with conductor casing shoe at 100 ft)

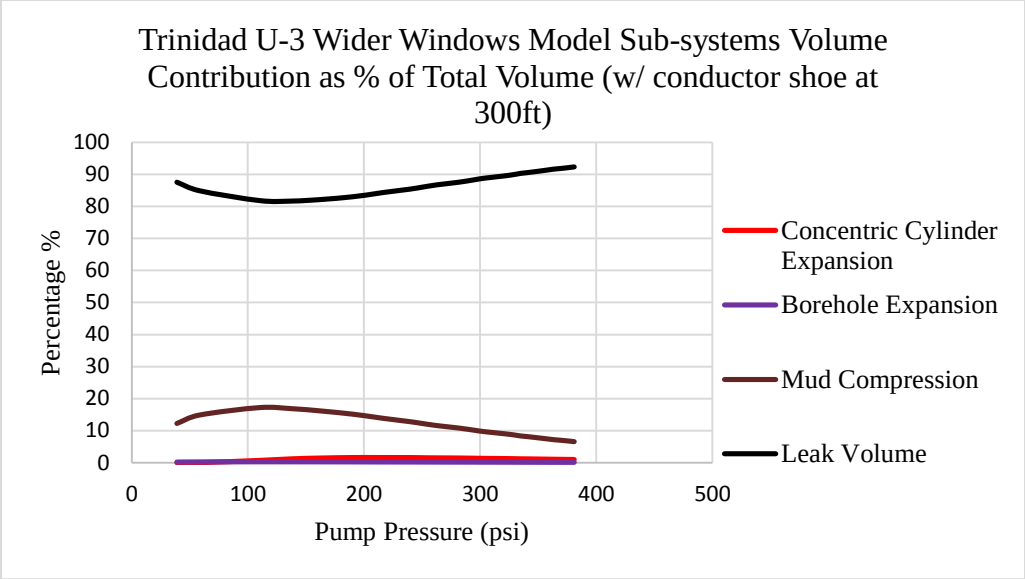

Figure 4.50 Trinidad U-3 Wider Windows model sub-systems volume contributions as percentages of total volume (with conductor casing shoe at 300 ft)

4.4.4.6 WW model with conductor vs. WW model without conductor

Adding a layer of conductor casing did not make noticeable changes in the results. Theoretically, when the conductor casing is in place, the portion of the 20" casing inside the conductor would expand less (shown in Figures 4.39 through 4.41). However, because the reduction in casing displacement is very small, the overall volume change can be negligible.

4.4.4.7 Linear Components vs. Non-linear Components

In this section, the combined volume from linear components (mud compression, concentric cylinder expansion, and borehole expansion) is plotted with the volume contribution from the non-linear component (leak volume) and the actual LOT data. The results are shown as follows.

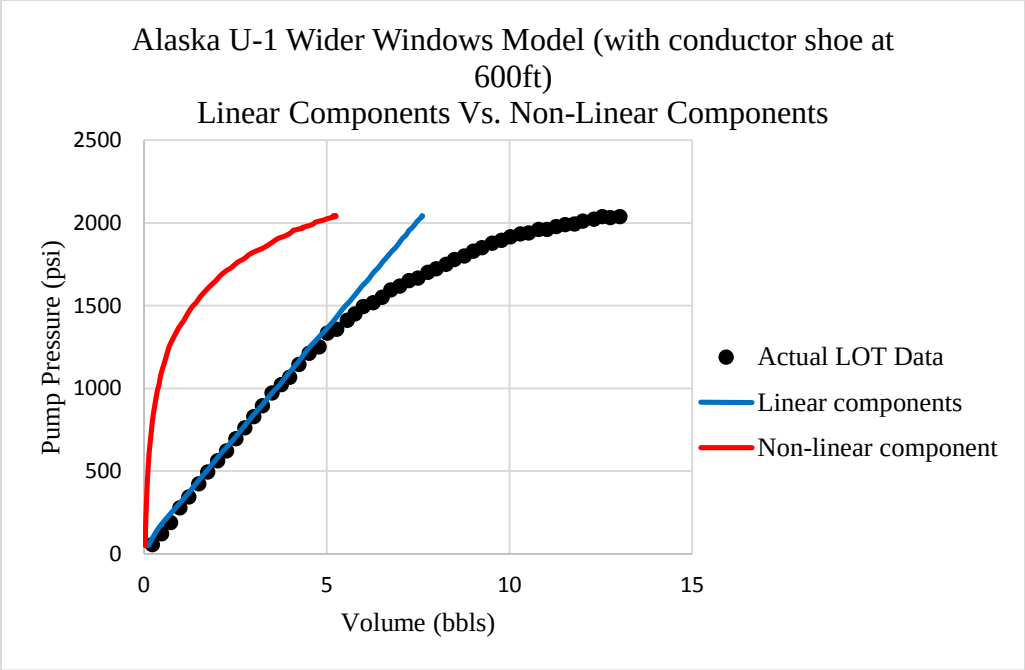

Figure 4.51 Alaska U-1 Wider Windows model linear vs. non-linear components (with conductor casing shoe at 600 ft)

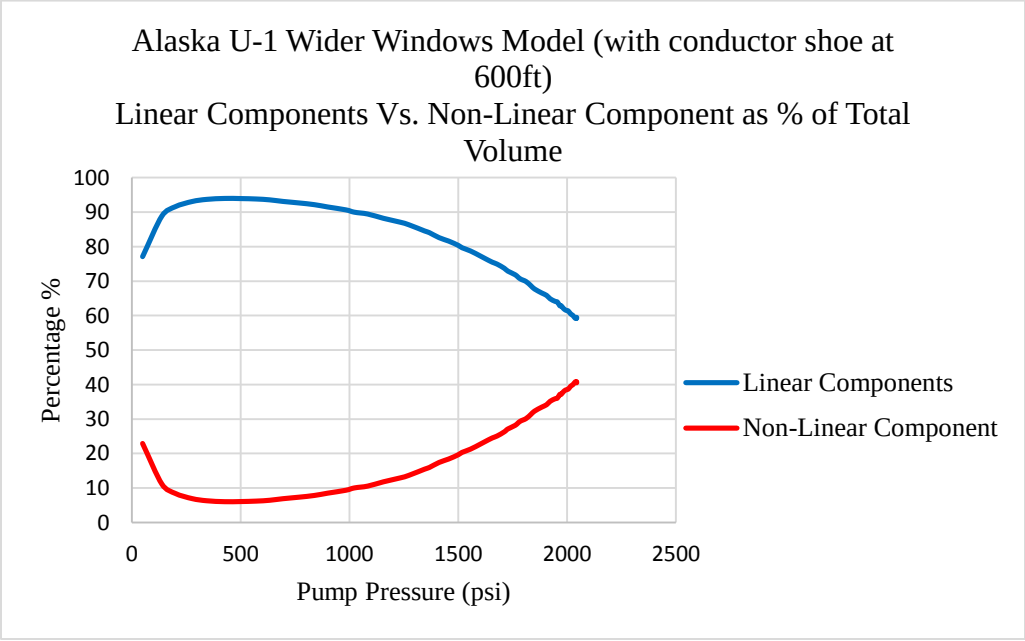

Figure 4.52 Alaska U-1 Wider Windows model linear vs. non-linear components as percentages of total volume (with conductor casing shoe at 600 ft)

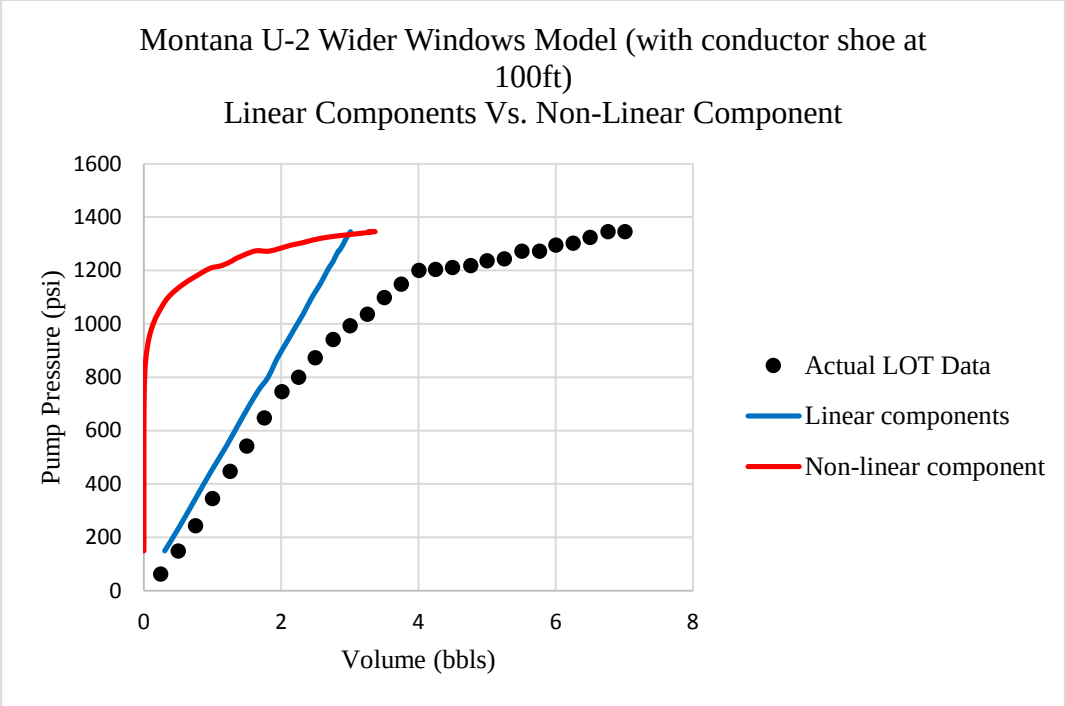

Figure 4.53 Montana U-2 Wider Windows model linear vs. non-linear components (with conductor casing shoe at 100 ft)

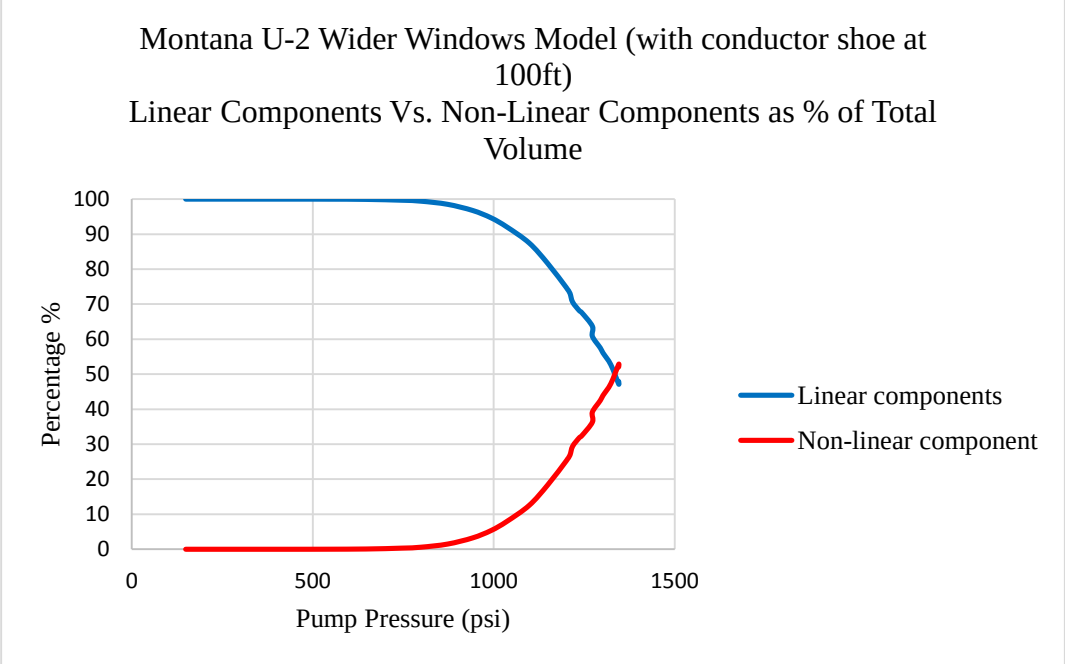

Figure 4.54 Montana U-2 Wider Windows model linear vs. non-linear components as percentages of total volume (with conductor casing shoe at 100 ft)

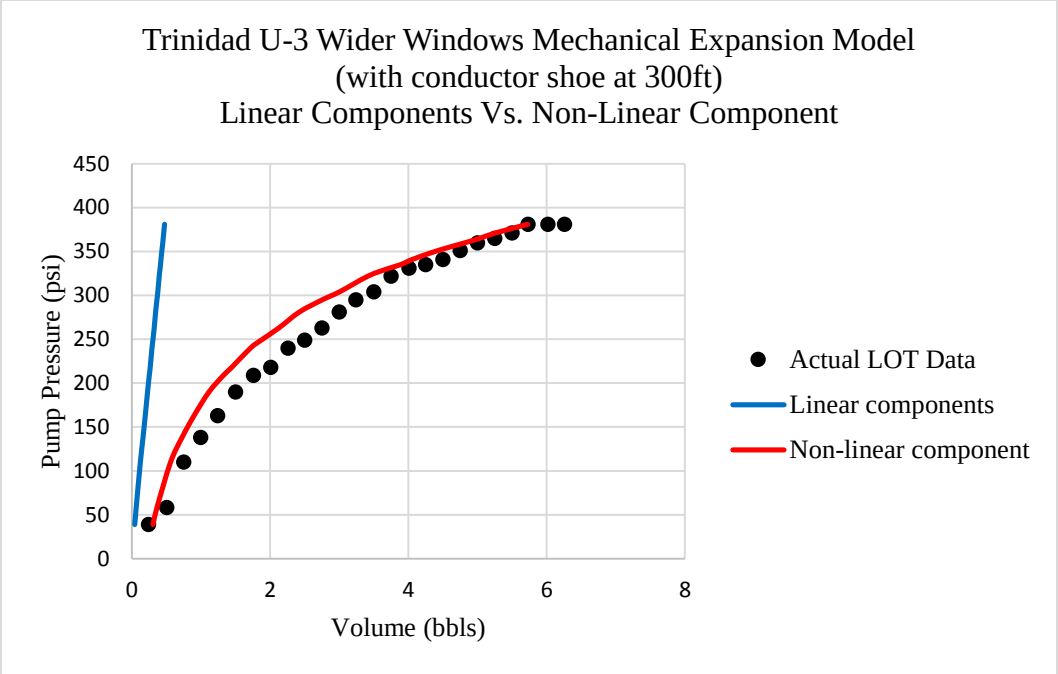

Figure 4.55 Trinidad U-3 Wider Windows model linear vs. non-linear components (with conductor casing shoe at 300 ft)

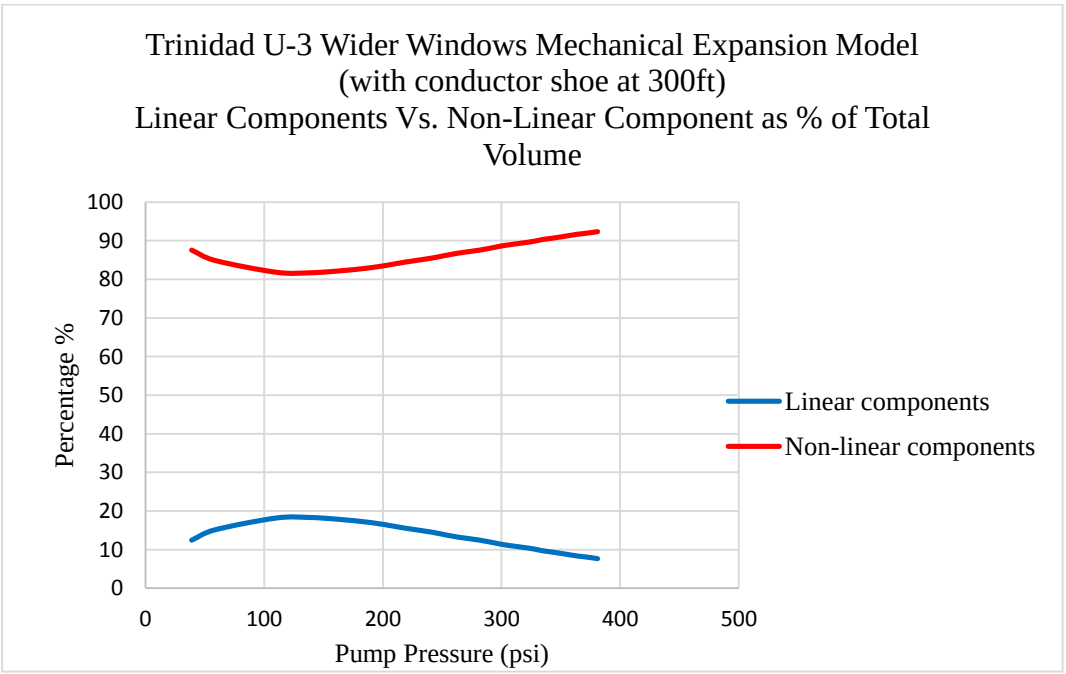

Figure 4.56 Trinidad U-3 Wider Windows model linear vs. non-linear components as percentages of total volume (with conductor casing shoe at 300 ft)

For Alaska U-1, fluid leakage contributed very little to total leak-off volume before pump pressure reaches 1000 psi. The actual leak-off volume, as shown in Figure 4.51, remained close to the linear components approximation and exhibits a linear trend. After 1000 psi, the contributions from fluid leakage becomes significant relative to the other volume contributions. Therefore, the total leak-off volume starts to demonstrate a non-linear behavior.

Similar observations can be seen from Montana U-2 as well. Figure 4.53 shows that prior to pump pressure reaching 1000 psi, the actual leak-off volume stays close to the linear components approximation and exhibits a linear trend. As leakage contribution becomes significant after 1000 psi, the total leak-off volume starts to display a non-linear behavior.

On the other hand, Trinidad U-3 shows different behaviors. Because the length of casing is much shorter than that of Alaska U-1 and Montana U-2, the volume of mud pumped to compress the mud already in the wellbore is greatly reduced. Therefore, mud compression generates small contribution to the total volume as shown in Figure 4.50. The leakage volume makes up the majority throughout the LOT. The overall leak-off volume stays close to the leakage volume approximation and the shape of LOT plot stays non-linear for Trinidad U-3.

4.4.4.8 Relative Errors

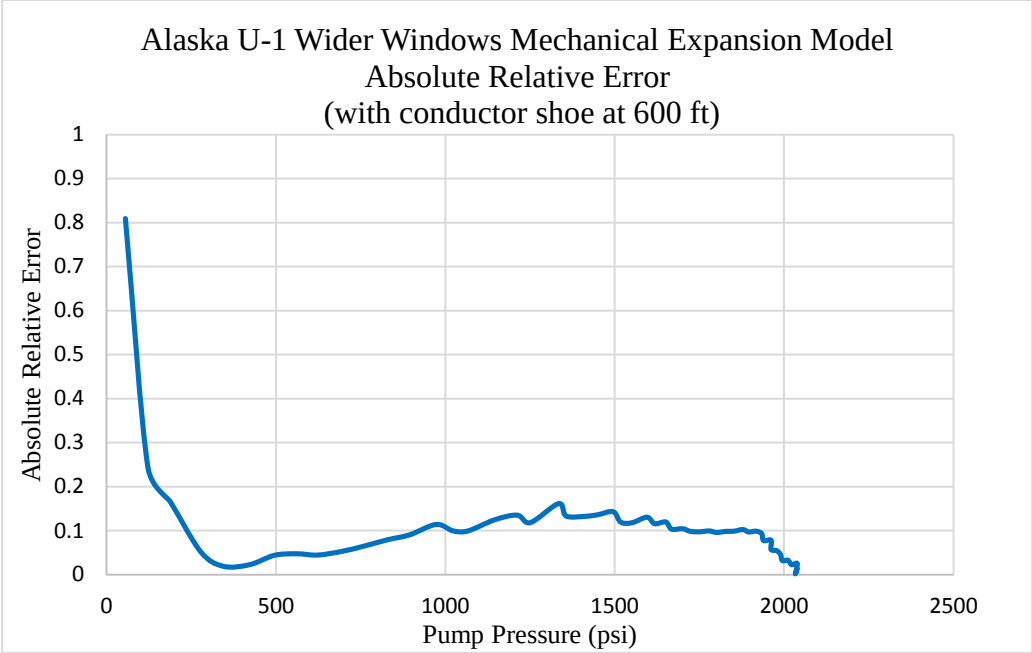

Figure 4.57 Alaska U-1 Wider Windows model absolute relative error (with conductor casing shoe at 600 ft)

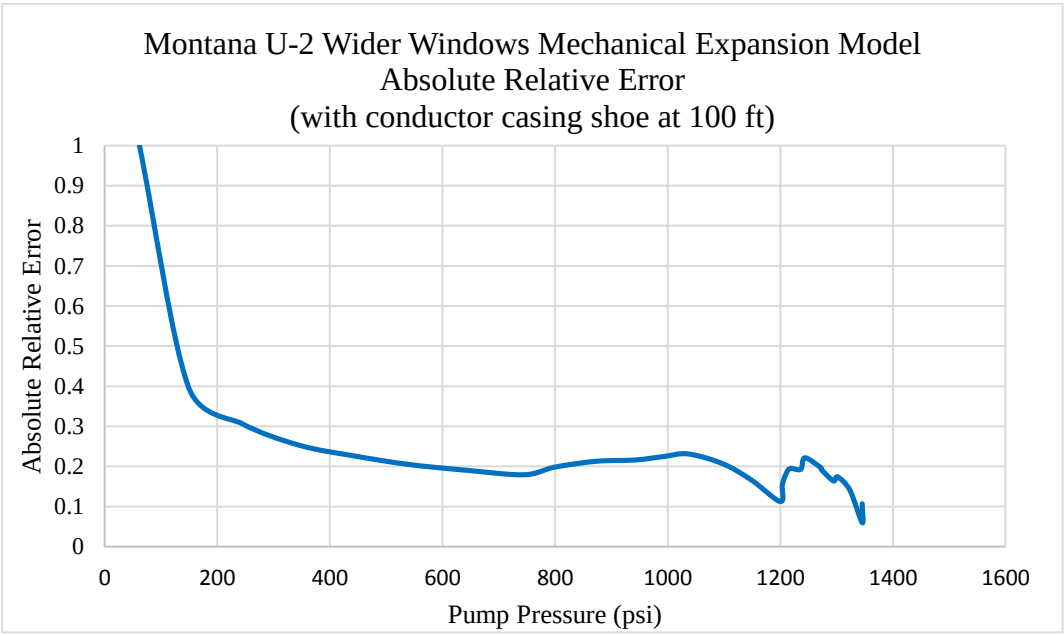

Figure 4.58 Montana U-2 Wider Windows model absolute relative error (with conductor casing shoe at 100 ft)

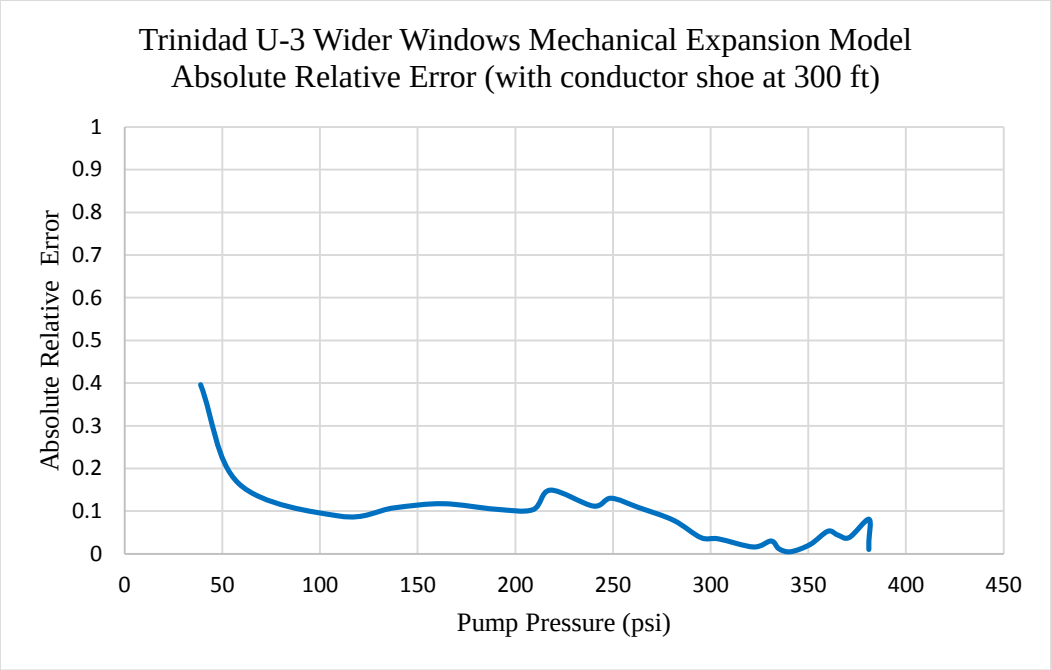

Figure 4.59 Trinidad U-3 Wider Windows model absolute relative error (with conductor casing shoe at 300 ft)

It can be seen that the absolute relative errors changed very little again from the previous study. Overall, the WW model provides good estimation of leak-off volume for Trinidad U-3. The average errors and standard deviations are shown in Table 4.9.

Table 4.9 Wider Windows mechanical expansion with conductor casing average errors

Well ID	Casing length (ft)	Average absolute relative error %	Standard deviation
Alaska U-1	5767	10.31	0.110
Montana U-2	1765	22.60	0.169
Trinidad U-3	833	8.31	0.080

4.5 Comparison of LOT Models

The results obtained from the enhanced Altun model and the WW models are plotted against the actual LOT data and the Altun model predictions. The results are shown in this section.

4.5.1 Overall Volume Comparisons

The results from Altun model, enhanced Altun model, WW model without conductor casing, and WW model with conductor casing are compared in this section.

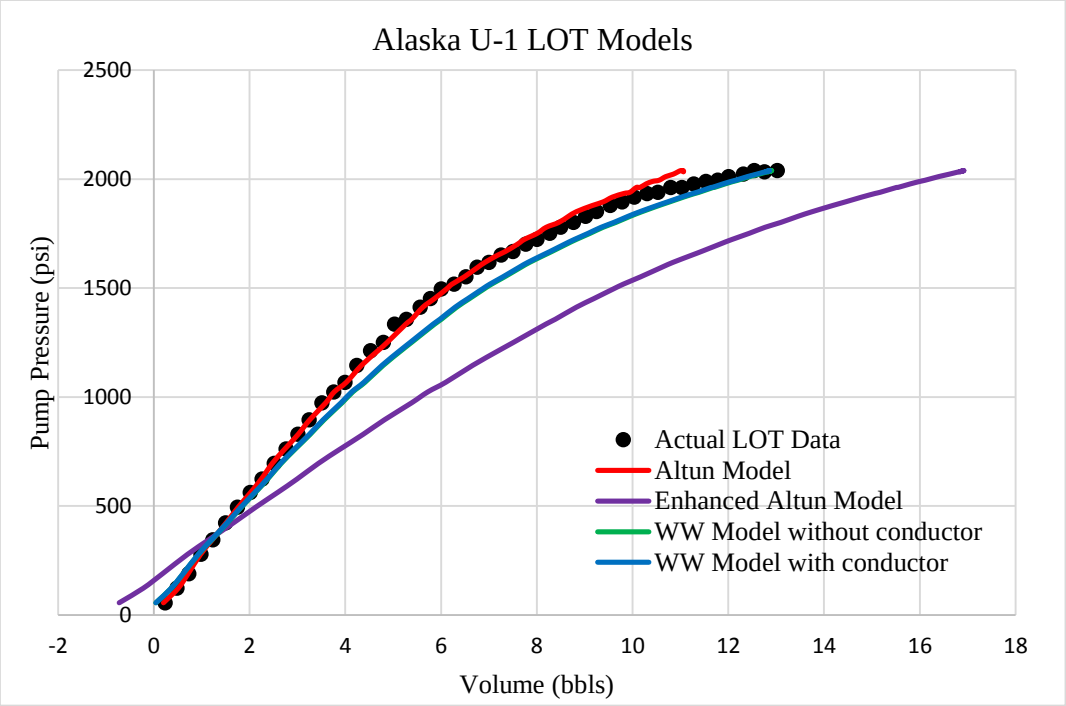

Figure 4.60 Alaska U-1 LOT Models

Figure 4.60 shows the overall volume predictions from all four LOT models for Alaska U-1the actual LOT data and LOT models for Alaska U-1. From pumping start to approximately 500 psi of pump pressure, the Altun model and the WW models provide good volume estimations. Between 500 psi and 1800 psi, the Altun model predictions are slightly better and fit closer to the actual LOT data. After 1800 psi, Altun model slightly underestimates leak-off volumes and the WW models become more accurate toward the end of the LOT. On the other hand, the enhanced Altun model severely overestimates leak-off volumes for the majority of the LOT, the largest difference between model prediction and the actual LOT data is nearly 4 barrels at 1500 psi.

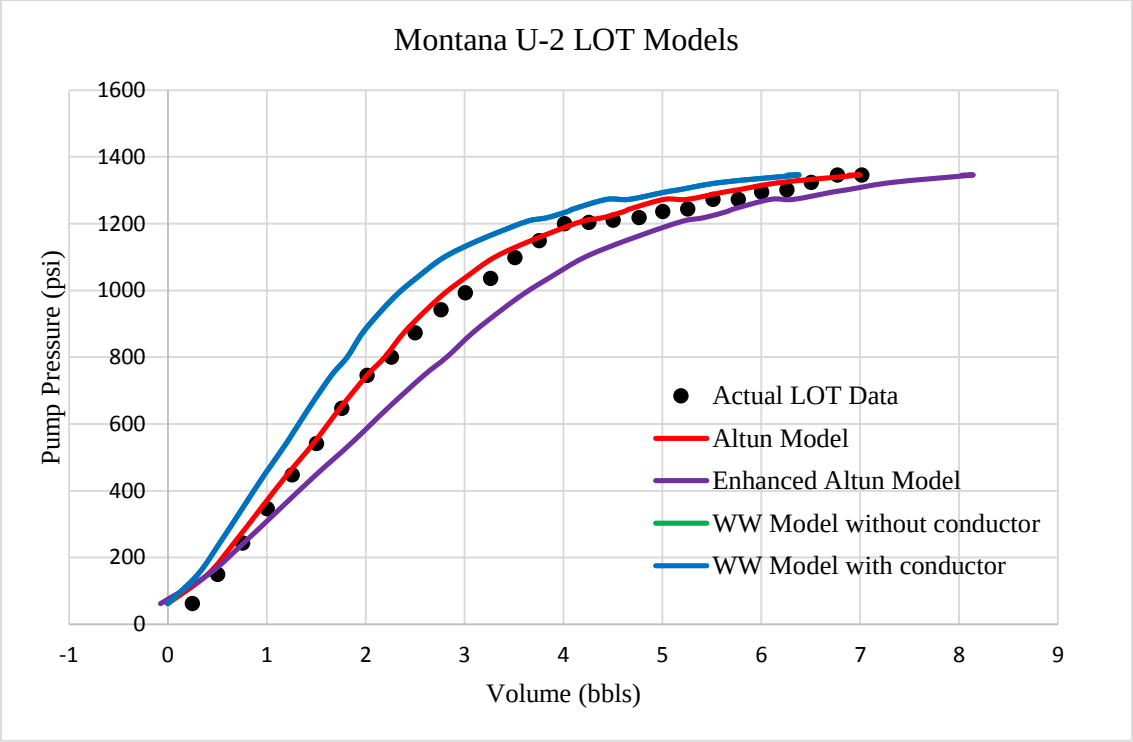

Figure 4.61 Montana U-2 LOT Models

Figure 4.61 shows the LOT models' volume predictions for Montana U-2. Overall, the Altun model provides the best fit to the actual data. The enhanced Altun model clearly overestimates leak-off volume whereas the WW models underestimate the leak-off volume.

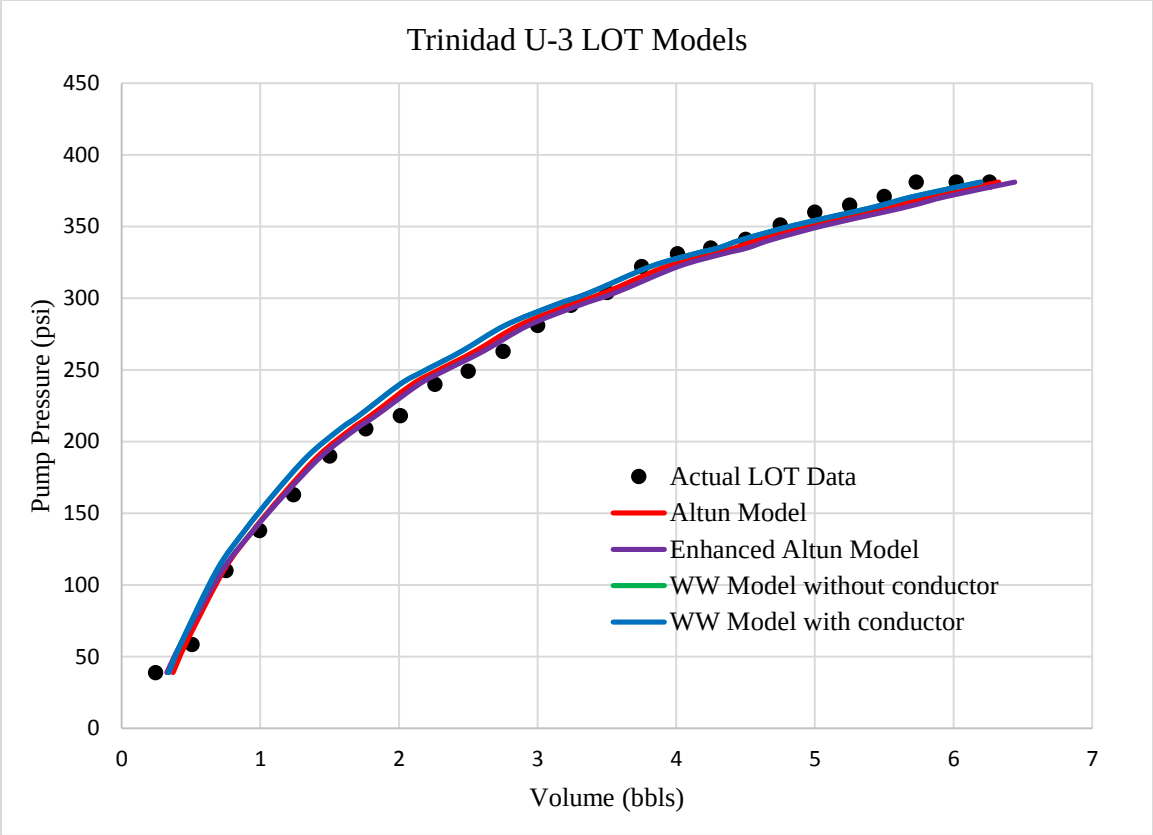

Figure 4.62 Trinidad U-3 LOT Models

For Trinidad U-3. All the LOT models provide excellent estimations of overall leak-off volume. The plot can be divided into two parts: before pump pressure reaches 300 psi, the enhanced Altun model appears to be the closest to actual data; after pump pressure reaches 300 psi, the WW model with conductor casing provides the best estimations.

4.5.2 Error Comparisons

This section compares the overall performances of the enhanced Altun model and the WW models.

4.5.2.1 Absolute Relative Error

The absolute relative errors from all 4 LOT models are plotted for each tested well and are shown in this section.

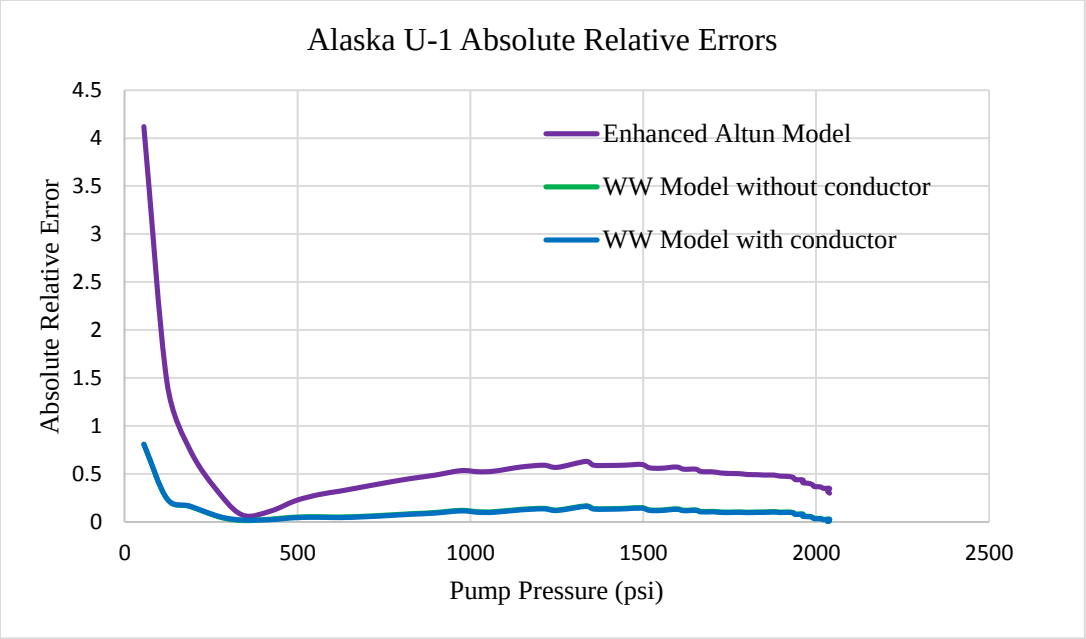

Figure 4.63 Alaska U-1 absolute relative errors from LOT models

Figure 4.63 shows the trends in errors for the three models. For all three models, the highest errors are recorded at the early stage of pumping. As pump pressure increases, errors decrease rapidly. Also, the difference between the enhanced Altun model and the WW models is noticeable. The WW models are significantly more accurate when compared with the enhanced Altun model. This finding confirms the importance to calculate leak-off volume along the cased hole should be based on the compounded expansion of casing, cement, and rock.

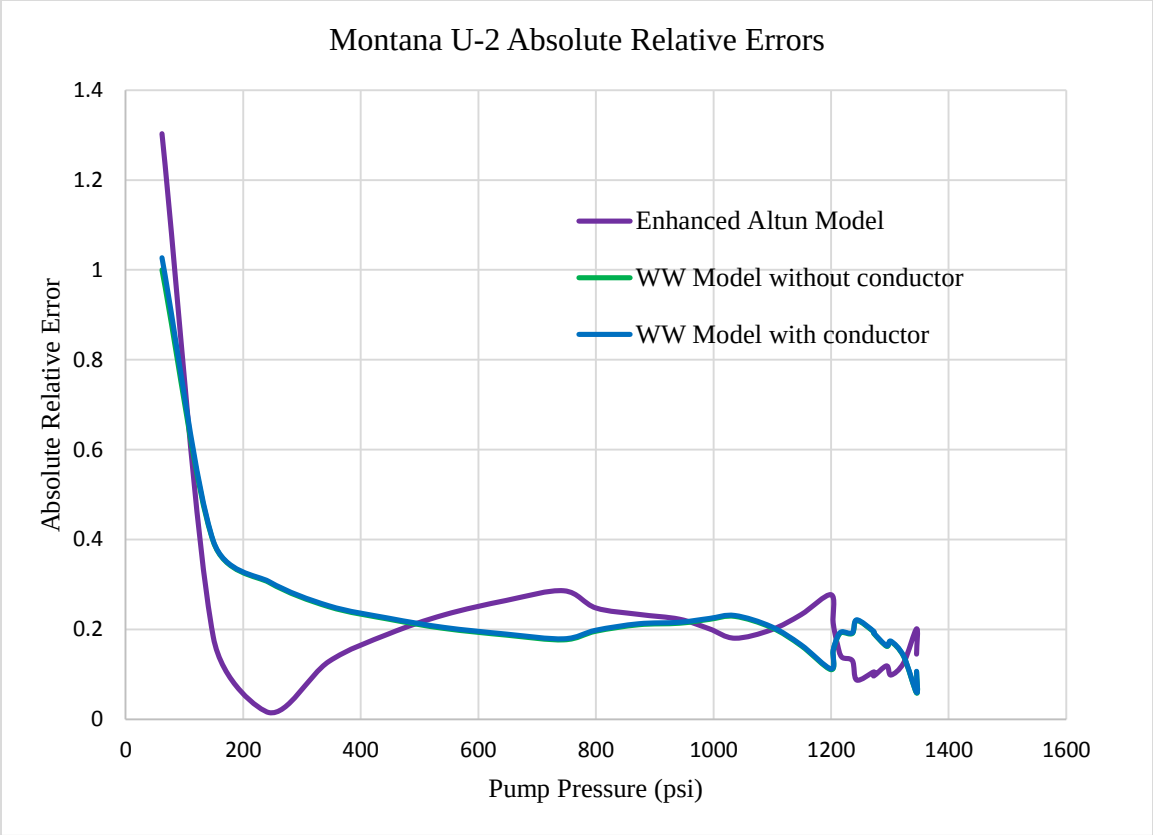

Figure 4.64 Montana U-2 absolute relative errors from LOT models

The error analysis for Montana U-2 can be divided into sections. The WW models demonstrate less relative errors at the beginning of pumping compared to the enhanced Altun model and errors from all three models decrease rapidly after the beginning of LOT. From approximately 200 psi to 500 psi of pump pressure, the enhanced Altun model displays less error than the WW models. From 500 psi to approximately 950 psi of pump pressure, the WW models have less errors compared to the enhanced Altun model. However, after pump pressure passes 1000 psi, the enhanced Altun model shows less errors.

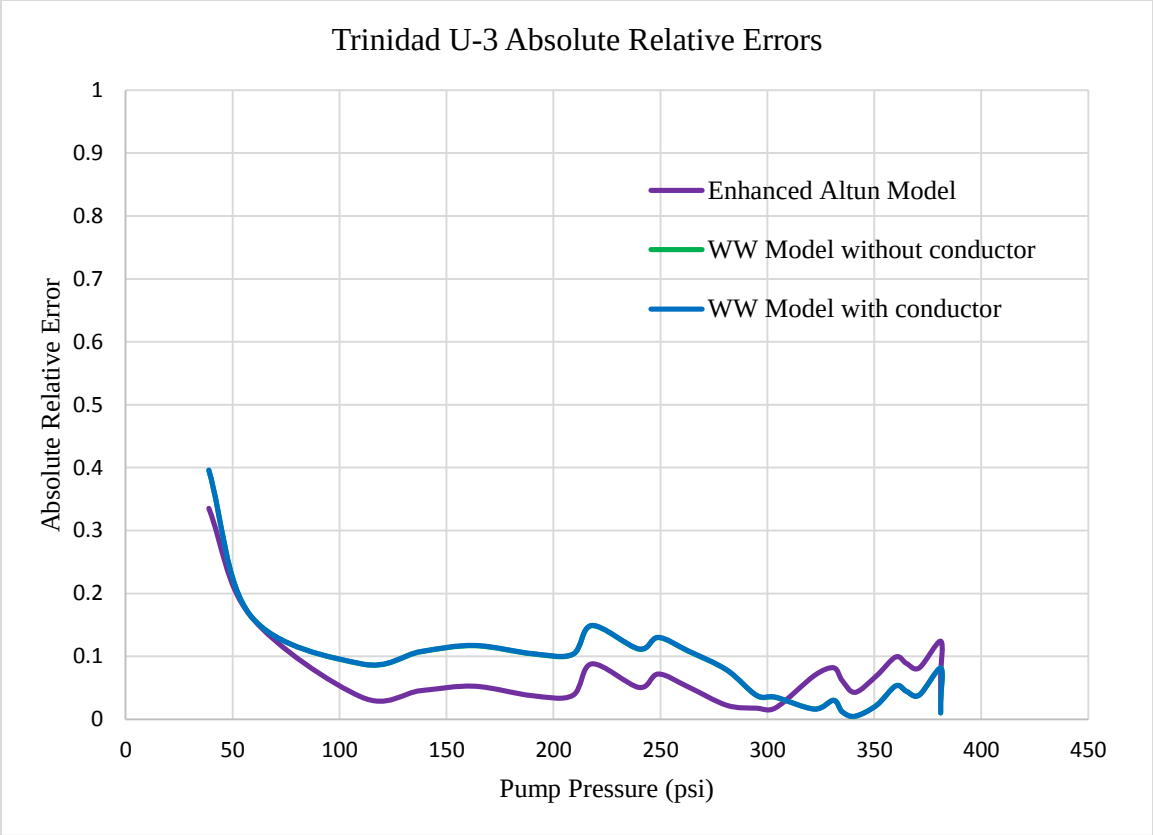

Figure 4.65 Trinidad U-3 absolute relative errors from LOT models

The error analysis for Trinidad U-3 can also be divided into sections. The enhanced Altun model is more accurate before pump pressure reaches 300 psi, as shown in Figure 4.65. However, after pump pressure passes 300 psi, the WW models appear to be more accurate.

4.5.2.2 Average Absolute Relative Error and Standard Deviation

Table 4.10 Overall average absolute relative errors and standard deviations for LOT models

Alaska U-1		
	Average Error	Standard Deviation
Enhanced Altun Model	0.548071602	0.538948448
WW without conductor	0.10713215	0.109326533
WW with conductor	0.103084494	0.109774919
Montana U-2		
	Average Error	Standard Deviation
Enhanced Altun Model	0.21526739	0.222898259
WW without conductor	0.223351954	0.164050471
WW with conductor	0.226029213	0.168542273
Trinidad U-3		
	Average Error	Standard Deviation
Enhanced Altun Model	0.073927493	0.064113223
WW without conductor	0.082919356	0.080065024
WW with conductor	0.08306406	0.080274755

4.6 Deficiencies of LOT Models and Future Research Suggestions

The deficiencies of the LOT models are discussed in detail in this section.

4.6.1 Altun Model

A closer inspection upon Altun's dissertation reveals that Altun uses pump pressure as the pressure terms in both the casing expansion calculations and borehole expansion calculations. However, pump pressure does not reflect the actual pressure loading on the inner surfaces of the casing and the borehole. In a real time LOT, the pressures acting on the casing and borehole depend not only on the pump pressure, but also the head of mud above.

Altun's leak model is based on Poiseuille's flow in channels. In the original reference, Craft and Hawkins (1991) stated that the change in pressure term is defined by the difference in pressure between the tip of the flow channel and the heel of the crack. It

was not certain how Altun recognized this pressure difference in his calculations. In addition, Altun assumed that the preexisting crack has the length of 15 ft. With this length, the crack would have extended well beyond the near wellbore stress region. However, questions remain regarding the validity of this assumption as many believe that a crack cannot extend very long during a LOT.

4.6.2 Wider Windows Mechanical Expansion Model

The data obtained from Altun's dissertation and published paper were originally provided by Unocal, Amoco, and Amerada Hess Corporation. The original field data has been furnished and was not available for this study. Therefore, considerable amount of assumptions on key parameters were made to enable model calculations. Certain uncertainties and errors from assumptions can affect the accuracy of the volume calculations by the WW model.

One of the assumptions that can affect the accuracy of volume calculation is the depth of conductor casing shoe. For example, Alaska U-1's 20" section is drilled to 5869 ft. Because this depth has exceeded the usual setting depth of a surface casing, it is likely that a 26" section has been drilled and cemented before. In deeper wells like Alaska U-1, the volume contribution from concentric cylinder expansion has shown to be significant. Therefore, uncertainties in wellbore schematics can certainly affect the accuracy of total volume prediction.

The WW mechanical expansion model utilizes Lame's solution in 2D to calculate inner casing surface displacements. As shown in Figure 4.4.19 to Figure 4.4.21, there exist gaps in inner cylinder displacement when an outer casing is present. This is because the WW mechanical model calculates displacements based on each concentric cylinder system, the model cannot handle 3D effects near the boundaries of concentric cylinder systems. Although the gap is considered to be local, it creates errors and uncertainties in the analysis.

4.6.3 Future Research Suggestions

Ishijima (1973) and Postler (1997) suggested that fluid penetrating properties affect LOT behaviors. In deep water drilling, the conductor and surface sections are normally drilled with seawater. However, as the well deepens, drill engineers commonly switch to OBM or SYM. OBM and SYM are considered to be penetrating fluids and their effects on leak-off behaviors have been shown in chapter 2. Therefore, a more realistic fluid flow model coupled with hydraulic fracturing mechanisms can be helpful to enhance the simulation of fluid flow and leakage during a LOT.

Van Oort (2007) suggested that temperature can affect the near wellbore thermal stresses and downhole effective mud density. In this study, the highest errors are all recorded at low pump pressures. During the early stages of the LOT, new mud is introduced into the system, the temperature difference between the new mud and the formation is not accounted for. Therefore, future studies should take into account the temperature effect on LOT behaviors.

If cracks are created during a LOT with WBM, mud cakes are likely to buildup not only in the open hole, but also along the length of the fracture. Previous studies have shown that mud cake can affect crack stability and propagation (Postler, 1997). Therefore, the effect of mud cake buildup can be further investigated by future works.

4.7 CHAPTER SUMMARY

From the sub-system volume contribution plots, it is clear that only fluid leakage displays non-linear trend during pressure buildup. Therefore, the non-linearity observed in the general LOT behaviors from all three tested wells is the result of the leak effect. The leak effect in Trinidad U-3 is the most dominant among the three tested wells, indicating that a channel likely exists to provide fluid flow near the casing shoe. In addition, borehole expansion volumes are very small compared to all the other sub-systems. From the

calculated results, it was concluded that borehole volume contributions are more than 100 times smaller than the second smallest sub-system. Therefore, borehole expansion along with the volumes pumped to compress other sub-system volumes are neglected from total volume calculations.

The enhanced Altun model, which added the effects from cement expansion and formation rock expansion, seems to provide the best fit of actual LOT data for Montana U-2 and Trinidad U-3. However, for the well with the longest length of casing under loading, Alaska U-1, the error for enhanced Altun model increased significantly. This suggests that leak-off volume is characterized by a combined effect of casing, cement, and formation rock expansion under both internal pressure in the wellbore and the external pressure exerted on the formation rock.

Chapter 5 Conclusions

This research produced several important findings relevant to modeling linearly behaved LOTs and non-linearly behaved LOTs.

5.1 LOT Model sub-systems

The sub-system volume plots showed that the leakage volume is the only source of non-linear LOT behavior. In addition, the overall LOT trend depends on the magnitudes of the linearly behaved systems (mud compression, casing expansion, borehole expansion, and concentric cylinder expansion) and the non-linearly behaved system (leak volume). When the leak volume is dominant, the overall LOT plot generally duplicate the behaviors and signatures observed on the leak volume plot. On the other hand, when the linearly behaved systems dominate, the LOT plot exhibits a linear behavior up until the leak volume becomes significant.

5.2 The Added Volumes from Cement Expansion and Formation Expansion

The results from the enhanced Altun model with additional volumes generated by cement sheath expansion and formation rock expansion suggested that the leak-volume along the cased hole is a compounded effect. When the length of the cased hole is short, such as in Trinidad U-3, the gap between model prediction and the actual LOT data is not obvious. However, as the length of cased hole gets longer, as in Alaska U-1 and Montana U-2. The difference between actual data and model volume prediction becomes significant. Therefore, it was concluded that it is necessary to use the WW mechanical expansion model to simulate the leak volume along the cased hole.

5.3 CONCENTRIC CYLINDER EXPANSION

The WW mechanical expansion model adopted the concentric cylinder theory developed by Norris (2003) to accurately simulate the volume produced by the expansion of the casing, cement, and formation rock during a LOT. The first advantage of this model is that it incorporated both the pressure in the wellbore as well as the pressure out in the far field stress region, which accurately determines the casing displacements at different pump pressures during the LOT. Based on the casing displacements, the model can simulate the leak-off volume generated by the compounded effect of casing, cement, and rock expansion.

Most offshore wells have complicated designs and layers of casing strings before reaching the targeted formation. Previous LOT models, such as the Altun model and the Paknejad model, can only investigate the leak-off volume by modeling the expansion of the particular casing string that the LOT is testing. However, the WW model, describes the wellbore by using layers of concentric cylinders and can be modified to give the total system response during a LOT.

List of Acronyms

BOP: Blow out preventer

ELOT: Extended leak-off test

EMW: Equivalent mud weight

FCP: Fracture closure pressure

FIP: Fracture initiation pressure

FIT: Formation integrity test

FPP: Fracture propagation pressure

FRP: Fracture reopening pressure

GOM: Gulf of Mexico

HPHT: High pressure and high temperature

ISIP: Instantaneous shut in pressure

LOP: Leak-off pressure

LOT: Leak-off test

LP: Limit pressure

LWD: Logging while drilling

MD: Measured depth

OBM: Oil based mud

ppg: pounds per gallon

SBM: Synthetic based mud

SMS: Shallow marine sediments

SPP: Stop pump pressure

TVD: True vertical depth

UFP: Unstable fracture pressure

WBM: Water based mud

WW: Wider Windows

XLOT: Extended leak-off test

References

Aadnoy, B.S., Mostafavi, V., and Hareland, G. 2009. Fracture Mechanics Interpretation of Leak-Off Tests. SPE 126452 presented at 2009 Kuwait International Petroleum Conference and Exhibition, Kuwait City, Kuwait, 14-16 December 2009.

Addis, M.A., Hanssen, T.H., Yassir, N., Willoughby, D.R., and Enever, J. 1998. A Comparison of Leak-Off Test and Leak-Off Test Data for Stress Estimation. SPE 47235 presented at SPE/ISRM Eurock '98, Trondheim, Norway, 8-10 July 1998.

Alberty, M.W., Hafle, M.E., Mingle, J.C., and Byrd, T.M. 1999. Mechanisms of Shallow Waterflows and Drilling Practices for Intervention. SPE 56868 presented at Offshore Technology Conference, Houston, Texas, 5-8 May, 1997.

Altun, G. 1999. Analysis of Non-linear Formation Fracture Resistance Tests Obtained During Oil Well Drilling Operations. PhD dissertation, Louisiana State University, Baton Rouge, Louisiana.

Altun, G., Langlinais, J., and Bourgoyne Jr., A.T. 2001. Application of a New Model to Analyze Leak-Off Tests. SPE 72061 presented at SPE Annual Technical Conference and Exhibition, Houston, Texas, 3-6 October 1999.

Craft, B.C. and Hawkins, M.F. 1991. *Applied Petroleum Reservoir Engineering*. Englewood Cliffs, N.J.: Prentice Hall, 225-226.

Edwards, S.T., Meredith, P.G., and Murrell, S.A.F. 1998. An Investigation of Leak-Off Test Data for Estimating In-situ Stress Magnitudes: Application to a Basinwide Study in the North Sea. SPE 47272 presented at SPE/ISRM Eurock '98, Trondheim, Norway, 5-10 July 1998.

Haimson, B., and Fairhurst, C. (1967, September 1). Initiation and Extension of Hydraulic Fractures in Rocks. Society of Petroleum Engineers. DOI:10.2118/1710-PA

Heger, A. and Spoerker, H.F. 2011. Understanding XLOTs. SPE 140028 presented at SPE/IADC Drilling Conference and Exhibition, Amsterdam, The Netherlands, 1-3 March 2011.

Horsrud, P., Risnes, R., and Bratli, R.K. 1982. Fracture Initiation Pressures in Permeable Poorly Consolidated Sands. International Journal of Rock Mechanics and Mining Sciences. Volume (19): 255-266.

Hubbert, M.K. and Willis, D.G. 1957. Mechanics of Hydraulic Fracturing. Transactions of American Institute of Mining, Metallurgical, and Petroleum Engineers. Volume (210): 153-166, 167-168.

Ishijima, Y. and Roegiers, J.C. 1983. Fracture Initiation and Breakdown Pressure – Are they Similar? Proc. 24th U.S. Symposium on Rock Mechanics, pp. 761-772.

Lee, D., Birchwood, R., and Braton, T. 2004. Leak-Off Test Interpretation and Modeling with Application to Geomechanics. ARMA 04-547 presented at Gulf Rocks 2004 the 6th North American Rock Mechanics Symposium, Houston, Texas, 5-9 June 2004.

Li, G., Lorwongngam, A., and Roegiers, J.C. 2009. Critical Review of Leak-Off Test as a Practice for Determination of In-situ Stresses. ARMA 09-3 presented at the 43rd US Rock Mechanics Symposium and 4th U.S.-Canada Rock Mechanics Symposium, Asheville, North Carolina, 28 June-1 July 2009.

Norris, T. Algorithm Derivation. Toby Norris's website. www.tobynorris.com/work/prog/cpp/mfc/concyl_hlp/algorithmderivation.htm. Downloaded 1 May 2013.

Økland, D., Gabrielsen, G.K., Gjerde, J., Sinke, K., and Williams, E.L. 2002. The Importance of Extended Leak-Off Test Data for Combatting Lost Circulation. SPE 78219 presented at SPE/ISRM Rock Mechanics Conference, Irving, Texas, 20-23 October 2002.

Paknejad, A., Schubert, J., and Amani, M. 2007. A New Method to Evaluate Leak-Off Tests in Shallow Marine Sediments (SMS). SPE 110953 presented at SPE Saudi Arabia Technical Symposium, Dhahran, Saudi Arabia, 7-8 May 2007.

Postler, D.P. 1997. Pressure Integrity Test Interpretation. SPE 37589 presented at 1997 SPE/IADC Drilling Conference, Amsterdam, The Netherlands, 4-6 March 1997.

Rezmer-Cooper, I.M., Rambow, F.H.K., Arasteh, M., Hashem, M.N., Swanson, B., and Gzara, K. 2000. Real-Time Formation Integrity Tests Using Downhole Data. SPE 59123 presented at IADC/SPE Drilling Conference, New Orleans, Louisiana, 23-25 February 2000.

van Oort, E. and Vargo, R. 2007. Improving Formation Strength Tests and Their Interpretation. SPE 105193 presented at 2007 SPE/IADC Drilling Conference, Amsterdam, The Netherlands, 20-22 February 2007.

Wojtanowicz, A.K. and Zhou, D. 2001. Shallow Casing Shoe Integrity Interpretation Technique. SPE 67777 presented at SPE/IADC Drilling Conference, Amsterdam, The Netherlands, 27 February-1 March 2001.

Zoback, M.D. 2007. *Reservoir Geomechanics.* New York, N.Y.: Cambridge University Press, 221.